Photochemical and Logic-Based Regulation over the Cellular Microenvironment

Emily Rose Ruskowitz

A dissertation

submitted in partial fulfillment of the

requirements for the degree of

Doctor of Philosophy

University of Washington

2020

Reading Committee:

Cole A. DeForest, Chair

Elizabeth Nance

James M. Carothers

Program Authorized to Offer Degree:

Chemical Engineering

University of Washington

Abstract

Photochemical and Logic-Based Regulation over the Cellular Microenvironment

Emily Rose Ruskowitz

Chair of the Supervisory Committee:
Assistant Professor Cole A. DeForest
Department of Chemical Engineering and Bioengineering

The biological microenvironment is a complex, constantly changing space featuring varying amounts of many cell-secreted signaling molecules that serve as the communicatory elements of biology. By better understanding how well-defined combinations of individual biochemical signals including proteins presented in this space operate in (a)synchrony to direct cellular and integrated tissue function, we can begin to unravel irregularities within diseased systems and utilize this information to engineer therapies that promote healthy recovery. As photochemical reactions can be uniquely modulated in time and space, this dissertation develops and subsequently exploits novel light-based strategies to spatiotemporally control biochemical microenvironments and cellular signaling. First, we establish the cytocompatibility of near-ultraviolet light treatments common to photochemical manipulation through mammalian cell survival assays and global proteomic analyses. Expanding on existing concepts of photoresponsive drug delivery, we then introduce a generalizable strategy to govern biochemical signal presentation

within biomaterials in response to precise combinations of environmental factors following user-programmable Boolean logic. Finally, we introduce the first genetically encoded protein-protein photoligation chemistry, and demonstrate its utility in irreversibly directing protein binding, function, and interactions both intra- and extracellularly. Employing this versatile photoreaction, we demonstrate 3D patterned immobilization of full-length proteins within biomaterials and user-guided intracellular protein activity. Such newly afforded 4D control over biological systems is expected to further basic biological understanding and advance medicine through enhanced tissue engineering and therapeutic delivery approaches.

.

TABLE OF CONTENTS

LIST OF FIGURES

ACKNOWLEDGEMENTS

It’s fascinating to think about all the events that felt very minor yet had a significant impact in generating this document. But in reality, many of those events circle back to someone extending mentorship of some form. This document speaks to the power of offering advice, support, and inclusivity to those around us and to the quality of people I was fortunate enough to have guide me throughout my career. To each one of those people, thank you.

Cole DeForest, thank you for taking a chance on me and helping me find my place as a scientist. Your excitement for life, dedication to family and students, and pure enthusiasm for science made generating the work in this document enjoyable and fun. Thank you for being both a mentor and a friend through this process and for challenging and inspiring me to be a passionate researcher, teacher, and mentor to others.

I’d also like to thank my committee for guiding my work and dedicating their time, effort, and resources to my success. Particularly, I’d like to thank Elizabeth Nance for being a role model and a mentor over the years. I will always feel fortunate to have been a founding officer of WChE and for the opportunity to work with Elizabeth and my fellow officers to create an organization that empowers women and their supporters to find inspiration in STEM.

A large part of this work is here purely due to the talent and self-motivation of Sebastian Kurniawan and Alder Strange. Thank you for your dedication to our work. Additionally, the support both mentally and scientifically that the first-generation DeForest lab members (Mike Comerford, Barry Badeau, Jared Shadish, and Chris Arakawa) provided was quintessential. I am also grateful for the many lab-mates, fellow graduate students, and collaborative labs I was able to work with and learn from.

And finally, I’d like to thank my family and friends for their continued support and relentless belief in me. I was fortunate to be raised in an environment that prioritized education and problem solving. Mom and Dad, thank you for always being there. Jeffrey Ruskowitz, thank you for being my first scientific mentor and leading me research and chemical engineering. Jeri Ruskowitz, thank you for inspiring me to pursue graduate school and for endless support. And finally, Cody King, thank you for believing in me from the moment we met and becoming the most supportive partner imaginable.

DEDICATION

This work is dedicated to my endlessly supportive husband, family, pets, and Grandma Charlotte whose kindness and humor inspire me daily.

Chapter 1: INTRODUCTION

Adapted from Ruskowitz, E.R., DeForest, C.A. Photoresponsive Biomaterials for Targeted Drug Delivery and 4D cell culture *Nature Reviews Materials*, **3**, 17087 (2018).

1.1 ABSTRACT

Biological signaling is regulated through a complex and tightly choreographed interplay between cells and their extracellular matrix. The spatiotemporal control of these interactions is essential for tissue function, and disruptions to this dialogue often result in aberrant cell fate and disease. When disturbances are well understood, correct biological function can be restored through the precise introduction of therapeutics. Moreover, model systems with modifiable physiochemical properties are needed to probe the effects of therapeutic molecules and to investigate cell-matrix interactions. Photoresponsive biomaterials benefit from spatiotemporal tunability, which allows for site-specific therapeutic delivery *in vivo* and 4D modulation of synthetic cell culture platforms to mimic the dynamic heterogeneity of the human body *in vitro*. In this chapter, we discuss how light can be exploited to modify different biomaterials in the context of photomediated drug delivery and phototunable cell culture platforms. We survey various photochemistries for their applicability *in vitro* and *in vivo*, and for the biochemical and biophysical modification of materials. Finally, we highlight emerging tools and closely investigate applications of biochemical reactions including optogenetic tools to mediate intra- and extracellular control.

1.2 INTRODUCTION

Photochemistry plays a fundamental role in many biological processes, including photosynthesis, maintenance of circadian periodicity and sight. Visual interpretation of one's surroundings relies on a photo-induced isomerization reaction that triggers a signaling cascade responsible for vision[1]. Inspired by nature, chemists, biologists and material scientists have long sought to control biological functions through light-driven reactions[2] owing to several advantages over chemistries triggered with enzymes, small molecules, temperature, ultrasound, or changes in pH. First, light can be directed to specific 3D locations at user-defined times (**Figure 1.1**), enabling 4D control over system dynamics. Second, functional tunability can be obtained by varying the administered light dosage. Third, independent control over different biological processes can be achieved in a wavelength-specific manner, and finally, the optical tissue window permits regulation *in vivo*. Properly engineered photochemistries open up opportunities to examine and alter biological processes with high precision.

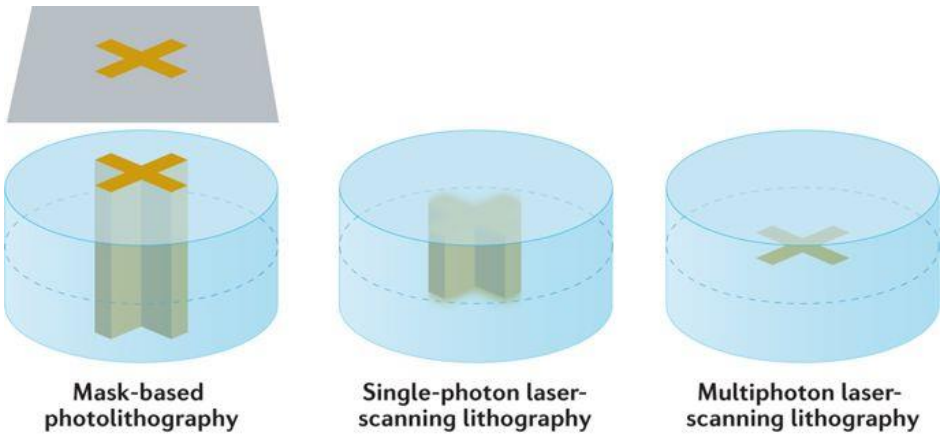

Figure 1.1. Selective exposure of phototunable biomaterials to light allows for the modification of specific volumes of a material. Directed light exposure can be obtained through lithographic techniques. **Mask-based photolithography** Substrates are exposed to light that is partially obstructed by a designed photomask inserted between the sample and the photonic source. Mask-defined 2D geometric shapes can be applied throughout the thickness of the material. Although limited by the inability to achieve 3D control, traditional photolithography is inexpensive and provides scalable patterning with an x,y-resolution on the order of tens of microns. **Single-photon**

laser-scanning lithography Laser light is directed to a specific area within a material to localize photoreactions to regions near the focal point. Programmed laser rastering permits some degree of 3D patterning, although x,y-resolution (sub-micron) exceeds z-resolution (typically > 25 μm) owing to the unavoidable reaction initiation above and below the focal plane. Despite longer processing times associated with sample scanning, the technique employs readily accessible equipment and provides some degree of 3D patterning within photoresponsive biomaterials. **Multiphoton laser-scanning lithography** Limitations of single-photon laser-scanning lithography can be addressed through the use of a pulsed near-infrared (NIR) laser source. Near-instantaneous absorption of two low-energy photons confines photoreactions to the focal plane, which improves z-resolution (typically 2-3 μm). NIR light permits deeper sample penetration and avoids cell damage and deterioration of photosensitive molecules surrounding the region of interest. However, this technique is time-consuming and relies on specialized, expensive equipment.

Over the past several decades, the library of light-responsive synthetic reactions has vastly expanded with photochemical tools for bond formation, cleavage, isomerization and other molecular rearrangements (**Table 1.1**)[3–5]. Reaction specifics including excitation wavelength, conversion efficiency and chemical response must be carefully matched to the desired application. In one of the first applications of photochemistry to control biological activity, the function of adenosine triphosphate (ATP) was masked with a photolabile nitrobenzyl-based protective 'photocage', which could be removed with ultraviolet (UV) light to liberate the bioactive species[6]. Photocages represent covalently linked chemical moieties that can be removed through a photoreaction to reveal a biochemical functionality[7]. When incorporated into biomaterials, photochemistries give rise to a variety of photoresponsive constructs[8], which have found widespread application in both drug delivery and tissue engineering (**Figure 1.2**).

The growing interest in smart therapeutic dosing has led to a recent surge in the development of light-based strategies for targeted drug delivery[9,10]. Many therapeutics are tainted with severe off-target effects, limited effectiveness owing to short circulation times, and the requirement for invasive techniques to administer or monitor their concentration within a patient[11]. In addition to mitigating many of these concerns, photochemical tools enable therapeutic dosage to be locally controlled and precisely dictated at specific times through external, pulsed light

exposure. Therefore, photochemical strategies are an appealing approach to engineer smart delivery vehicles.

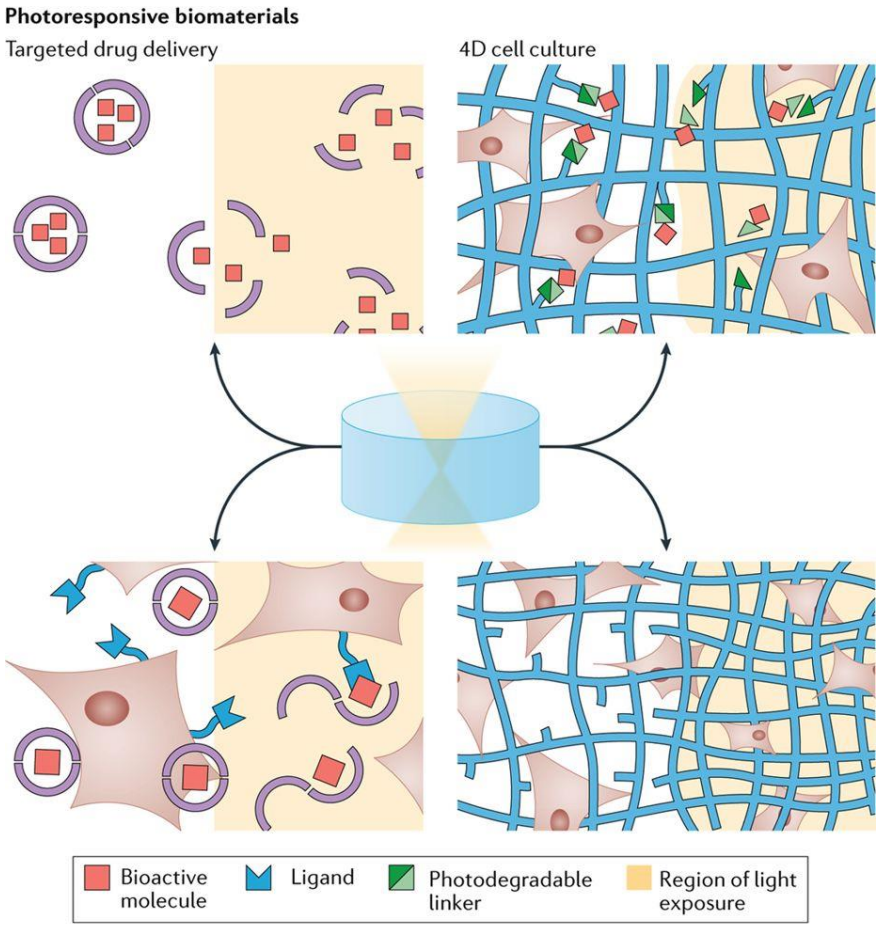

Figure 1.2. Photoresponsive biomaterials as platforms for targeted drug delivery and 4D cell culture. Localized, on-demand therapeutic release can be controlled through selective light exposure to a photoresponsive delivery vehicle, or through photomediated activation of a bioactive molecule, which becomes available for specific-ligand binding. Similarly, photoresponsive hydrogels can be modified with a photodegradable linker, which enables spatiotemporally defined patterning of biochemical and biophysical cues to recreate the dynamic, heterogeneous cellular microenvironment.

Table 1.1. Photochemistries for the control of biomaterial function

				Relative Use	
Type of reaction	**Functional group or reaction**	**Representative Mechanism**	**Relative Rate**	**Drug Delivery**	**4D Cell Culture**
Cleavage	Nitrobenzyl	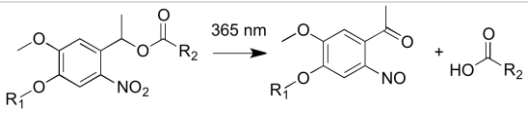	+ +	✓✓✓	✓✓✓
	Coumarin	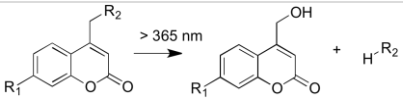	+ + +	✓✓	✓✓
	Disulfide	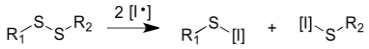	++	–	✓
Isomerization	Azobenzene	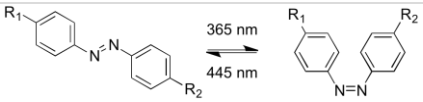	+ +	✓✓	✓
	Spiropyran/ Merocyanine	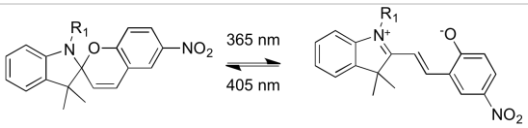	+ +	✓	✓
Rearrangement	DNQ	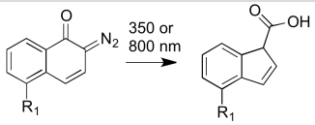	+ +	✓	–
	RAFT	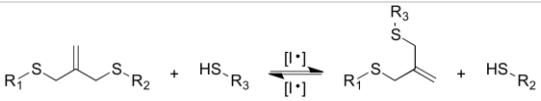	+++	–	✓
Addition	Acrylate	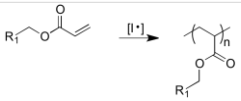	+++	–	✓✓✓
	Photocaged Michael Addition	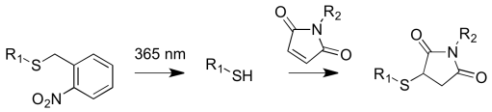	+ +	–	✓✓
	Thiol-ene	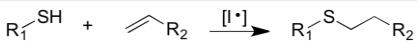	+++	–	✓✓

DNQ,2-diazo-1,2-napthoquinone; RAFT, reversible addition-fragmentation chain-transfer; CuAAC, copper-catalyzed azide-alkyne cycloaddition; Factor XIIIa, FXIIIa. Relative reaction rate is indicated with plus signs (+). Relative usage for each reaction for both drug delivery and 4D cell culture is indicated with check marks.

The spatiotemporal tunability provided by photoreactions for therapeutic delivery has also proven invaluable in the creation of dynamic cell culture platforms. Hydrogels are a class of biomaterials that mimic many properties of native tissue, and are commonly used for tissue engineering and 3D cell culture. Although gels can be cast with well-defined initial physiochemical properties, next-generation strategies seek to create biomaterials that capture the dynamic and heterogeneous characteristics of the native extracellular matrix (ECM). Light exposure can be controlled in 4D and therefore, local attributes of photoresponsive biomaterials can be governed on demand and in the presence of live cells. Such dynamic platforms allow for the investigation of disease progression and tissue morphogenesis, and ultimately the engineering of complex functional tissues.

In this chapter, we highlight advances in photoresponsive biomaterial engineering for controlled drug delivery, investigating photoreaction mechanisms and applications of different photochemistries in the targeted release of bioactive therapeutics. We then examine phototunable cell culture platforms with special emphasis on the photochemical reactions that govern 4D material responsiveness, physicochemical tunability and biophysical alterations. Finally, we discuss exciting opportunities for next-generation photoresponsive systems, highlighting novel protein-based chemistries and optogenetic tools.

1.3 PHOTOMEDIATED DRUG DELIVERY

Controlled drug delivery ideally introduces bioactive compounds to precise locations at defined times, and therapeutic concentrations are maintained by providing protection from biodegradation and clearance *in vivo*. Drug delivery strategies should have high loading efficiency, cytocompatibility and on-demand, dose-controlled release only at desired sites. Of externally controllable stimuli, such as light, magnetic fields or ultrasound, light affords near-instantaneous

release with precise on and off spatiotemporal control in a minimally invasive manner. Photochemistries are further wavelength-specific, offering the opportunity to exploit multiple reactions for on-demand delivery of different therapeutics from a single system. Reactions are being developed that are active in the near-infrared (NIR) range, because they are less damaging to tissue and afford increased penetration depth[12]. Photoresponsive drug delivery vehicles can be categorized based on their underlying photochemical mechanism: an explicit molecular cleavage event, isomerization, rearrangement, or whether light is used in conjunction with additional species to initiate thermal or free-radical processes.

1.3.1 *Bond photolysis*

Photoscissable covalent bonds can be cleaved with a sufficient dose of wavelength-matched irradiation, forcing molecular dissociation. This photolabile property offers a robust approach to release compounds of interest at a target location through directed light exposure, which is particularly useful for drug delivery. Photosensitive drug delivery vehicles most commonly use nitrobenzyl and coumarin derivatives, because of their synthetic tractability, favorable absorbance properties and photokinetics. They can be either applied as a cleavable linker between a therapeutic and a stable delivery vehicle, within the structural support of a photodegradable carrier, or as a photocage to inhibit biological activity (**Figure 1.3a**).

Nitrobenzyl derivatives

Nitrobenzyl chemistry has been first applied in a biological setting to demonstrate the photoliberation of nitrobenzyl-caged ATP to serve as a substrate for an ATPase upon release[6]. Building on this foundational work, nitrobenzyl derivatives have been extensively employed to release small molecule therapeutics[13–15], proteins[16,17] and oligonucleotides[18–22] from various materials.

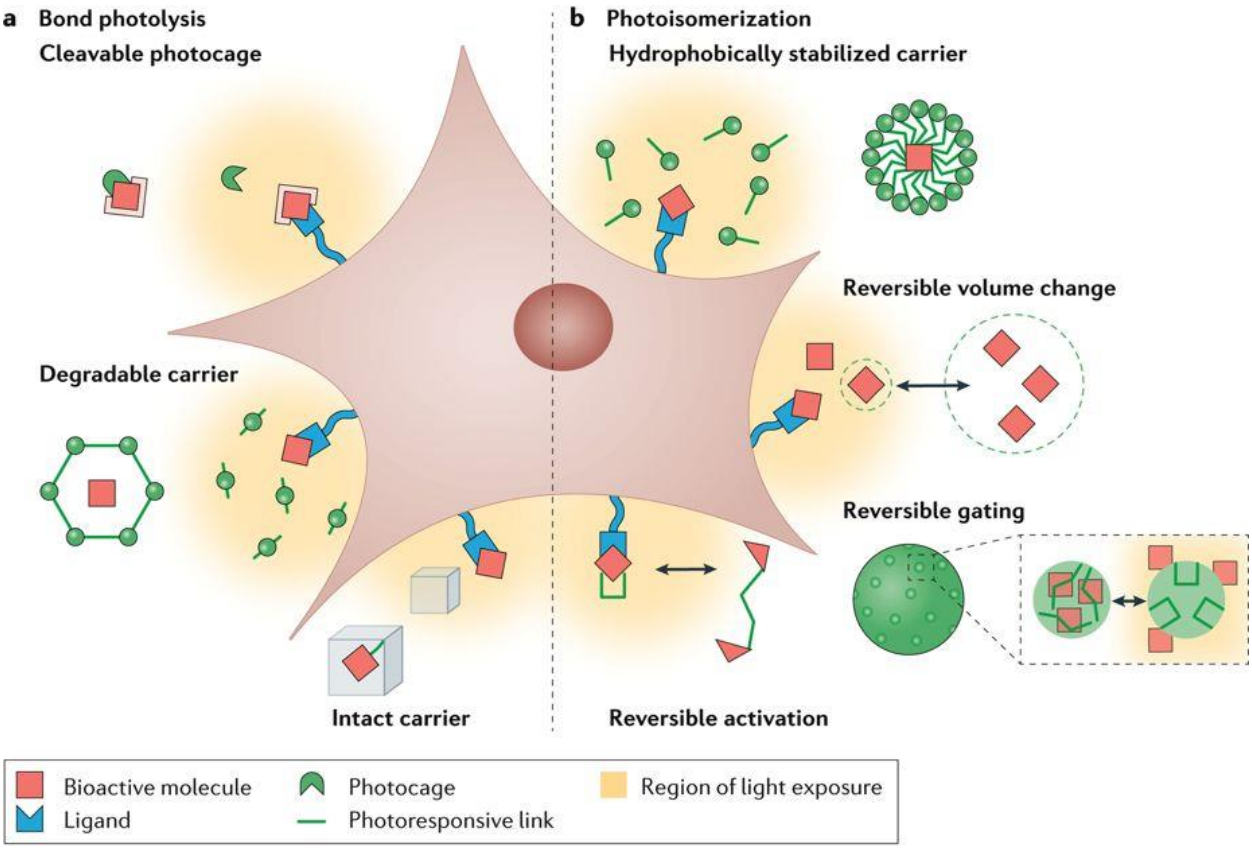

Figure 1.3. Photocontrolled delivery of bioactive molecules. **a**, Bond photolysis can be used to confine therapeutic release to specific locations at specific times. Approaches have been developed, which rely on photoliberation of caged species, photodegradation of therapeutic delivery vehicles, or photoscission of molecular tethers between a nondegradable carrier and a bioactive molecule. **b**, Photomediated isomerization reactions can be exploited to degrade hydrophobically stabilized delivery vehicles, to trigger changes in payload release rates through the reversible adjustment of the size of the delivery vehicle, for the reversible gating of therapeutics in stable delivery vehicles, and for the reversible activation of therapeutic activity through conformational changes.

Release profiles are largely dependent on the chemical linkage between the therapeutic and the photoactive nitrobenzyl group. Through the incorporation of a nitrobenzyl ester crosslink in a poly(ethylene glycol) (PEG)-2-aminoethyl methacrylate hydrogel containing short interfering RNA (siRNA), degradation of the material and release were induced upon exposure to UV light[21]. Although nitrobenzyl photolysis enables controlled delivery through light exposure, the lack of long-term stability associated with gradual ester hydrolysis is a potential limitation. In order to

minimize hydrolytic degradation upon intradermal injection, therapeutic cargos can be linked through a nitrobenzyl ester derivative to insoluble polymeric microbeads. In this manner, human insulin has been remotely released from polystyrene matrices through short external exposures at 365 nm to regulate blood levels *in vivo*[23]. Replacing the ester with hydrolytically stable linkages (such as amides or carbonate) offers a method to decrease non-specific release[24]. For example, a nitrobenzyl carbonate linker between a box-like DNA nanostructure and the therapeutic cargo has been developed to release small molecules and large proteins[17]. Nitrobenzyl photocleavage at 302 nm releases the biomolecule from the nanostructure, eliciting a biological response within milliseconds. This approach allows for the release of a molecule with intact biological activity. However, the toxicity of the short wavelengths and the limited depth of tissue penetration of light limit the *in vivo* applicability of this system. Alternatively, hydrophobic therapeutic release under UV irradiation can be achieved using 4,5-dimethoxy-2-nitrobenzyl containing poly(lactic-co-glycolic acid) nanoparticles[25]. The carbamate linkage employed here increases particle stability and facilitates the controlled release of a small molecule therapeutic 10 weeks post-injection in a rat model of choroidal neovascularization[26].

Substantial efforts have been dedicated to improving photocleavage kinetics and redshifting compound absorbances to enhance species cytocompatibility and expand the application of nitrobenzyl-based photochemistry in living systems[27]. Substituent effects can be used to increase nitrobenzyl photocleavage rates at higher wavelengths ($\lambda > 360$ nm)[28]. Three differently substituted nitrobenzyl-based linkers with different wavelength photoresponsiveness (365-436 nm) enable wavelength-dependent release of three model therapeutics from a single material[29]. Another nitrobenzyl derivative, 2-(2-nitrophenyl)propyloxycarbonyl (NPPOC), can be efficiently cleaved using multiphoton NIR[30,31] and red light[32] excitation, which makes it applicable

for higher wavelength (λ > 360 nm) drug delivery techniques. Single-photon IR-initiated photocleavage has been achieved through the combination of nitrobenzyl moieties with silicon quantum dots[15] and upconverting nanoparticles[33–37]. The diverse library of nitrobenzyl linkers, which are responsive to a variety of wavelengths, allows for the development of dynamic, smart delivery vehicles for sequential therapeutic release.

Directed release of biological molecules to a specific cell type or tissue within the body by locally concentrating the delivery vehicle can reduce minimum effective therapeutic dosages, increase efficacy and eliminate off-target effects. Specific targeting can be achieved through on-site gelation of photodegradable materials[21] or by exploiting key markers and features of the local microenvironment. For example, cancer cells, which overexpress folate receptors, can be targeted by decorating the vehicle with folic acid residues[38–41]. Micelle carriers modified with folic acid and containing a nitrobenzyl-photocaged camptothecin prodrug improve cellular uptake; chemotherapeutic release into the cytosol is triggered by subsequent light exposure[41]. Similarly, cell-penetrating peptides, that is amino acid sequences that mediate transport across the cell membrane, can be conjugated to drug delivery vehicles to increase intracellular delivery[42,43], or can be photocaged with nitrobenzyl-derived nitroveratryloxycarbonyls (NVOC) to control cellular uptake[44–46].

Orthogonal chemistries have been used in conjunction with nitrobenzyl-based linkers to create multi-stimuli responsive systems[47–51]. For example, a poly(2-hydroxyethyl methacrylate-co-methacrylic acid) microgel containing myoglobin undergoes pH-dependent (de)swelling for slow release and photomediated NVOC-crosslinker cleavage for rapid delivery following vehicle photodegradation[50]. Mesoporous silica nanoparticles (MSNs) have been employed to create a triple-stimuli responsive vehicle containing a disulfide linkage, which is cleaved under reductive

conditions, pH-sensitive poly(2-(diethylamino)-ethyl methacrylate polymer caps and an *ortho*-nitrobenzyl ester photolinker[51]. Even though these systems represent an important step towards the development of multiple stimuli-sensitive chemistries within a single device, they are limited by leakiness and UV-unresponsiveness. Ideally, delivery vehicles remain fully stable until therapeutic release is required. Hydrogels can be programmed to exhibit Boolean logic-based degradation of material crosslinks in response to precise combinations of external stimuli for triggered drug delivery[52]. When nitrobenzyl moieties are connected in series with another degradable functionality, the cleavage of either group causes material dissolution (OR gate); when scissile moieties are connected in parallel, cleavage of both is required for degradation (AND gate). Multiple gates combined hierarchically enable complex logic-based delivery to light alongside other dynamic stimuli.

Coumarin compounds

Coumarin derivatives have become popular phototriggers, since their early demonstration as efficient photocleavable moieties[53]. High absorption efficiencies, fast cleavage rates, ease of redshifting their absorption profiles and affinity for multiphoton-induced reactions make coumarin derivatives favorable alternatives to nitrobenzyl-based linkers[54,55]. As such, efforts have been dedicated towards the development of new photolabile coumarin compounds, which have been applied to micelles[56], microgels[57], MSNs[58–60] and as simple cages[54,61] for photomediated drug delivery. Similar to nitrobenzyl-based delivery vehicles, folic acid residues[60,62,63], complimentary mRNA sequences[64] and dual-caging strategies[65] have been used in conjunction with coumarin compounds to target specific cells or tissues.

Minor chemical modifications of coumarin compounds result in significant absorption shifts to higher, biocompatible wavelengths without a significant reduction in the quantum yield

for cleavage[66]. For example, a 7-amino coumarin modified with vinyl groups for radical chain polymerization undergoes photocontrolled swelling and degradation of polystyrene microgels upon exposure to light at 400-450 nm[57]. Similarly, a redshifted, synthetically tractable 7-diethylamino-4-thiocoumarinylmethyl protecting group has a peak absorption above 450 nm and minimal response to UV light, which can be exploited for wavelength-orthogonal photoinduction of distinct phenotypes in zebrafish with UV and blue light[67]. The coumarinylmethyl backbone can be further modified to create a library of cyan light-responsive (470-500 nm) cages[68]. These photolabile molecules offer a narrow activation window at various wavelengths and thus, represent an important step towards the controlled release of different therapeutics from a common material through wavelength specificity.

In addition to their high quantum yield under single-photon excitation, coumarin moieties are highly sensitive to multiphoton absorption, providing the possibility for therapeutic delivery to deep tissue. 6-bromo-7-hydroxycoumarin esters and carbamates, which have been used for controlled un-caging of glutamate in brain tissue[69], require lower light intensities to elicit photocleavage and exhibit a relatively large multiphoton absorption cross-section compared with unmodified coumarins. NIR-responsive, coumarin-containing block copolymer micelles have also been used for drug delivery[70,71]. Additionally, the delivery of hydrophilic payloads, such as cells and proteins, has been achieved through NIR-based degradation of a short, water-soluble coumarin crosslinker[72]. Coumarin-based materials show significant promise for *in vivo* drug delivery, because of the ease to redshift absorption, high quantum yield and cytocompatibility.

1.3.2 *Photomediated isomerization*

Photoexcitation can induce the reversible isomerization of selected organic compounds, such as azobenzenes and spiropyrans, by providing the required energy to reach a π^* state. This

conversion initiates a molecular switch from one stereoisomer to the other without a molecular by-product. The *trans*-to-*cis* conversion of azobenzene occurs under UV light (365 nm) through a π–π^* transition; the *cis* conformation relaxes to the thermodynamically stable *trans* isomer in the dark or under visible light (445 nm)[73]. Spiropyran undergoes a photoinitiated (365 nm) ring-opening isomerization to an unstable zwitterionic merocyanine. The reverse reaction rate is highly dependent on molecular substituents, but can be accelerated through visible light exposure. These reversible isomerizations can serve as building blocks for the creation of smart drug delivery vehicles (**Figure 1.3b**).

Azobenzene isomerization

Since the first application of an azobenzene photoisomerization for the construction of photoresponsive membrane systems[74], this photoreaction has been used to destabilize micelles and vesicles by disrupting the interactions of the amphiphilic components for burst release[75–78] and as a photoswitch in which drug efficacy is dependent on the conformation[79]. Azobenzene-carrier conjugation has further been applied to create delivery systems[80–83]; for example, vehicles that harness an impeller-type motion, which is induced by repeated *cis*-*trans* isomerizations, have been developed to increase diffusion rates out of an MSN[81]. These techniques have been used to release cholesterol[84] and to deliver DNA[85].

Significant effort has also been put forth to redshift the absorbance of azobenzene-based photoswitches with the assistance of upconverting nanoparticles[86] and through *ortho*- and *para*-substitutions[87–89]. For example, redshifted photoswitchable control can be gained through the tetra-*ortho*-chlorination of a fatty acid azobenzene designed to mimic capsaicin to regulate a non-specific cation channel[90]. NIR-absorbing azobenzene compounds show promise to be able to control biological targets *in vivo*[91,92].

Spiropyran-merocyanine isomerization

Spiropyran photoisomerizes from a hydrophobic closed-ring structure to a hydrophilic, zwitterionic open-ring merocyanine. This change in polarity can be exploited for the photoinitiated disruption of hydrophobic and ionic interaction-dependent structures[93–97]. For example, spiropyran-indoline-PEG nanoparticles loaded with the chemotherapeutic docetaxel undergo a reversible, UV-initiated (365 nm) shrinkage from 103 to 49 nm in diameter[98,99]. Treatment of subcutaneous HT-1080 tumors in nude mice with these nanoparticles using a single light exposure leads to increased tumor penetration and increased intratumoral vessel diameter through apoptosis-induced vascular decompression, which results in a decreased tumor size compared to treatments solely involving docetaxel[99]. NIR light (980 nm) can also be used in conjunction with upconverting nanoparticles to release a chemotherapeutic from a spiropyran-containing amphiphilic polymer system *in vitro*[96]. Although only few applications have been developed so far, reversible isomerization reactions provide a possibility to introduce cyclic on and off control of the activity of a biologic *in vivo*, a desirable trait towards inhibiting off-target activity or to achieve repetitive dosing.

1.3.3 *Light-induced rearrangement*

Photo-induced molecular rearrangement events can be exploited for therapeutic release. In response to UV light, diazocarbonyl compounds are converted to a ketene intermediate followed by a [2+2] cycloaddition adduct or a nucleophilic substituted product in the presence of a weakly or strongly acidic nucleophile – a mechanism referred to as a Wolff rearrangement[100]. Such systems can be designed to yield photoproducts with a shift in hydrophobicity strong enough to disrupt amphiphilic systems. 2-Diazo-1,2-naphthoquinone (DNQ) rearranges to a strongly hydrophilic carboxylic acid under UV (350 nm) and multiphoton excitation (800 nm)[101]. The first

IR-controlled delivery of a hydrophobic model therapeutic using DNQ was not performed in the presence of cells[102], but a DNQ-containing poly(ethylene oxide)-dendritic polyester micelle affords cytocompatible triggered release[103]. DNQ coupled with tumor-targeting sugar residues in a dendritic nanoparticle[104] or in the backbone of a brush copolymer[105] exhibits particle degradation because of NIR-induced shifts in hydrophobicity.

1.3.4 *Photothermally induced delivery*

The absorption properties and the resulting local heating of conductive nanomaterials have been extensively used to control drug delivery[106]. Although not directly falling into the category of photochemical reactions, such systems can be applied for indirect photomediated therapy. With the correct wavelength, conductive materials absorb incident photons and convert energy into local heating to increase membrane permeability[107], disrupt endosomes after endocytosis[108,109] and induce phase transitions of temperature-responsive systems[110–113]. Therapeutic release has been demonstrated using light ranging from UV to NIR[114–116], from a variety of carriers including MSNs[115,117,118], gold nanocages[119], nanorods[116,120], polymer nanoparticles[121–124], nanocrystals[125] and black phosphorous nanosheets[126]. For example, local heating from visible light-absorbing magnetite nanoparticles dispersed in poly(N-isopropylacrylamide-co-vinyl-2-pyrrolidinione) hydrogel beads induces a volume change leading to the release of dexamethasone from a transdermal patch[127]. Thermally conductive nanoparticle-based systems are very versatile; however, local heating may damage surrounding tissue and limits the application of these systems to ones in which cell death is desired.

1.3.5 *Photosensitization*

Photosensitizers produce reactive oxygen species for photodynamic therapy[128,129], prodrug activation[130–132], liposome disruption[133] and drug release from endocytic vesicles through photochemical internalization (PCI)[134–136]. PCI-based gene delivery using a dendrimer complex increases transcription relative to basal levels by 100-fold *in vitro* and *in vivo*[137]. Alternatively, an NIR-absorbing phthalocyanine photosensitizer can be used to locally release an anesthetic through lipid peroxidation of a phosphocholine liposome carrier[133]. This technique is limited by an initial burst release, in which the area is immediately anesthetized for 10 h; however, controlled release can be achieved with subsequent exposures. Although photosensitization techniques do not show detectable local temperature changes[138], the produced radical species can induce vascular damage[139]. Applying this effect in a tumor microenvironment to disrupt the endothelium increases the bioavailability of a chemotherapeutic within the tumor. Harsh radical-based chemistries may be appealing to cancer treatment, but side effects and possible tissue damage must be considered for other therapeutic regimes.

1.4 PHOTORESPONSIVE CELL CULTURE PLATFORMS

There is a growing interest in the development of 3D cell culture substrates to investigate fundamental biology, interrogate disease physiology and engineer functional tissue. However, most 3D systems are static with defined physiochemical properties, which cannot capture the dynamics of the ECM. Therefore, tunable 4D biomaterials are being developed that recapitulate the key variable and heterogeneous aspects of native tissues[140]. Hydrogels are crosslinked polymeric networks, which are powerful platforms for 4D cell culture because their chemical and physical properties can be customized to mimic *in vivo* microenvironments. Just as photochemistry has proven beneficial for controlled drug delivery, photoresponsive hydrogels can be used to

recreate the spatiotemporal variations of native tissue, including the dynamic presentation of signaling cues and moduli changes that accompany morphogenesis, disease and healing.

1.4.1 *Biochemical alteration of biomaterials*

The native cellular microenvironment is characterized by the heterogeneous presentation of biochemical cues, that is, small molecules, peptides and proteins, with varying local concentrations. Therefore, efforts have focused on the development of *in vitro* culture platforms that enable spatial and temporal control over biochemical presentation within synthetic materials. One approach is to introduce, remove or reversibly control biochemical functionality using photochemistry.

Photomediated introduction of biochemical functionalities into biomaterials

Photochemical addition reactions are essential for the immobilization of bioactive ligands in hydrogels. The gold standard of hydrogel formation has long been based on the free-radical chain photopolymerization of PEG diacrylate (PEGDA). The hydrophilicity, biocompatibility and bioinertness of PEGDA provide a 'blank slate', in which cells, proteins and small molecules can be encapsulated with high fidelity. Moreover, photopolymerization can be achieved within minutes using cytocompatible photoinititators[141]. Biochemical cues can be introduced to PEGDA by spatially controlled addition (**Figure 1.4a**)[141–143]. Not every acrylate group needs to be consumed for gelation; thus, unreacted moieties remain available for the immobilization of cues. Initially, these free moieties have been labelled with an acrylate-PEG-Arg-Gly-Asp (RGD) polymer-peptide through secondary light exposure at selected volumes within the gel. Local concentrations of the immobilized biomolecule can be tuned through in-solution precursor concentration and irradiation time[145]. Since then, PEGDA hydrogels have been photochemically modified with multiple cues[144]

by both bulk biochemical gradients[146] and tissue-inspired 3D computer-generated patterns to control 3D cellular organization[147].

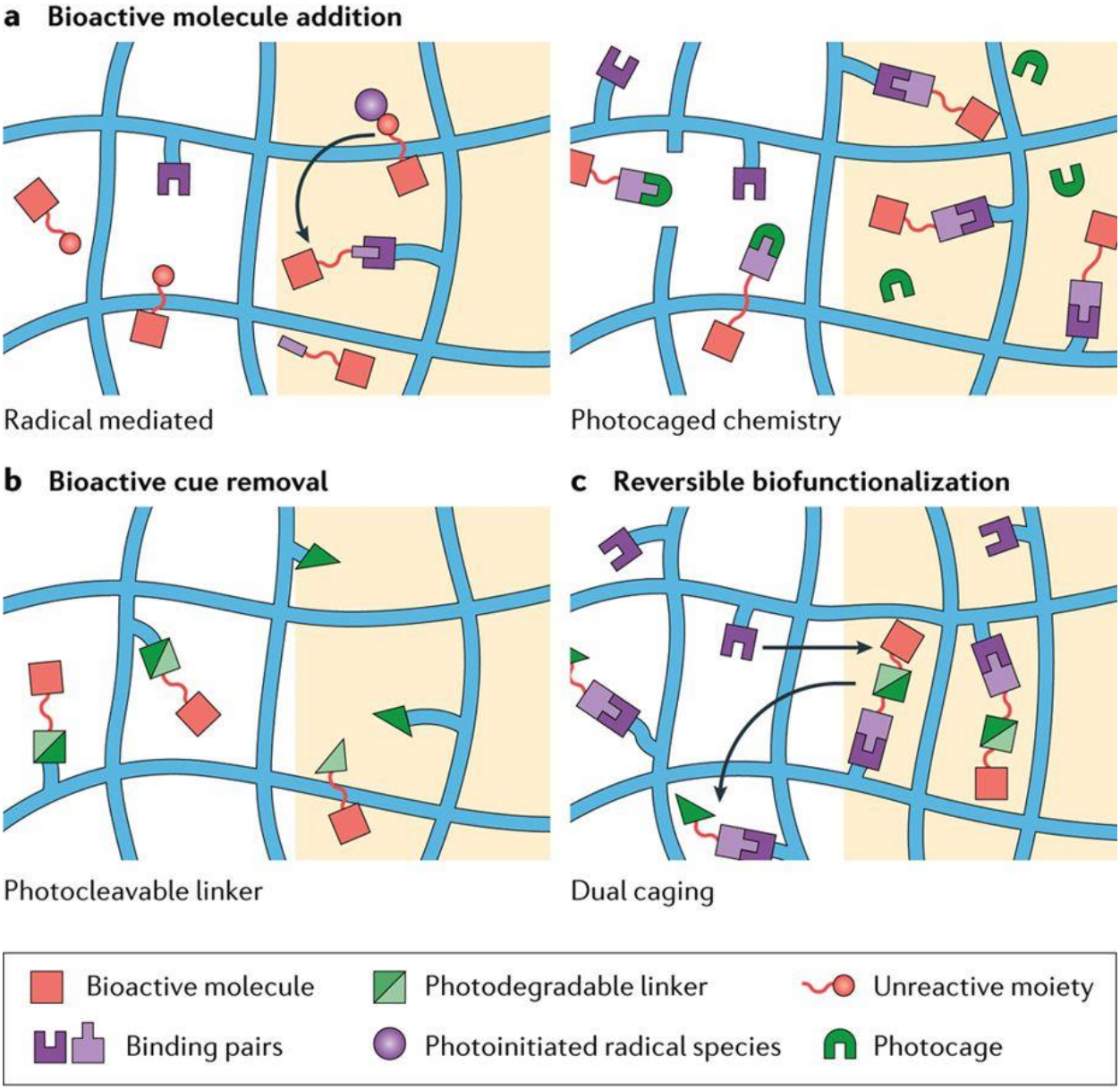

Figure 1.4. Photomediated biochemical alteration of biomaterials. **a**, Hydrogels can be biochemically functionalized through photoinitiated, radical-mediated addition reactions and through the selective de-protection of photocaged reactive groups. **b**, Photocleavable linkers allow for the local removal of functional moieties upon light exposure. **c** Dual caging is a combination of photoaddition and photoremoval techniques to reversibly control the presentation of biochemical cues using sequential, often orthogonal, light exposures.

These techniques have been extensively used to unravel the cellular response to biochemical signals ranging from short adhesion peptides[148] to full-length proteins[149]. For example, photopatterned hydrogels enable the formation of complex, vascularized systems to overcome diffusion limitations associated with large 3D constructs. Endothelial cells seeded on the surface of a PEGDA hydrogel functionalized with strips (≥ 50 μm wide) of the adhesion peptide Arg-Gly-Asp-Ser (RGDS) undergo concentration- and width-dependent angiogenesis[148]. Additional patterning with vascular endothelial growth factor (VEGF) initiates spontaneous formation of endothelial tubules in the gel[149]. The degree of polymerization of PEGDA determines the mechanical properties of the gel; therefore, crosslink formation reduces the finite number of free acrylate groups available for further biochemical functionalization. Additionally, keeping a certain amount of acrylate groups unreacted is difficult to control and characterize. This issue can be addressed by uniformly including photocaged reactive species throughout the material, which can be uncaged for biochemical anchoring. This strategy was first demonstrated in agarose-based gels modified with photocaged thiols[150–153]. Applying UV light to selected volumes of the gel triggers the uncaging of thiols that are subsequently available for Michael-type addition reactions with maleimide-functionalized biomolecules. This method allows for the selective modification of the gel in UV-exposed regions. In contrast to acrylate-based patterning, the mechanical properties of the gel remain the same, because the immobilization of biomolecules is not related to the crosslinking of the gel. This technique has been used to promote dorsal root ganglia cell invasion into RGDS-patterned gels in a concentration-dependent manner[150,154]. The photomediated Michael addition can be extended to the sequential patterning of one protein of a binding pair into a gel, for example, biotin-streptavidin[152], barnase-barstar[152] or human serum albumin-albumin binding domain[153]. Thereby, the gel can be functionalized with a protein of choice by fusing it to the

respective binding partner. Although innovative, the limited cytocompatibility of the maleimide-thiol reaction resulting from cross-reaction with native thiols as well as slow reaction rates limit applications in the presence of cells.

'Click chemistry' has also been explored as a bioconjugation strategy for the development of well-defined hydrogels, which can be biochemically functionalized. Click reactions, such as the thiol-ene addition or copper-catalyzed azide-alkyne cycloaddition (CuAAC), enable a one-to-one addition with high reaction yields and specificity[155,156]. The thiol-ene reaction can be photochemically initiated with an appropriate cytocompatible photoinitiatior (for example, lithium phenyl-2,4,6-trimethlbenzoylphosphinate[141], Irgacure 2959[157] or Eosin Y[158]), resulting in a radical-mediated step-growth reaction between a free thiol and an alkene[159]. Unlike chain reactions, step-growth polymerizations generally evolve into homogenous networks, forming a uniform material for post-gelation photopatterning. The first photoinitiated thiol-ene based biochemical patterning was demonstrated by conjugating cysteine-containing peptides into CuAAC-based PEG networks without modification of the gel mechanics[155]. To circumvent the use of cytotoxic CuAAC, a bioorthogonal, cytocompatible polymerization, strain-promoted azide-alkyne cycloaddition (SPAAC), can be used, which is compatible with thiol-ene based photopatterning[160]. The degree of photopatterning can be precisely controlled by light dosage. Furthermore, this reaction can be iteratively performed to create complex biochemical gradients and to functionalize a single hydrogel with multiple bioactive peptides[160,161]. Such materials can be used to control 3D cell spreading in gels patterned with islands of RGDS, representing true photo-directed control over 3D cell migration.

Further improvements to thiol-ene-based modification include patterning with allyloxycarbonyl (alloc)-functionalized peptides of gels formed between thiol-functionalized

multi-arm PEGs and di-alloc end-functionalized peptide crosslinks[162]. Moreover, strained norbornene functionalities show improved reactivity for the immobilization of cues in PEG hydrogels[163,164]. Likewise, gel stiffness can be increased through further thiol-norbornene-based crosslinking of electrospun coil-like nanofibrous hyaluronic acid (HA) gels, which closely mimic natural ECM[165,166]. Cell protrusions and alignment can be directed by patterns of RGD on the surface of the hydrophilic networks[166].

Ideally, photochemistries retain reactivity in complex medium and in the presence of live cells. Photo-modulated enzymatic reactions fulfil these requirements owing to their high selectivity towards target sequences, fast reaction rates and inherent biocompatibility; for example, Factor XIIIa (FXIIIa)-catalyzes an addition reaction between a free amine and a carboxamide residue of glutamine[167,168]. 6-nitroveratryloxycarbonyl (NVOC)-photocaged lysine-containing peptides can be covalently incorporated in a PEG-based hydrogel, and after photocleavage with laser light (405 nm), a glutamine-labelled biomolecule and the FXIIIa enzyme are swollen into the network, resulting in a stable amide linkage between the two species[167]. Such a patterning strategy can be used to direct cell invasion from human mesenchymal stem cell (hMSC) microclusters into a gel modified with RGD, recombinant fibronectin fragments ($FN_{9\text{-}10}$) or platelet-derived growth factor B (PDGF). Similarly, photoinitated, FXIIIa-catalyzed immobilization can be applied to an HA-based hydrogel containing *ortho*-nitrobenzyl photocaged lysine-containing peptides for the *in situ* control of cell spreading and proliferation[168]. Enzyme-based patterning schemes will prove useful for the conjugation of small molecules, peptides and full-length proteins into 3D tissue constructs.

Light can also be explored for the spatial control of bioactivities through the photoactivation of biologics, which are uniformly present throughout a material. RGD, photocaged

at its critical aspartic acid residue, can be activated to selectively promote cell attachment, spreading and migration[169–171]. For example, transdermal irradiation of a photoactivatable 3-(4,5-dimethoxy-2-nitrophenyl)-2-butyl ester-caged RGD moiety has been applied to regulate cell adhesion and to reduce fibrous capsule formation associated with the foreign body response following subcutaneous implantation of PEG hydrogels in mice[172], marking the first demonstration of how photopatterning can be used for the biochemical alteration of a hydrogel material *in vivo*. Photouncaging of synthetic peptides has also been shown to promote enhanced cell attachment and proliferation; however, using this strategy for the activation of bioactive proteins that regulate more complex cellular functions has yet to be demonstrated.

Photomediated removal of biochemical functionalities from biomaterials

3D cell culture systems can be made photoresponsive to specifically remove biochemical cues, addressing the biological importance of ligand dynamics in cellular plasticity. Such systems are used to activate or deactivate signaling pathways, to deliver soluble species to encapsulated cells or to create biochemically patterned substrates. For example, chondrogenic differentiation of MSCs is accompanied by fluctuating fibronectin production that influences differentiation signaling pathways. Fibronectin-derived RGDS peptides, which are covalently linked to PEGDA hydrogels through a nitrobenzyl-based photolabile linker, can be stochastically incorporated into the gel during polymerization[173], representing a simple and robust methodology to photorelease bioactive species from mechanically stable materials. Encapsulated MSCs interact with the bioactive peptide and remain in an undifferentiated state in the gel. After UV-initiated photocleavage, the cells exhibit increased signs of chondrogenesis owing to the removal of RGDS peptides from the microenvironment (**Figure 1.4b**).

An individual compound can significantly influence cell function, but controlling several chemical signals within the same system better mimics in vivo signaling. Wavelength-selective release of multiple signals was first demonstrated through the selective and simultaneous or independent release of three model therapeutics from a hydrogel to create multistage release profiles[29]. Two nitrobenzyl-based crosslinkers can be used for wavelength-specific, but not fully orthogonal, cell release from materials[174]. Coupling a coumarin-based photodegradable linker (405 nm) with a classic nitrobenzyl compound (365 nm) allows staggered release of bone morphogenic protein (BMP)-2 and -7 from a PEG-based hydrogel to investigate hMSC osteogenesis[175]. Using this approach, relative rates of protein photorelease can be preferentially influenced by wavelength; however, full orthogonality has not been achieved. Strategies that offer true wavelength-dependent control of biomaterial properties remain elusive.

Reversible control of hydrogel functionality

Advanced biomaterial platforms afford the reversible control of biofunctionalities (**Figure 1.4c**). The first reversible biochemical patterning of PEG-based hydrogels exploited a visible light-initiated thiol-ene reaction to immobilize thiol-functionalized peptides. UV exposure then triggers cleavage of the nitrobenzyl linkage resulting in the release of the peptides[176]. Although reversible immobilization has been demonstrated using both photolithographic and multiphoton laser scanning lithography, the approach does not provide repeatable reversibility, because reactive alkenes are continuously consumed throughout each immobilization event. Fully dynamic functionalization can be achieved by applying a reversible addition-fragmentation-chain transfer (RAFT) reaction for the iteratively repeatable immobilization of thiol-containing peptides. Using this technique, a PEG-based hydrogel can be functionalized with complex, dynamic patterns of multiple fluorescent molecules[177]. However, this approach relies on free-radical chemistry, which

hinders its application for complex, sensitive molecules, such as proteins. Alternatively, a bioorthogonal photomediated oxime ligation can be used for the immobilization and subsequent removal of full-length proteins through nitrobenzyl photocleavage[178,179]. For example, patterned tethering and release of vitronectin allows for the reversible and spatially controlled osteogenesis of hMSCs[178]. This method requires repeated patterning cycles, which are limited by the finite number of available reactive groups. Thus, strategies for the fully reversible immobilization of biomolecules remain of prime interest towards recapitulating the complexity of the cellular microenvironment.

1.4.2 *Biophysical alteration of biomaterials*

Tissue biomechanics are crucial for tissue function, and physical forces establish an intimate relationship between cells and their microenvironment. Focal adhesions are protein complexes that connect the cell cytoskeleton to the proteins of the ECM, thereby translating biophysical signals. The stiffness and elasticity of the ECM influence cell adhesion, spreading and morphogenesis and thus, cell fate[180,181]. The mechanical properties of the cell microenvironment undergo drastic changes throughout tissue homeostasis, development, disease progression and healing[182], reflected in the dynamic interactions between cells and their ECM. 4D control of phototunable materials offers a way to recapitulate the biophysical dynamics that occur *in vivo*. The fast kinetics of photochemistry and the high resolution of exposure techniques allow for the spatial and temporal control of hydrogel elasticity and degradation.

Photomediated increase in biomaterial stiffness

In a covalently crosslinked network, the elastic modulus (G') or stiffness is dictated by the crosslink density and thus, can be increased with spatiotemporal control through the formation of secondary crosslinks post-gelation (**Figure 1.5**). For example, PEGDA gels can be formed without

the consumption of all acrylates; chain-growth extension of the remaining reactive groups through patterned secondary photopolymerization of additional PEGDA results in localized increases in elastic moduli from 3 to 7 kPa[142]. This approach allows for the examination of stiffness-dependent biological processes within one material. Macrophages seeded on mechanically graded hydrogels (G'~ 5-100 kPa) preferentially migrate towards stiffer substrate regions[183] – a process known as durotaxis. Hepatic stellate cells cultured on the surface of a photopatterned HA-based hydrogel differentiate into myofibroblasts in stiffer areas of the gel, mimicking a key event in liver fibrosis, which is characterized by matrix stiffening[184]. The formation of myofibroblasts is dependent on the size of the stiff region, and re-seeding of the cells onto a 3D substrate of original stiffness initiates a reversion to quiescence. Such photomediated gel stiffening strategies are not limited to synthetic systems; crosslinking of artificial proteins containing a photosensitive, non-canonical amino acid, *p*-azidophenylalanine, which undergoes non-specific photoaddition upon exposure to UV light, leads to selective stiffening of elastin-based hydrogels[185]. Crosslink formation occurs in a dose-dependent manner such that patterning can be finely tuned across a high range of moduli (~ 0.3-1.0 MPa) through variation of exposure duration.

Photostiffening also proves valuable for examining cell-ECM interactions in nonpolarizing, native-like 3D environments. Methacrylated-hyaluronic acid (MeHA) gels can be formed through Michael addition with bis(cysteine)-containing, enzymatically degradable peptide crosslinkers. Some acrylates can be left unreacted for the spatiotemporally controlled photo-addition of non-degradable crosslinks[186,187]. These non-degradable bonds prevent cellular matrix remodeling, thus, restricting cell shape changes and differentiation. Human MSCs forced into a spherical morphology undergo adipogenesis, whereas cells permitted to spread preferentially

differentiate into osteoblasts. Cell traction forces, which are established through cell-mediated matrix remodeling, are responsible for directed hMSC differentiation[188].

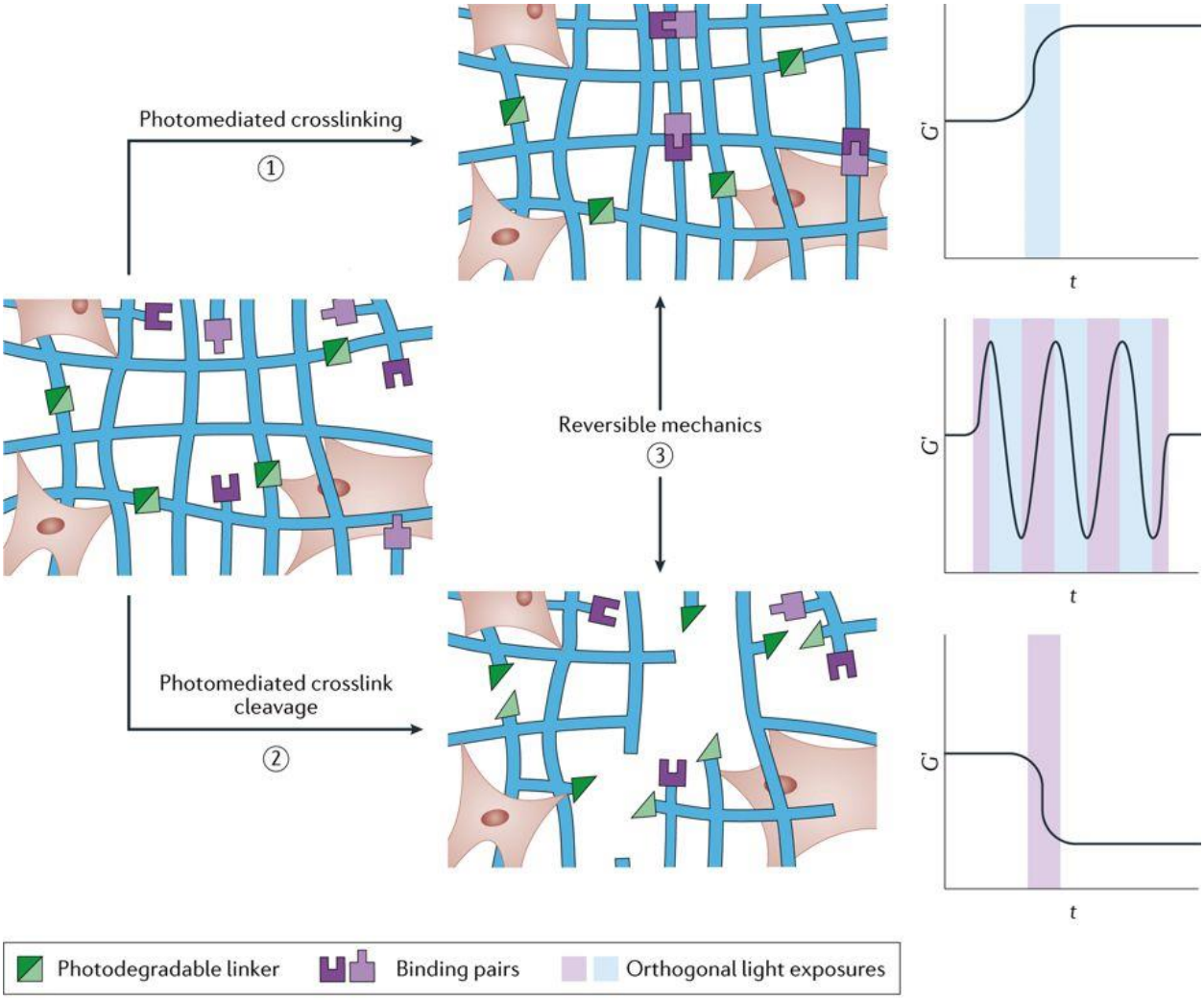

Figure 1.5. Photomediated biophysical alteration of biomaterials. The biophysical properties of a hydrogel can be controlled through photomediated crosslinking and cleavage of photodegradable linkers. Photomediated crosslinking can be exploited to increase the elastic modulus (G') of a hydrogel at specific times, through the formation of additional crosslinks. Softening of a hydrogel can be achieved through the selective degradation of photolabile crosslinks within the gel network. Combining both strategies allows for reversible and spatiotemporal control over hydrogel mechanics, mimicking extracellular matrix dynamics *in vivo*.

In addition to photo-addition reactions, photo-liberation of reactive functionalities can be used to form new crosslinks post-gelation[189,190]. Using photocaged thiols, the crosslinking density of PEG-based biomaterials can be increased through a photo-driven Michael addition[190]. The

exposure-dependent nature of the chemistry enables the formation of substrates with different stiffness gradients (3-8 kPa). Human MSCs seeded on top of materials with a G' ≥ 5.5 kPa exhibit durotaxis, suggesting a mechanical threshold to induce a cellular response. A photomediated oxime ligation has also been exploited for gel stiffening, enabling localized material alterations in a fully bioorthogonal manner[179]. Alternatively, the ionic crosslinking of alginate gels can be controlled through the phototriggered release of a divalent cation, such as calcium[191,192], or a calcium chelator[192] to stiffen or soften the gels, respectively.

Photomediated decrease in biomaterial stiffness

Light can be applied to reduce the crosslink density in a hydrogel, softening the material in a time-independent, controlled manner. High-intensity focused laser light can photoablate transparent materials to create channels and voids[193,194]. Cells can sense these topographical features as demonstrated by axonal regeneration and neurite outgrowth from dorsal root ganglia into photoablated microchannels[195]. However, material photoablation applies indiscriminate bond photolysis and therefore, leaves behind unpredictable degradation products. Photocleavable linkers, which dissociate in a predictable manner, offer a low-intensity and cytocompatible alternative to photoablation (**Figure 1.5**)[172,195–200]. PEGDA-based hydrogel networks containing nitrobenzyl groups formed through redox-initiated radical chain polymerization degrade upon UV light exposure[173]. These materials have been extensively used to examine how bulk changes of material properties can influence cell migration[173], how microtopographies impact cell morphology and alignment[202], how elastic gradients influence cell function[203], and how erosion of adhesive ligands induce subcellular detachment[204]. For example, linear gradients of G' (7-32 kPa) can be created through graded photodegradation of PEGDA hydrogels, to probe the influence of biomechanics on cell phenotype[205] and to control the de-differentiation of myofibroblasts into

quiescent fibroblasts[206]. The reversion into fibroblasts occurs within 6 hours of gel softening, mimicking the tissue healing process. Such photodegradable hydrogels have also been used to investigate whether cells possess a mechanical memory of substrate conditions. By modifying the elastic properties of the substrate, it has been demonstrated that the influence of the mechanical characteristics on cell fate is dynamic and reversible[207].

Bioorthogonal, step-growth polymerization chemistries offer a homogenous backbone with improved mechanical integrity and rapid erosion compared to chain-growth polymerized gels[208]. Independent control over biochemical and biophysical properties has been achieved using photodegradable SPAAC-based networks through the inclusion of a vinyl moiety for thiol-ene photoconjugation, which is initiated by visible light[158]. In this system, physical channels can be eroded and decorated with RGD to direct fibroblast motility in 3D. Similarly, channels can be created through photodegradation of nitrobenzyl-containing SPAAC networks to encourage encapsulated motor neurons derived from embryonic stem cells to form neuronal axons[209]. Fully eroded channels offer the opportunity to engineer complex cellular networks and to mimic complex biological features, for example the vasculature[210] and multicellular aggregation[211–213], by directing cell migration.

Alternatively to nitrobenzyl cleavage, disulfide-crosslinked networks can be degraded through a radical-mediated disulfide fragmentation reaction[214]. In the presence of a photoinitiator, light exposure generates chemical radicals that propagate and cause multiple crosslink degradation events within seconds. This classic degradation chemistry can be applied for the rapid release of encapsulated cells from biomaterials, which is used for harvesting specific cell populations from heterogeneous cultures *ex vivo* for a downstream analysis of single cell types[158,215,216].

Redshifted chemistries can have a unique absorption spectrum and therefore, enable the precise control of multiple functionalities at the same location in a single system. For example, a thiol-ene hydrogel polymerized with visible light undergoes UV-mediated photodegradation through a nitrophenylalanine photoscission reaction, which facilitates dual-wavelength control over network mechanics[217]. Photochemistries that extend material degradation further into the visible range are also being developed; for example, coumarin-based photodegradable units can be included, which are cleaved under visible light exposure (405 nm)[218,219].

Reversible control over physical properties

The functional control of most of the techniques discussed above is unidirectional. However, to capture the dynamic nature of cell-ECM interactions, materials with photoreversible stiffness are being engineered (**Figure 1.5**). PEG macromers can be decorated with moieties that reversibly dimerize to sequentially stiffen or soften materials. For example, cinnamylidene acetyl moieties dimerize when exposed to UV light (> 300 nm)[220–222], which can be reversed to a certain degree upon exposure to higher-energy UV light (254 nm). However, this strategy suffers from photocleavage inefficiencies, undesired side reactions, poor molecular stability and requires extended periods (0.5-1 h) of cytotoxic UV light to modulate the material[222]. Substituting a nitrocinnamate for cinnamylidene acetyl moieties increases photo-reactivity and storage stability[223]. Photodimerization of anthracene[224,225] and coumarin[226,227] have also been explored for the reversible alteration of network mechanics, although undesired photocleavage reactions limit their cyclability. Despite their ability to offer nearly reversible mechanical modulation, these systems have only found limited application in tissue engineering owing to the long exposures to cytotoxic light (< 300 nm).

By contrast, azobenzene undergoes efficient photoisomerization under cytocompatible exposure conditions and can be used to disrupt host-guest interactions in a reversible, wavelength-specific manner[228]. An azobenzene moiety can act as a junction between a cyclodextrin-polymer complex, thus, exhibiting cyclic gel-to-sol transitions. Azobenzene can also be incorporated within PEG gel backbones, resulting in the reversible modulation of the mechanical properties of the gel following exposure with UV (365 nm) or visible (400-500 nm) light[229]. Hydrogel stiffness decreases ~ 200 Pa upon photoisomerization of *trans*- to *cis*-azobenzene, attributed to hydrogen bond disruption. Reversion to a stiffer substrate is induced through exposure to visible light or thermal relaxation ($t_{1/2}$ ~ 9 h at 37 °C). Primary porcine aortic valvular interstitial cells can be encapsulated in such a material prior to either light treatments, demonstrating cytocompatibility. The development of effective strategies to reversibly and repetitively modulate changes in gel mechanics in the presence of live cells remains an ongoing effort in the field.

1.4.3 *Independent physiochemical tunability*

Biochemical and biophysical matrix cues usually act cooperatively to influence cell function. Therefore, design principles need to be developed to simultaneously and precisely control both aspects within synthetic cell culture systems (**Figure 1.6**). So far, only few strategies have enabled the recapitulation of the physiochemical heterogeneity of native ECM. The combination of different wavelength-orthogonal photochemistries allows for the independent control of material stiffness and biochemical cues[158]. Distinct wavelengths of light can be used to dictate local substrate mechanics and the presentation of fibronectin to regulate cell function in a MeHA hydrogel[230]. Stiffness gradients can be created by a two-step Michael addition and a visible light-based crosslinking procedure, and biochemical patterning of a gel can be accomplished through nitrobenzyl-photocage removal, liberating a thiol for a maleimide-based reaction with

biomolecules. Dual patterning constitutes a high-throughput technique to probe cell-ECM interactions; however, the cytotoxicity of thiol-maleimide chemistry prevents the translation to 3D cell studies. Whereas each of these strategies represents an important step towards the independent control of physicochemical properties, capturing the entire physiochemical aspects of native ECM remains elusive as of yet.

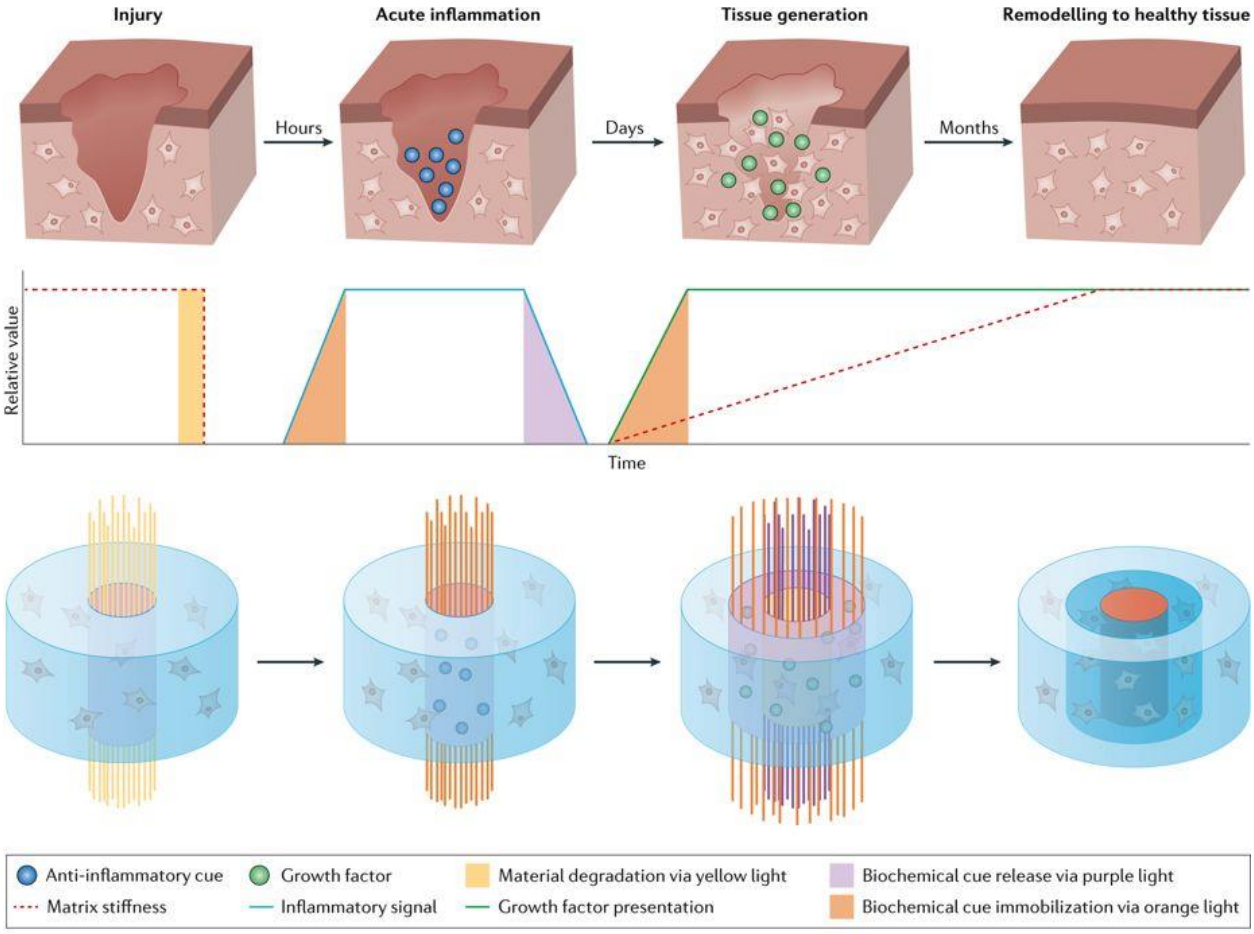

Figure 1.6. Independent physiochemical tuning of biomaterials to mimic *in vivo* processes. Dynamic biological processes, such as wound healing, can be recapitulated using appropriately designed photochemistries, which allow for the complete orthogonal control over the physiochemical properties of a cell culture substrate *in vitro*. The treatment of the three physiochemically and temporally distinct stages of a tissue repair process can be modelled through the reversible local presentation of inflammatory signals, growth factors, and through variations of matrix stiffness. After injury resulting in the complete elimination of local cells and their extracellular matrix, damaged tissue activates an acute inflammatory response marked by the infiltration of key inflammatory cues from the blood plasma. Following, cells proliferate at an increased rate for tissue generation promoted through the differential presentation of growth

factors. Finally, the extracellular matrix is remodeled to restore tissue mechanics. Sequential exposure to different wavelengths of light triggers specific and orthogonal modifications of the material: yellow – mechanical degradation, orange – biochemical cue immobilization, purple – biochemical cue release. Thereby, an engineered tissue can be guided by light through the different stages of wound healing *in vitro*.

1.5 LOOKING FORWARD

Photochemistry can be near-instantaneously controlled in 4D, providing a powerful tool for targeted drug delivery and advanced cell culture. Many photoresponsive biomaterial systems have already been designed that provide high precision for probing and directing living processes, and the field continues to explore photochemistry for a variety of applications, especially for the dynamic photomodulation of material properties *in vivo*[172,231,232]. Future prospects exist in optically activating reactions at deeper locations within living human tissue; currently, the limited tissue penetration of commonly utilized light sources restricts the application of photoresponsive biomaterials to transdermal patches, the eye, or sites just a few millimeters below the surface of the skin. While substantial effort has been dedicated to redshifting reactive moieties, chemistries that are hyperactive within the NIR optical window of biological tissue (λ = 600 – 1200 nm) are needed. A critical design constraint is to create reactive components that are responsive to the low energy supplied by high-wavelength light. Additionally, the species must remain stable and photochemically inert in dark and physiological conditions. Reactants with enhanced quantum yields and tunable absorbance properties will enable biocompatible photochemistries, which can be performed fast and in deep tissue.

Another area of active development addresses the request to independently conduct several different photoreactions within the same material system. Fluorescent microscopes now permit simultaneous visualization of ≥ 4 fluorophores within one sample, and even more when spectral deconvolution is employed; however, independent photomodulation of even two biomaterial

properties remains challenging. Continued effort must be made towards generating libraries of photoactive species for reactions that can be initiated in a wavelength-orthogonal manner. Components must not only have well-separated maximum absorbances, but also narrow absorption peak widths, to ensure minimal spectral overlap and independent activation[233]. This will enable the design of combinatorial drug delivery systems that release therapeutics in a medically relevant manner and to determine the biological importance of distinct physiochemical cues that are independently regulated within a common material.

The majority of photoresponsive biomaterials engineered to date rely on reactions that proceed only in one direction. The establishment of photoreactions that can be reversibly triggered using cytocompatible wavelengths remains of prime importance to control therapeutic activities within the body and to dynamically manipulate the physiochemical properties of synthetic cell culture platforms. Incorporation of allyl sulfides, originally developed as agents for addition-fragment chain polymerization, into materials has shown promise in creating reversible constructs[177,234], as has azobenzene-mediated host-guest chemistry[235,236]. Borrowing from biology, reaction schemes using photoresponsive proteins, which can undergo reversible dimerization or conformational changes, may greatly improve the dynamic control over local material properties.

Many photoreactions commonly employed for biomaterial alteration, for example, thiol-ene or methacrylate/acrylate-based chain polymerization, are driven by free radicals, which can elicit damaging and non-specific reactions with cells and tissues. Other reactions, such as photocaged Michael additions, rely on moieties that exhibit undesired cross-reactions with functional groups found in biomacromolecules, including DNA or proteins. Many reactions proceed exothermally or operate through a photothermal effect, generating heat, which can damage the surrounding tissue. Reaction bioorthogonality has to be considered to ensure that phototools

can be safely and effectively performed within living systems. The development of novel bioorthogonal chemistries extends well past the field of photochemistry, and therefore, the establishment of general strategies to photoregulate reactions will prove invaluable.

Technological advances are also needed to direct light exposure onto and within materials. Multiphoton lithography enables material control in 3D, but the high equipment costs and slow processing speeds limit its application and scale-up. This issue can be addressed by the use of low-cost light sources with narrow emission spectra of tunable wavelengths over a broad range of power. Next-generation optical fibers and endoscopic techniques may further extend the reach of photomodulation techniques to light-impenetrable regions of the body. Collaborations with physicists and machinists specializing in optics will be crucial in achieving these goals.

Emerging optogenetic tools, combining aspects of both genetics and optics, facilitate the precise control over intracellular processes. In addition to governing specific signaling events using light, strategies involving photoactivated Cre recombinase[237,238] (Cre-Lox recombination) and Clustered Regularly Interspaced Short Palindromic Repeats (CRISPR)/CRISPR-associated protein-9 nuclease (Cas9)[239,240] are providing opportunities to optically guide targeted genome editing. Through the combination of optogenetics and photoresponsive biomaterial platforms, independent manipulation of signaling events both within and around cells could be achievable. Such hybrid systems would provide complete control towards probing and directing 4D cell fate.

Photochemistry will continue to enrich the development of next generation biomaterials to meet clinical needs and further our understanding of dynamic biological processes. Clearly, the future for photoresponsive biomaterials remains bright.

1.6 BIOCHEMISTRY FOR BIOMATERIAL ALTERATION

Protein-based chemistries can be applied to manipulate crosslinking and biochemical cue presentation with biomaterials. These chemistries uniquely offer specificity, scalability, mild reaction conditions compatible with sensitive biomolecules (i.e., radical-free, low temperature, buffered aqueous environments) and typically can be performed without multistep procedures or specialized equipment. Selecting the ideal bioreaction for a given application requires consideration of substrate specificity, location of the modification/reaction, stability of the final product, and rate of reaction[241]. Many different protein-based chemistries are commonly used to form, modify, decorate, and degrade cell-laden hydrogels by exploiting protein-mediated binding events and stimuli-triggered refolding/cleavage events.

1.6.1 *Protein-mediated binding events*

Protein-mediated binding events can be used to functionalize and crosslink biomolecules within hydrogels. Transient functionalization of biomaterials with bioactive proteins can be achieved by exploiting natural protein-(bio)molecule affinities like heparin-containing materials which sequester heparin-binding proteins (e.g., basic fibroblast growth factor, beta-nerve growth factor, vascular endothelial growth factor, bone morphogenetic protein)[242–246] or similar binding pairs such as Src homology 3 (SH-3)-SH-3 fusion proteins[247], biotin-streptavidin[152], and albumin-albumin binding domain[153] (**Figure 1.7a**). While non-covalent protein-protein binding of native species can be exploited to immobilize proteins within materials previously functionalized with its binding partner, systems are limited to known protein-protein interactions and are limited by leaky release governed by the affinity of the non-covalent interaction. Though such leakiness is often a limitation, these systems can provide well-defined protein release profiles useful for *in vivo* therapeutic delivery[247].

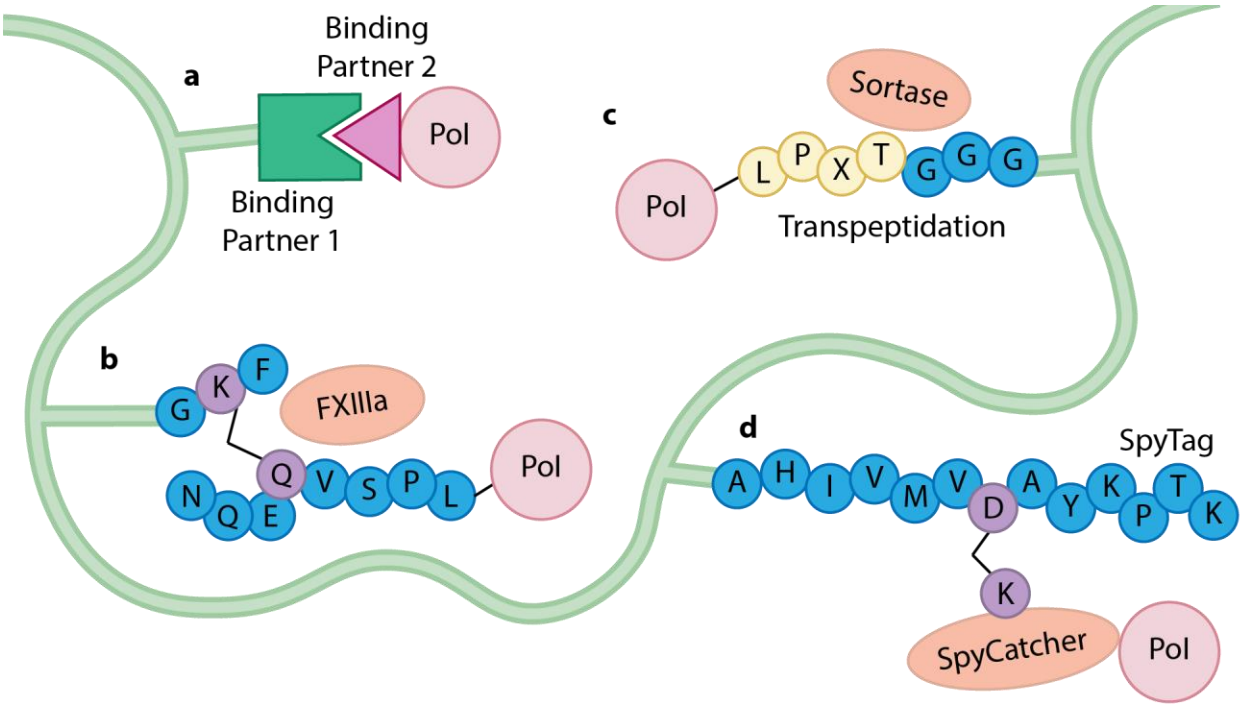

Figure 1.7. Protein-mediated binding events are commonly used to link bioactive proteins of interest (PoIs) to biomaterials. **a**, Non-covalent associations between two binding partners enable reversible PoI conjugation with varying kinetics depending on the binding pairs used. **b**, Stable transamidation between lysine and the second glutamine residue of NQEQVSPL- are catalyzed by transglutaminase FXIIIa. However, increased substrate specificity is achievable with **c**, Sortase-based transpeptidation which occurs between a C-terminal LPXTG motif and an N-terminal polyglycine substrate. **d**, The spontaneous protein-peptide amidation of SpyCatcher and SpyTag offers favorable kinetics, high specificity and versatility in peptide tag location.

For improved stability, techniques generating new covalent bonds are common in forming new crosslinks and immobilizing biomolecules to gain control of the mechanical and biochemical space. Transglutaminases, a class of enzymes that ligate a free amine to the carboxamide residue of glutamine, were an early choice in making and modifying hydrogels because the newly formed bond is highly stable[248]. In an early example, tissue transglutaminase (tTG) formed network crosslinks between glutaminamide-modified PEG macromers and poly(lysine-phenylalanine) peptides to generate a hydrogel. Since then, tTG has been used to form hydrogels[249] and subsequently immobilize heterogeneous populations of proteins within biomaterials[250]. However, since reaction occurs spontaneously with side-chain amines of native lysines, controlling these

reactions in protein-containing media with high specificity is not possible. Thrombin activating factor XIIIa (FXIIIa), the key enzyme in crosslinking fibrin clots, exhibits increased specificity for terminal substrates (**Figure 1.7b**). As such, FXIIIa conjugated the bioactive peptides RGD and DGEA into fibrin matrices during polymerization. The presence of these peptides improved neurite outgrowth from an encapsulated dorsal root ganglion[251]. FXIIIa has since been applied to crosslink networks by including reactive substrates on the backbone components of PEG gels[252], microgel particles[253], and hyaluronan gels[254,255], and has been spatially controlled by photocaging the reactive lysine residues[167,168]. Although increased specificity has been demonstrated by engineering glutamyl- or amine- donor peptides, it remains challenging to control the reaction when plasma proteins and other natural substrates are present.

With increased specificity over transglutaminases, the bacterial membrane transpeptidase Sortase A (SrtA) has found numerous applications in forming and breaking bonds between biomolecules[256]. SrtA catalyzes a condensation reaction between its substrate -LPXTG and an N-terminal poly(glycine) species by cleaving between the threonine and glycine residues of the substrate to form a substrate-enzyme intermediate. This intermediate then undergoes a nucleophilic attack by an N-terminal GGG- species (GGG-Y) forming the ligated product -LPXT-GGG-Y (**Figure 1.7c**) [257]. In the first demonstration of biomolecule coupling to a synthetic material via SrtA, eGFP-LPETG was purified from cell lysate using SrtA and GGG-modified beads[258]. Building from this work, SrtA can be used to stiffen[259,260], degrade[260–262], and biochemically modify hydrogels[263,264] by exploiting the ligation or reverse hydrolysis reactions. Additionally, SrtA remains active when expressed as a fusion with its substrate which can be exploited to install GGG peptides functionalized with a reactive moiety of choice for biomaterial conjugation at the C-terminus of a recombinantly expressed protein of interest (PoI) during

purification[265–268]. The versatility of this ligation technique is growing as mutants characterized by faster kinetics and orthogonal substrates are engineered[269]. These engineered SrtAs can be paired for unique dual-enzymatic approaches to orthogonally modify the biochemical and biophysical properties of biomaterials[262]. Since genetic installation of both the short recognition sequence or a poly(glycine) moiety is straightforward and the reaction exhibits minimal cross-reaction in complex biological samples, SrtA-based biomaterial systems will continue to rise.

Another useful protein ligation chemistry originates from the membrane surface fibronectin binding domain FbaB from *Streptococcus pyogenes*. The CnaB2 domain of FbaB is stabilized by a spontaneously formed covalent bond between the side chains of Lys31 and Asp117. This isopeptide bond is an extremely stable linkage formed within minutes in complex biological mixtures or buffers even after the CnaB2 domain is split into a 138-residue protein containing Lys31 (SpyCatcher) and a 13-residue peptide containing Asp117 (SpyTag)[270] (**Figure 1.7d**). Owing to the ease of genetically encoding the protein/peptide pair, favorable reaction conditions, and high selectivity, the SpyCatcher/SpyTag system has helped create modular techniques to form and functionalize hydrogels[271]. By combining fusions of three SpyTag sequences separated by elastin-like proteins (ELPs) with a construct containing two SpyCatchers fused through an RGD-containing ELP domain, a soft protein-based hydrogel (i.e., "Network of Spies") can be formed upon spontaneous crosslinking between SpyCatcher and SpyTag. These gels can be functionalized with biologically active peptides such as RGD or full-length proteins by simply encoding the sequence between ELPs within the backbone[272]. The genetic encodability can be further exploited to tether full-length proteins into both protein-based[273–275] and synthetic[276] hydrogels. To ensure unreacted SpyTag tether-points exist after gelation, a backbone SpyTag of a Network of Spies can be sterically blocked with a redox-responsive immunoglobulin G domain such that a disulfide

bridge is cleaved under reducing conditions, exposing the unreacted SpyTag for reaction with SpyCatcher-PoI fusions[275]. Alternatively, the orthogonal reactive pair SnoopCatcher/SnoopTag which undergo a spontaneous transamidation between an asparagine and lysine[277], can be combined with a Network of Spies to decouple biochemical functionalization and gel crosslinking[278]. Although these binding pairs offer versatility without additional synthetic reactions to functionalize sensitive proteins, *in vivo* applications remain limited to modular vaccines[279,280] or other systems in which an immune response is desired because of their bacterial origin. Nature has evolved many naturally occurring ligation reactions that have yet to be utilized[281,282], let alone even discovered. The future in using protein-based reactions to perform a desired chemical reaction is promising.

1.6.2 *Stimuli-responsive proteins for biomaterial modification*

Varying levels of spatiotemporal control of the mechanical and biochemical landscape of biomaterials can be achieved by using proteins responsive to a stimulus (e.g., small molecules, sonication, light). Some proteins require a small molecule or cofactor catalyst that initiates a desired function, thus controlling when to present the cue selects when a protein will become active (**Figure 1.8a**). For example, rapamycin addition induces rapid dimerization of FK506-binding protein (FKBP) and the FKBP-rapamycin binding domain (FRB). By expressing individual pentamers of FKBP or FRB each separated by a small linker, hydrogel-like synthetic RNA stress granules can be formed intracellularly upon addition of rapamycin[283]. Similarly, the varied binding affinities between Gyrase B and two different small-molecule antibiotics (i.e., coumermycin, novobiocin) has been used to create a molecular switch for material degradation, where Gyrase B's dimerization with coumermycin can be competitively displaced with novobiocin. The release of a cargo such as a vaccine can be pharmacologically triggered *in vivo* upon oral ingestion of

novobiocin[284]. Towards overcoming the exogenous addition of a chemical cue, the initiator can be encapsulated in a liposome and then liberated through user-directed ultrasound to trigger transglutaminase-mediated crosslinking of fibrinogen gels[285]. This technique could be further expanded to other calcium-dependent enzymes (e.g., SrtA) for gel degradation or modification. However, there is lack of spatial control often sought out when recreating cellular microenvironments.

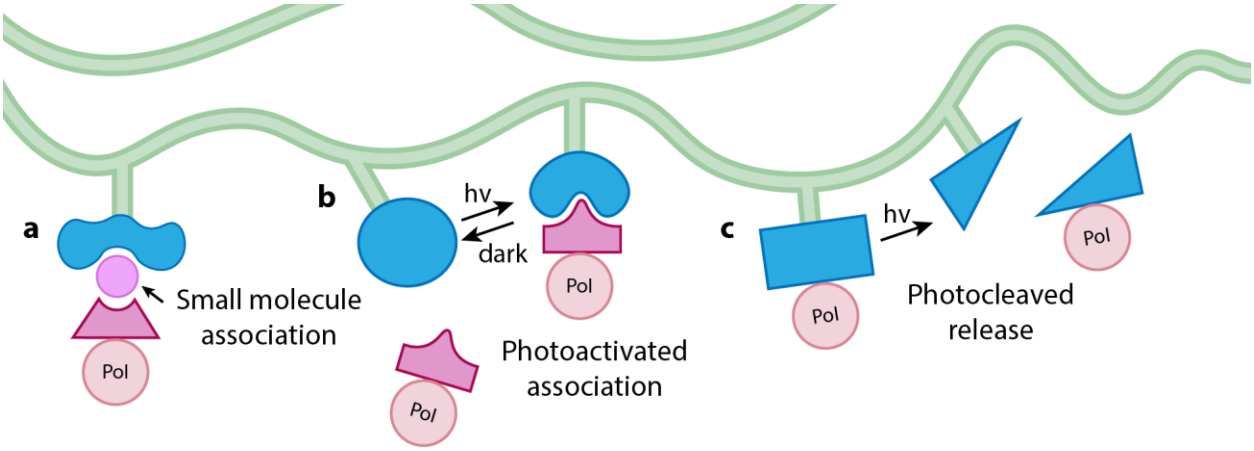

Figure 1.8. Stimuli-responsive proteins are used to control the binding and release of proteins of interest (PoIs) from biomaterials. **a**, Small molecules offer temporal control of protein-protein interactions with varying affinities. **b**, Photoactivated interactions exhibit reversible control of PoI tethering and release, though associations demonstrate uncontrolled reversion characteristic of the chosen photoresponsive protein. **c**, Photocleavable proteins stably tether a PoI to a material until direct light exposure irreversibly releases the PoI.

As photoresponsive tools uniquely offer high spatiotemporal control, proteins that bind, refold, or cleave in response to light can have exciting applications in biomaterials (**Figure 1.8b**). Gelation can be controlled by exploiting proteins that change oligomeric state with light exposure such as the photoswitching of Dronpa145N which forms a green fluorescent tetramer under violet light and disassembles to a monomeric state under cyan light. By combining a tri-functionalized SpyCatcher fusion and SpyTag-functionalized Dronpa145N, gelation and dissolution can be controlled through exposures of violet and cyan light, respectively[286]. Similarly, the

photoresponsive C-terminal adenosylcobalamin ($AdoB_{12}$) binding domain ($CarH_c$) forms a tetramer in the presence of $AdoB_{12,}$ but upon exposure to green or white light the $CarH_c$ tetramer disassembles to a monomeric state which can be used to degrade protein-based hydrogels[287,288]. Alternatively, large conformational changes induced by light exposures can be harnessed to cyclically modulate the mechanical properties of a gel. By installing light, oxygen, and voltage sensing domain 2 (LOV2) and the C-terminal Jα helix binding domain within the backbone of a covalently crosslinked gel, blue light initiated a relaxation and softening of the gel by up to 15% while dark conditions quickly restored the tightly bound protein structure and original gel stiffness[266]. The LOV2 binding domain Zdk which cleaves under blue light, can be used to biochemically decorate gels with immobilized LOV2[289]. Unlike the cyclic nature of these systems, the photocleavable protein PhoCl offers a genetically encodable approach to irreversibly cleave a PoI from a gel with spatial control (**Figure 1.8c**)[290]. While PhoCl breaks a covalent linkage in response to light, there are currently no examples of a photoresponsive protein capable of forming a covalent bond – a clear void in current capabilities.

1.7 Gaining Spatiotemporal Control of Biological Processes

Substantial work has resulted in numerous methods, often utilizing photochemistries, to control processes occurring directly within biological systems. While many of these techniques have been applied in biomaterials with substantial success, some powerful tools have yet to find their way into the field. Specifically, many optogenetic and protein engineering tools popularized by genetically encoded parts, could provide the unique ability to direct single-cell fate and function in 3D. By repurposing light-responsive proteins from nature, cellular processes [e.g., protein-protein interactions (PPIs), membrane composition, gene transcription, protein/organelle translocation] can be controlled on a (sub)cellular level[291]. Rhodopsins – photoreceptors embedded

in the cellular membrane – isomerize their all-*trans*-retinal chromophore with light treatment, cascading to an overall function such as controlling ion channels (Type I Rhodopsins) or G protein pathways (Type II Rhodopsins). Similarly, photoactivated adenylyl cyclases (PACs) and LOV domains can be used to directly photomodulate biological function by controlling cellular levels of cyclic AMP and protein (in)activation through steric hindrance, respectively.

Apart from controlling specific functions, photoreceptors such as phytochromes, LOV domains, and cryptochromes (proteins containing a flavin adenine dinucleotide (FAD) chromophore) can direct PPIs[292]. Biologically active proteins can be split in an unstructured region to generate inactive N- and C-terminal fragments that properly refold and regain activity when held in proximity (**Figure 1.9**). Photoactivatable PPIs can reversibly and with spatiotemporal control, restore activity to these split proteins[293]. Phytochromes such as phytochrome B (PhyB) or the bathy phytochrome RpBphP1 (BphP1) reversibly transition between active and inactive states under red-shifted light and utilize a chromophore readily abundant in mammalian cells – beneficial for *in vivo* applications[294]. Blue light-responsive LOV domains have been incorporated in many photoactivatable PPI systems (FKF1/GIGANTEA, TULIPS, iLID/SspB, and LOVTRAP) each varying by binding pair size, affinity, and dissociation rate[295]. Alternatively, Cryptochrome 2 (Cry2) and its binding partner cytochromes-interacting basic-helix-loop-helix protein 1 (CIB1) or a truncated version CIBN heterodimerize with sub-second resolution under blue light or multiphoton excitation[296]. Magnets, an alternative blue light-responsive cryptochrome characterized by its small tag (150 amino acids, 17.1 kDa), minimal dark association, and quick photoswitching kinetics compared to PhyB, LOV, and Cry2 systems, has been used to photoregulate a variety of split proteins with high success (Cas9[297,298], recombinases[299], antibodies[300], etc.). The system consists of two VVD variants in which an N-terminal series of

neutral amino acids have been mutated to a series of either positively or negatively charged amino acids, pMag and nMag, respectively. Through charge repulsion and photoactivation of both species, only pMag and nMag heterodimerize avoiding undesired homodimers[301]. The inherent reversibility of these photoswitching systems typically limit applications to pulsed or cyclic activation unless continual light treatment is feasible.

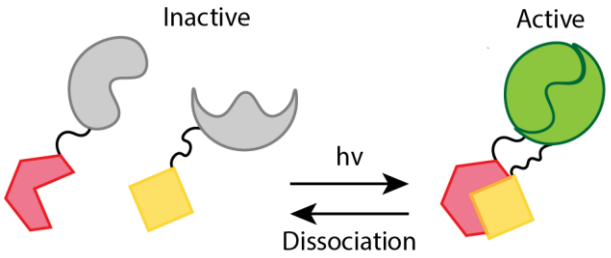

Figure 1.9. Split proteins (grey) are reconstituted to an active form (green) upon directed light exposure, mediated through photodimerization of genetically fused protein partners. The light-induced interaction slowly dissociates under dark conditions, offering temporary protein activation.

To avoid bulky protein fusions associated with photoswitches, researchers have applied genetic engineering techniques to selectively insert stimuli responsive chemical mutations into the protein of interest to provide user-control over activity. By expanding the genetic code, or including an orthogonal tRNA/tRNA synthetase pair within the expression system to override the rarely used amber stop codon (TAG), proteins can be expressed with an unnatural amino acid site-specifically incorporated by mutating the location of interest in the gene to TAG (**Figure 1.10**)[302]. While directed evolution is necessary to optimize the tRNA synthetase for orthogonality and the new unnatural amino acid, optimized systems are becoming more readily accessible and computational methods may expedite the development of new orthogonal tRNA synthetases[303]. Towards achieving spatiotemporal control of biological events, photocaged variants of naturally occurring amino acid can be installed at a critical site, such that photolytic cleavage restores the native protein and its activity. Lysines, serines, cysteines, and tyrosines have been caged with

ortho-nitrobenzyl- and coumarin-based derivatives and utilized to control diverse classes of proteins (e.g., kinases, nucleases, proteases, polymerases) inside mammalian cells and *in vivo*[304]. Spatiotemporal genome editing of zebrafish embryos can be achieved through a photoactivatable Cre recombinase containing a hydroxycoumarin lysine at a key DNA binding site[305]. Applications of encoded photocaged amino acids have grown significantly and created a unique toolkit for spatiotemporal control of biological systems with promising application in biomaterials. The field is ripe for development.

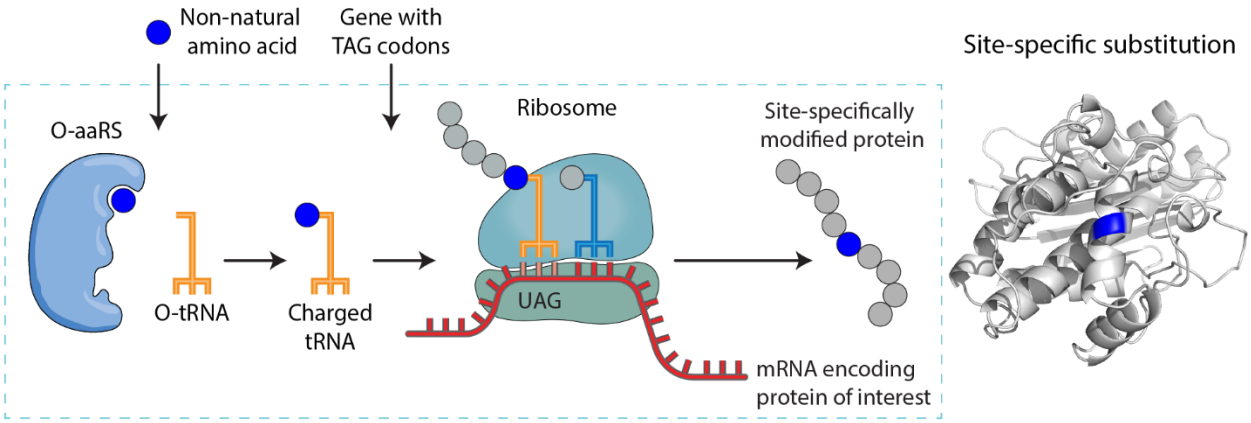

Figure 1.10. Non-natural amino acid incorporation through genetic code expansion. By programming unnatural machinery engineered to override the amber stop codon, UAG, an orthogonal tRNA synthetase (O-aaRS) aminoacylates an orthogonal tRNA (O-tRNA) with a non-natural amino acid. The charged tRNA lands at the UAG site of the mRNA to translate the non-natural amino acid into a protein of interest with single-site specificity. Figure reproduced from original article by Shadish and DeForest[241].

1.8 REFERENCES

1. Palczewski, K. Chemistry and biology of vision. *J. Biol. Chem.* **287**, 1612–9 (2012).
2. Brieke, C., Rohrbach, F., Gottschalk, A., Mayer, G. & Heckel, A. Light-Controlled Tools. *Angew. Chemie Int. Ed.* **51**, 8446–8476 (2012).
3. Yu, H., Li, J., Wu, D., Qiu, Z. & Zhang, Y. Chemistry and biological applications of photo-labile organic molecules. *Chem. Soc. Rev.* **39**, 464–73 (2010).
4. Zhu, C., Ninh, C. & Bettinger, C. J. Photoreconfigurable Polymers for Biomedical Applications: Chemistry and Macromolecular Engineering. *Biomacromolecules* **15**, 3474–3494 (2014).
5. Cui, J., Miguel, V. S. & del Campo, A. Light-Triggered Multifunctionality at Surfaces Mediated by Photolabile Protecting Groups. *Macromol. Rapid Commun.* **34**, 310–329 (2013).
6. Kaplan, J. H., Forbush, B. & Hoffman, J. F. Rapid photolytic release of adenosine 5'-triphosphate from a protected analog: utilization by the sodium:potassium pump of human red blood cell ghosts. *Biochemistry* **17**, 1929–1935 (1978).
7. Klán, P. *et al.* Photoremovable protecting groups in chemistry and biology: reaction mechanisms and efficacy. *Chem. Rev.* **113**, 119–191 (2013).
8. Ercole, F., Davis, T. P. & Evans, R. A. Photo-responsive systems and biomaterials: photochromic polymers, light-triggered self-assembly, surface modification, fluorescence modulation and beyond. *Polym. Chem.* **1**, 37–54 (2010).
9. Wang, Y., Shim, M. S., Levinson, N. S., Sung, H.-W. & Xia, Y. Stimuli-Responsive Materials for Controlled Release of Theranostic Agents. *Adv. Funct. Mater.* **24**, 4206–4220 (2014).
10. Barhoumi, A., Liu, Q. & Kohane, D. S. Ultraviolet light-mediated drug delivery: Principles, applications, and challenges. *J. Control. Release* **219**, 31–42 (2015).
11. Velema, W. A., Szymanski, W. & Feringa, B. L. Photopharmacology: Beyond Proof of Principle. *J. Am. Chem. Soc.* **136**, 2178–2191 (2014).
12. Olejniczak, J., Carling, C.-J. & Almutairi, A. Photocontrolled release using one-photon absorption of visible or NIR light. *J. Control. Release* **219**, 18–30 (2015).
13. Breitinger, H.-G. A., Wieboldt, R., Ramesh, D., Carpenter, B. K. & Hess, G. P. Synthesis and Characterization of Photolabile Derivatives of Serotonin for Chemical Kinetic Investigations of the Serotonin 5-HT 3 Receptor. *Biochemistry* **39**, 5500–5508 (2000).
14. Shi, Y. *et al.* Light-triggered release of ciprofloxacin from an in situ forming click hydrogel for antibacterial wound dressings. *J. Mater. Chem. B* **3**, 8771–8774 (2015).
15. Paul, A. *et al.* Photoresponsive real time monitoring silicon quantum dots for regulated delivery of anticancer drugs. *J. Mater. Chem. B* **4**, 521–528 (2016).
16. Cabane, E., Malinova, V., Menon, S., Palivan, C. G. & Meier, W. Photoresponsive polymersomes as smart, triggerable nanocarriers. *Soft Matter* **7**, 9167–9176 (2011).
17. Kohman, R. E., Cha, S. S., Man, H.-Y. & Han, X. Light-Triggered Release of Bioactive Molecules from DNA Nanostructures. *Nano Lett.* **16**, 2781–2785 (2016).
18. Shestopalov, I. A., Sinha, S. & Chen, J. K. Light-controlled gene silencing in zebrafish embryos. *Nat. Chem. Biol.* **3**, 650–651 (2007).
19. Inlay, M. A. *et al.* Synthesis of a photocaged tamoxifen for light-dependent activation of Cre-ER recombinase-driven gene modification. *Chem. Commun. (Camb).* **49**, 4971–4973 (2013).

20. Li, L. *et al.* Aptamer photoregulation in vivo. *Proc. Natl. Acad. Sci.* **111**, 17099–17103 (2014).
21. Huynh, C. T. *et al.* Photocleavable Hydrogels for Light-Triggered siRNA Release. *Adv. Healthc. Mater.* **5**, 305–310 (2015).
22. Faal, T. *et al.* 4-Hydroxytamoxifen probes for light-dependent spatiotemporal control of Cre-ER mediated reporter gene expression. *Mol. Biosyst.* **11**, 783–90 (2015).
23. Sarode, B. R., Kover, K., Tong, P. Y., Zhang, C. & Friedman, S. H. Light Control of Insulin Release and Blood Glucose Using an Injectable Photoactivated Depot. *Mol. Pharm.* **13**, 3835–3841 (2016).
24. D'Souza, A. J. M. & Topp, E. M. Release from polymeric prodrugs: Linkages and their degradation. *J. Pharm. Sci.* **93**, 1962–1979 (2004).
25. Fomina, N., McFearin, C., Sermsakdi, M., Edigin, O. & Almutairi, A. UV and near-IR triggered release from polymeric nanoparticles. *J. Am. Chem. Soc.* **132**, 9540–2 (2010).
26. Huu, V. A. N. *et al.* Light-responsive nanoparticle depot to control release of a small molecule angiogenesis inhibitor in the posterior segment of the eye. *J. Control. Release* **200**, 71–7 (2015).
27. Aujard, I. *et al.* o-Nitrobenzyl Photolabile Protecting Groups with Red-Shifted Absorption: Syntheses and Uncaging Cross-Sections for One- and Two-Photon Excitation. *Chem. - A Eur. J.* **12**, 6865–6879 (2006).
28. Holmes, C. P. Model Studies for New *o* -Nitrobenzyl Photolabile Linkers: Substituent Effects on the Rates of Photochemical Cleavage. *J. Org. Chem.* **62**, 2370–2380 (1997).
29. Griffin, D. R. & Kasko, A. M. Photoselective Delivery of Model Therapeutics from Hydrogels. *ACS Macro Lett.* **1**, 1330–1334 (2012).
30. Donato, L. *et al.* Water-Soluble, Donor-Acceptor Biphenyl Derivatives in the 2-(o-Nitrophenyl)propyl Series: Highly Efficient Two-Photon Uncaging of the Neurotransmitter γ-Aminobutyric Acid at λ=800 nm. *Angew. Chemie Int. Ed.* **51**, 1840–1843 (2012).
31. Olejniczak, J., Sankaranarayanan, J., Viger, M. L. & Almutairi, A. Highest Efficiency Two-Photon Degradable Copolymer for Remote Controlled Release. *ACS Macro Lett.* **2**, 683–687 (2013).
32. Carling, C.-J. *et al.* Efficient Red Light Photo-Uncaging of Active Molecules in Water Upon Assembly into Nanoparticles. *Chem. Sci.* **7**, 2392–2398 (2015).
33. Yang, Y. *et al.* NIR light controlled photorelease of siRNA and its targeted intracellular delivery based on upconversion nanoparticles. *Nanoscale* **5**, 231–8 (2013).
34. Yang, Y., Velmurugan, B., Liu, X. & Xing, B. NIR photoresponsive crosslinked upconverting nanocarriers toward selective intracellular drug release. *Small* **9**, 2937–44 (2013).
35. Wang, W. *et al.* Efficient Triplet-Triplet Annihilation-Based Upconversion for Nanoparticle Phototargeting. *Nano Lett.* **15**, 6332–8 (2015).
36. Yan, B., Boyer, J.-C., Branda, N. R. & Zhao, Y. Near-infrared light-triggered dissociation of block copolymer micelles using upconverting nanoparticles. *J. Am. Chem. Soc.* **133**, 19714–7 (2011).
37. Yan, B., Boyer, J.-C., Habault, D., Branda, N. R. & Zhao, Y. Near Infrared Light Triggered Release of Biomacromolecules from Hydrogels Loaded with Upconversion Nanoparticles. *J. Am. Chem. Soc.* **134**, 16558–16561 (2012).
38. Sudimack, J. & Lee, R. J. Targeted drug delivery via the folate receptor. *Adv. Drug Deliv. Rev.* **41**, 147–162 (2000).

39. Fan, N.-C., Cheng, F.-Y., Ho, J. A. & Yeh, C.-S. Photocontrolled targeted drug delivery: photocaged biologically active folic acid as a light-responsive tumor-targeting molecule. *Angew. Chem. Int. Ed. Engl.* **51**, 8806–10 (2012).
40. Choi, S. K. *et al.* Light-controlled release of caged doxorubicin from folate receptor-targeting PAMAM dendrimer nanoconjugate. *Chem. Commun. (Camb).* **46**, 2632–4 (2010).
41. Hu, X., Tian, J., Liu, T., Zhang, G. & Liu, S. Photo-Triggered Release of Caged Camptothecin Prodrugs from Dually Responsive Shell Cross-Linked Micelles. *Macromolecules* **46**, 6243–6256 (2013).
42. Azagarsamy, M. A., Alge, D. L., Radhakrishnan, S. J., Tibbitt, M. W. & Anseth, K. S. Photocontrolled Nanoparticles for On-Demand Release of Proteins. *Biomacromolecules* **13**, 2219–2224 (2012).
43. Koren, E. & Torchilin, V. P. Cell-penetrating peptides: breaking through to the other side. *Trends Mol. Med.* **18**, 385–93 (2012).
44. Shamay, Y., Adar, L., Ashkenasy, G. & David, A. Light induced drug delivery into cancer cells. *Biomaterials* **32**, 1377–1386 (2011).
45. Yang, Y. Y., Yang, Y. Y., Xie, X., Cai, X. & Mei, X. Preparation and characterization of photo-responsive cell-penetrating peptide-mediated nanostructured lipid carrier. *J. Drug Target.* **22**, 891–900 (2014).
46. Lin, W. *et al.* Enhanced small interfering RNA delivery into cells by exploiting the additive effect between photo-sensitive peptides and targeting ligands. *J. Pharm. Pharmacol.* **67**, 1215–31 (2015).
47. Badeau, B. A., Comerford, M. P., Arakawa, C. K., Shadish, J. A. & DeForest, C. A. Engineered modular biomaterial logic gates for environmentally triggered therapeutic delivery. *Nat. Chem.* (2018) doi:10.1038/nchem.2917.
48. Lee, J. S., Deng, X., Han, P. & Cheng, J. Dual Stimuli-Responsive Poly(β-amino ester) Nanoparticles for On-Demand Burst Release. *Macromol. Biosci.* **15**, 1314–22 (2015).
49. Liu, G., Zhou, L., Guan, Y., Su, Y. & Dong, C.-M. Multi-responsive polypeptidosome: characterization, morphology transformation, and triggered drug delivery. *Macromol. Rapid Commun.* **35**, 1673–8 (2014).
50. Klinger, D. & Landfester, K. Dual Stimuli-Responsive Poly(2-hydroxyethyl methacrylate-co-methacrylic acid) Microgels Based on Photo-Cleavable Cross-Linkers: pH-Dependent Swelling and Light-Induced Degradation. *Macromolecules* **44**, 9758–9772 (2011).
51. Zhang, Y. *et al.* Polymer-Coated Hollow Mesoporous Silica Nanoparticles for Triple-Responsive Drug Delivery. *ACS Appl. Mater. Interfaces* **7**, 18179–87 (2015).
52. Badeau, B. A., Comerford, M. P., Arakawa, C. K., Shadish, J. A. & DeForest, C. A. Engineered modular biomaterial logic gates for environmentally triggered therapeutic delivery. *Nat. Chem.* **10**, 251–258 (2018).
53. Givens, R. S. & Matuszewski, B. Photochemistry of phosphate esters: an efficient method for the generation of electrophiles. *J. Am. Chem. Soc.* **106**, 6860–6861 (1984).
54. Suzuki, A. Z. *et al.* Coumarin-4-ylmethoxycarbonyls as phototriggers for alcohols and phenols. *Org. Lett.* **5**, 4867–70 (2003).
55. Geissler, D. *et al.* (Coumarin-4-yl)methyl esters as highly efficient, ultrafast phototriggers for protons and their application to acidifying membrane surfaces. *Angew. Chem. Int. Ed. Engl.* **44**, 1195–8 (2005).
56. Jin, Q., Mitschang, F. & Agarwal, S. Biocompatible drug delivery system for photo-triggered controlled release of 5-Fluorouracil. *Biomacromolecules* **12**, 3684–91 (2011).

57. Huang, Q., Bao, C., Ji, W., Wang, Q. & Zhu, L. Photocleavable coumarin crosslinkers based polystyrene microgels: phototriggered swelling and release. *J. Mater. Chem.* **22**, 18275 (2012).
58. Mal, N. K., Fujiwara, M., Tanaka, Y., Taguchi, T. & Matsukata, M. Photo-Switched Storage and Release of Guest Molecules in the Pore Void of Coumarin-Modified MCM-41. *Chem. Mater.* **15**, 3385–3394 (2003).
59. Lin, Q. *et al.* Anticancer Drug Release from a Mesoporous Silica Based Nanophotocage Regulated by Either a One- or Two-Photon Process. *J. Am. Chem. Soc.* **132**, 10645–10647 (2010).
60. Ji, W. *et al.* Coumarin-containing photo-responsive nanocomposites for NIR light-triggered controlled drug release via a two-photon process. *J. Mater. Chem. B* **1**, 5942 (2013).
61. Ando, H., Furuta, T., Tsien, R. Y. & Okamoto, H. Photo-mediated gene activation using caged RNA/DNA in zebrafish embryos. *Nat. Genet.* **28**, 317–25 (2001).
62. Seo, H. J. & Kim, J.-C. 7-acetoxycoumarin dimer-incorporated and folate-decorated liposomes: photoresponsive release and in vitro targeting and efficacy. *Bioconjug. Chem.* **25**, 533–42 (2014).
63. Long, Y.-B., Gu, W.-X., Pang, C., Ma, J. & Gao, H. Construction of coumarin-based cross-linked micelles with pH responsive hydrazone bond and tumor targeting moiety. *J. Mater. Chem. B* **4**, 1480–1488 (2016).
64. Ohtsuki, T. *et al.* Phototriggered protein syntheses by using (7-diethylaminocoumarin-4-yl)methoxycarbonyl-caged aminoacyl tRNAs. *Nat. Commun.* **7**, 12501 (2016).
65. Lin, Q. *et al.* Highly Discriminating Photorelease of Anticancer Drugs Based on Hypoxia Activatable Phototrigger Conjugated Chitosan Nanoparticles. *Adv. Mater.* **25**, 1981–1986 (2013).
66. Klán, P. *et al.* Photoremovable protecting groups in chemistry and biology: reaction mechanisms and efficacy. *Chem. Rev.* **113**, 119–91 (2013).
67. Fournier, L. *et al.* A Blue-Absorbing Photolabile Protecting Group for in Vivo Chromatically Orthogonal Photoactivation. *ACS Chem. Biol.* **8**, 1528–1536 (2013).
68. Fournier, L. *et al.* Coumarinylmethyl Caging Groups with Redshifted Absorption. *Chem. - A Eur. J.* **19**, 17494–17507 (2013).
69. Furuta, T. *et al.* Brominated 7-hydroxycoumarin-4-ylmethyls: Photolabile protecting groups with biologically useful cross-sections for two photon photolysis. *Proc. Natl. Acad. Sci.* **96**, 1193–1200 (1999).
70. Babin, J. *et al.* A new two-photon-sensitive block copolymer nanocarrier. *Angew. Chemie* **48**, 3329–32 (2009).
71. Kumar, S. *et al.* Near-infrared light sensitive polypeptide block copolymer micelles for drug delivery. *J. Mater. Chem.* **22**, 7252 (2012).
72. Lux, C. de G. *et al.* Short Soluble Coumarin Crosslinkers for Light-Controlled Release of Cells and Proteins from Hydrogels. *Biomacromolecules* **16**, 3286–3296 (2015).
73. Bandara, H. M. D. & Burdette, S. C. Photoisomerization in different classes of azobenzene. *Chem. Soc. Rev.* **41**, 1809–1825 (2012).
74. Kano, K. *et al.* Photoresponsive membranes. Regulation of membrane properties by photoreversible cis-trans isomerization of azobenzenes. *Chem. Lett.* **9**, 421–424 (1980).
75. Bisby, R. H., Mead, C. & Morgan, C. G. Active uptake of drugs into photosensitive liposomes and rapid release on UV photolysis. *Photochem. Photobiol.* **72**, 57–61 (2000).
76. Wang, Y. *et al.* Photocontrolled Self-Assembly and Disassembly of Block Ionomer

Complex Vesicles: A Facile Approach toward Supramolecular Polymer Nanocontainers. *Langmuir* **26**, 709–715 (2010).
77. Zhang, H. *et al.* Reversible morphology transitions of supramolecular polymer self-assemblies for switch-controlled drug release. *Chem. Commun. (Camb).* **51**, 15366–9 (2015).
78. Liu, D., Wang, S., Xu, S. & Liu, H. Photocontrollable Intermittent Release of Doxorubicin Hydrochloride from Liposomes Embedded by Azobenzene-Contained Glycolipid. *Langmuir* **33**, 1004–1012 (2017).
79. Sheldon, J. E., Dcona, M. M., Lyons, C. E., Hackett, J. C. & Hartman, M. C. T. Photoswitchable anticancer activity via trans-cis isomerization of a combretastatin A-4 analog. *Org. Biomol. Chem.* **14**, 40–49 (2015).
80. Angelos, S., Choi, E., Vogtle, F., DeCola, L. & Zink, J. I. Photo-Driven Expulsion of Molecules from Mesostructured Silica Nanoparticles. *J. Phys. Chem. C* **111**, 6589–6592 (2007).
81. Lu, J., Choi, E., Tamanoi, F. & Zink, J. I. Light-Activated Nanoimpeller-Controlled Drug Release in Cancer Cells. *Small* **4**, 421–426 (2008).
82. Guardado-Alvarez, T. M., Sudha Devi, L., Russell, M. M., Schwartz, B. J. & Zink, J. I. Activation of snap-top capped mesoporous silica nanocontainers using two near-infrared photons. *J. Am. Chem. Soc.* **135**, 14000–3 (2013).
83. Tarn, D. *et al.* A reversible light-operated nanovalve on mesoporous silica nanoparticles. *Nanoscale* **6**, 3335–3343 (2014).
84. Zhu, Y. & Fujiwara, M. Installing Dynamic Molecular Photomechanics in Mesopores: A Multifunctional Controlled-Release Nanosystem. *Angew. Chemie Int. Ed.* **46**, 2241–2244 (2007).
85. Yuan, Q. *et al.* Photon-manipulated drug release from a mesoporous nanocontainer controlled by azobenzene-modified nucleic acid. *ACS Nano* **6**, 6337–44 (2012).
86. Liu, J., Bu, W., Pan, L. & Shi, J. NIR-triggered anticancer drug delivery by upconverting nanoparticles with integrated azobenzene-modified mesoporous silica. *Angew. Chem. Int. Ed. Engl.* **52**, 4375–9 (2013).
87. Bléger, D., Schwarz, J., Brouwer, A. M. & Hecht, S. *o* -Fluoroazobenzenes as Readily Synthesized Photoswitches Offering Nearly Quantitative Two-Way Isomerization with Visible Light. *J. Am. Chem. Soc.* **134**, 20597–20600 (2012).
88. Knie, C. *et al. ortho* -Fluoroazobenzenes: Visible Light Switches with Very Long-Lived *Z* Isomers. *Chem. - A Eur. J.* **20**, 16492–16501 (2014).
89. Konrad, D. B., Frank, J. A. & Trauner, D. Synthesis of Redshifted Azobenzene Photoswitches by Late-Stage Functionalization. *Chem. - A Eur. J.* **22**, 4364–4368 (2016).
90. Frank, J. A. *et al.* Photoswitchable fatty acids enable optical control of TRPV1. *Nat. Commun.* **6**, 7118 (2015).
91. Broichhagen, J., Frank, J. A. & Trauner, D. A Roadmap to Success in Photopharmacology. *Acc. Chem. Res.* **48**, 1947–1960 (2015).
92. Dong, M., Babalhavaeji, A., Samanta, S., Beharry, A. A. & Woolley, G. A. Red-Shifting Azobenzene Photoswitches for in Vivo Use. *Acc. Chem. Res.* **48**, 2662–2670 (2015).
93. Achilleos, D. S., Hatton, T. A. & Vamvakaki, M. Light-Regulated Supramolecular Engineering of Polymeric Nanocapsules. *J. Am. Chem. Soc.* **134**, 5726–5729 (2012).
94. Son, S., Shin, E. & Kim, B.-S. Light-Responsive Micelles of Spiropyran Initiated Hyperbranched Polyglycerol for Smart Drug Delivery. *Biomacromolecules* **15**, 628–634

(2014).
95. Chen, S., Jiang, F., Cao, Z., Wang, G. & Dang, Z.-M. Photo, pH, and thermo triple-responsive spiropyran-based copolymer nanoparticles for controlled release. *Chem. Commun.* **51**, 12633–12636 (2015).
96. Chen, S. *et al.* Nanocomposites of Spiropyran-Functionalized Polymers and Upconversion Nanoparticles for Controlled Release Stimulated by Near-Infrared Light and pH. *Macromolecules* **49**, 7490–7496 (2016).
97. Chang, D., Yan, W., Yang, Y., Wang, Q. & Zou, L. Reversible light-controllable intelligent gel based on simple spiropyran-doped with biocompatible lecithin. *Dye. Pigment.* **134**, 186–189 (2016).
98. Tong, R., Hemmati, H. D., Langer, R. & Kohane, D. S. Photoswitchable Nanoparticles for Triggered Tissue Penetration and Drug Delivery. *J. Am. Chem. Soc.* **134**, 8848–8855 (2012).
99. Tong, R., Chiang, H. H. & Kohane, D. S. Photoswitchable nanoparticles for in vivo cancer chemotherapy. *Proc. Natl. Acad. Sci.* **110**, 19048–53 (2013).
100. Wolff, L. About diazoanhydrides. *Liebigs Ann. der Chemie* **325**, 129–195 (1902).
101. Urdabayev, N. K. & Popik, V. V. Wolff Rearrangement of 2-diazo-1(2H)-naphthalenone induced by nonresonant two-photon absorption of NIR radiation. *J. Am. Chem. Soc.* **126**, 4058–9 (2004).
102. Goodwin, A. P., Mynar, J. L., Ma, Y., Fleming, G. R. & Fréchet, J. M. J. Synthetic Micelle Sensitive to IR Light via a Two-Photon Process. *J. Am. Chem. Soc.* **127**, 9952–9953 (2005).
103. Mynar, J. L. *et al.* Two-photon degradable supramolecular assemblies of linear-dendritic copolymers. *Chem. Commun.* 2081–2082 (2007).
104. Sun, L., Yang, Y., Dong, C.-M. & Wei, Y. Two-photon-sensitive and sugar-targeted nanocarriers from degradable and dendritic amphiphiles. *Small* **7**, 401–6 (2011).
105. Yuan, Y. *et al.* Conjugated polymer and drug co-encapsulated nanoparticles for Chemo- and Photo-thermal Combination Therapy with two-photon regulated fast drug release. *Nanoscale* **7**, 3067–3076 (2015).
106. Ahmad, R., Fu, J., He, N. & Li, S. Advanced Gold Nanomaterials for Photothermal Therapy of Cancer. *J. Nanosci. Nanotechnol.* **15**, 1–14 (2015).
107. Gu, L., Koymen, A. R. & Mohanty, S. K. Crystalline magnetic carbon nanoparticle assisted photothermal delivery into cells using CW near-infrared laser beam. *Sci. Rep.* **4**, 5106 (2014).
108. Febvay, S., Marini, D. M., Belcher, A. M. & Clapham, D. E. Targeted Cytosolic Delivery of Cell-Impermeable Compounds by Nanoparticle-Mediated, Light-Triggered Endosome Disruption. *Nano Lett.* **10**, 2211–2219 (2010).
109. Vivero-Escoto, J. L., Slowing, I. I., Wu, C.-W. & Lin, V. S.-Y. Photoinduced Intracellular Controlled Release Drug Delivery in Human Cells by Gold-Capped Mesoporous Silica Nanosphere. *J. Am. Chem. Soc.* **131**, 3462–3463 (2009).
110. Troutman, T. S., Leung, S. J. & Romanowski, M. Light-Induced Content Release from Plasmon Resonant Liposomes. *Adv. Mater.* **21**, 2334–2338 (2009).
111. Yavuz, M. S. *et al.* Gold nanocages covered by smart polymers for controlled release with near-infrared light. *Nat. Mater.* **8**, 935–939 (2009).
112. Rengan, A. K., Jagtap, M., De, A., Banerjee, R. & Srivastava, R. Multifunctional gold coated thermo-sensitive liposomes for multimodal imaging and photo-thermal therapy of breast cancer cells. *Nanoscale* **6**, 916–23 (2014).
113. Basuki, J. S. *et al.* Photo-Modulated Therapeutic Protein Release from a Hydrogel Depot

Using Visible Light. *Angew. Chemie Int. Ed.* **56**, 966–971 (2017).
114. Ghosh, P., Han, G., De, M., Kim, C. K. & Rotello, V. M. Gold nanoparticles in delivery applications. *Adv. Drug Deliv. Rev.* **60**, 1307–1315 (2008).
115. Aznar, E. *et al.* pH- and photo-switched release of guest molecules from mesoporous silica supports. *J. Am. Chem. Soc.* **131**, 6833–43 (2009).
116. Kang, H. *et al.* Near-infrared light-responsive core-shell nanogels for targeted drug delivery. *ACS Nano* **5**, 5094–9 (2011).
117. Lee, J., Park, H. & Kim, W. J. Nano 'Chocolate Waffle' for near-IR Responsive Drug Releasing System. *Small* **11**, 5315–23 (2015).
118. Tang, Y. *et al.* An aptamer-targeting photoresponsive drug delivery system using "off–on" graphene oxide wrapped mesoporous silica nanoparticles. *Nanoscale* **7**, 6304–6310 (2015).
119. Cobley, C. M., Au, L., Chen, J. & Xia, Y. Targeting gold nanocages to cancer cells for photothermal destruction and drug delivery. *Expert Opin. Drug Deliv.* **7**, 577–87 (2010).
120. Hribar, K. C., Lee, M. H., Lee, D. & Burdick, J. A. Enhanced Release of Small Molecules from Near-Infrared Light Responsive Polymer−Nanorod Composites. *ACS Nano* **5**, 2948–2956 (2011).
121. Niidome, T. *et al.* PEG-modified gold nanorods with a stealth character for in vivo applications. *J. Control. Release* **114**, 343–7 (2006).
122. MacLeod, M. J. & Johnson, J. A. PEGylated N-Heterocyclic Carbene Anchors Designed To Stabilize Gold Nanoparticles in Biologically Relevant Media. *J. Am. Chem. Soc.* **137**, 7974–7977 (2015).
123. Li, W. *et al.* Remote modulation of neural activities via near-infrared triggered release of biomolecules. *Biomaterials* **65**, 76–85 (2015).
124. Yu, H. *et al.* pH- and NIR Light-Responsive Micelles with Hyperthermia-Triggered Tumor Penetration and Cytoplasm Drug Release to Reverse Doxorubicin Resistance in Breast Cancer. *Adv. Funct. Mater.* **25**, 2489–2500 (2015).
125. Sherlock, S. P., Tabakman, S. M., Xie, L. & Dai, H. Photothermally enhanced drug delivery by ultrasmall multifunctional FeCo/graphitic shell nanocrystals. *ACS Nano* **5**, 1505–12 (2011).
126. Chen, W. *et al.* Black Phosphorus Nanosheet-Based Drug Delivery System for Synergistic Photodynamic/Photothermal/Chemotherapy of Cancer. *Adv. Mater.* **29**, 1603864 (2017).
127. Kim, H. *et al.* Visible Light-Triggered On-Demand Drug Release from Hybrid Hydrogels and its Application in Transdermal Patches. *Adv. Healthc. Mater.* **4**, 2071–2077 (2015).
128. Bonnett, R. Photosensitizers of the porphyrin and phthalocyanine series for photodynamic therapy. *Chem. Soc. Rev.* **24**, 19 (1995).
129. Ackroyd, R., Kelty, C., Brown, N. & Reed, M. The History of Photodetection and Photodynamic Therapy. *Photochem. Photobiol.* **74**, 656 (2001).
130. Bio, M. *et al.* Site-Specific and Far-Red-Light-Activatable Prodrug of Combretastatin A-4 Using Photo-Unclick Chemistry. *J. Med. Chem.* **56**, 3936–3942 (2013).
131. Hossion, A. M. L., Bio, M., Nkepang, G., Awuah, S. G. & You, Y. Visible Light Controlled Release of Anticancer Drug through Double Activation of Prodrug. *Acs Med. Chem. Lett.* **4**, 124–127 (2013).
132. Ke, M.-R. *et al.* A tumor-targeted activatable phthalocyanine-tetrapeptide-doxorubicin conjugate for synergistic chemo-photodynamic therapy. *Eur. J. Med. Chem.* **127**, 200–209 (2017).
133. Rwei, A. Y. *et al.* Repeatable and adjustable on-demand sciatic nerve block with

phototriggerable liposomes. *Proc. Natl. Acad. Sci.* **112**, 15719–15724 (2015).
134. Berg, K. & Moan, J. Lysosomes as photochemical targets. *Int. J. Cancer* **59**, 814–22 (1994).
135. Berg, K. *et al.* Photochemical Internalization: a novel technique for delivery of macromolecules into cytosol. *Cancer Res.* **59**, 1180–1183 (1999).
136. Selbo, P. K. *et al.* Photochemical internalization provides time- and space-controlled endolysosomal escape of therapeutic molecules. *J. Control. Release* **148**, 2–12 (2010).
137. Nishiyama, N. *et al.* Light-induced gene transfer from packaged DNA enveloped in a dendrimeric photosensitizer. *Nat. Mater.* **4**, 934–941 (2005).
138. Carter, K. A. *et al.* Porphyrin-phospholipid liposomes permeabilized by near-infrared light. *Nat. Commun.* **5**, 3546 (2014).
139. Luo, D. *et al.* Porphyrin-phospholipid liposomes with tunable leakiness. *J. Control. Release* **220**, 484–94 (2015).
140. DeForest, C. A. & Anseth, K. S. Advances in Bioactive Hydrogels to Probe and Direct Cell Fate. *Annu. Rev. Chem. Biomol. Eng.* **3**, 421–444 (2012).
141. Fairbanks, B. D., Schwartz, M. P., Bowman, C. N. & Anseth, K. S. Photoinitiated polymerization of PEG-diacrylate with lithium phenyl-2,4,6-trimethylbenzoylphosphinate: polymerization rate and cytocompatibility. *Biomaterials* **30**, 6702–6707 (2009).
142. Hahn, M. S., Miller, J. S. & West, J. L. Three-dimensional biochemical and biomechanical patterning of hydrogels for guiding cell behavior. *Adv. Mater.* **18**, 2679–2684 (2006).
143. Lee, S.-H. H., Moon, J. J. & West, J. L. Three-dimensional micropatterning of bioactive hydrogels via two-photon laser scanning photolithography for guided 3D cell migration. *Biomaterials* **29**, 2962–2968 (2008).
144. Hoffmann, J. C. & West, J. L. Three-dimensional photolithographic patterning of multiple bioactive ligands in poly(ethylene glycol) hydrogels. *Soft Matter* **6**, 5056–5063 (2010).
145. Hahn, M. S. *et al.* Photolithographic patterning of polyethylene glycol hydrogels. *Biomaterials* **27**, 2519–2524 (2006).
146. DeLong, S. A., Moon, J. J. & West, J. L. Covalently immobilized gradients of bFGF on hydrogel scaffolds for directed cell migration. *Biomaterials* **26**, 3227–3234 (2005).
147. Culver, J. C. *et al.* Three-Dimensional Biomimetic Patterning in Hydrogels to Guide Cellular Organization. *Adv. Mater.* **24**, 2344–2348 (2012).
148. Moon, J. J., Hahn, M. S., Kim, I., Nsiah, B. A. & West, J. L. Micropatterning of poly(ethylene glycol) diacrylate hydrogels with biomolecules to regulate and guide endothelial morphogenesis. *Tissue Eng. Part A* **15**, 579–585 (2009).
149. Leslie-Barbick, J. E., Shen, C., Chen, C. & West, J. L. Micron-Scale Spatially Patterned, Covalently Immobilized Vascular Endothelial Growth Factor on Hydrogels Accelerates Endothelial Tubulogenesis and Increases Cellular Angiogenic Responses. *Tissue Eng. Part A* **17**, 221–229 (2011).
150. Luo, Y. & Shoichet, M. S. A photolabile hydrogel for guided three-dimensional cell growth and migration. *Nat. Mater.* **3**, 249–253 (2004).
151. Wosnick, J. H. & Shoichet, M. S. Three-dimensional chemical Patterning of transparent hydrogels. *Chem. Mater.* **20**, 55–60 (2008).
152. Wylie, R. G. *et al.* Spatially controlled simultaneous patterning of multiple growth factors in three-dimensional hydrogels. *Nat. Mater.* **10**, 799–806 (2011).
153. Wylie, R. G. & Shoichet, M. S. Three-Dimensional Spatial Patterning of Proteins in Hydrogels. *Biomacromolecules* **12**, 3789–3796 (2011).
154. Luo, Y. & Shoichet, M. S. Light-activated immobilization of biomolecules to agarose

hydrogels for controlled cellular response. *Biomacromolecules* **5**, 2315–2323 (2004).
155. Polizzotti, B. D., Fairbanks, B. D. & Anseth, K. S. Three-dimensional biochemical patterning of click-based composite hydrogels via thiolene photopolymerization. *Biomacromolecules* **9**, 1084–1087 (2008).
156. Adzima, B. J. *et al.* Spatial and temporal control of the alkyne-azide cycloaddition by photoinitiated Cu(II) reduction. *Nat. Chem.* **3**, 258–261 (2011).
157. Bryant, S. J., Nuttelman, C. R. & Anseth, K. S. Cytocompatibility of UV and visible light photoinitiating systems on cultured NIH/3T3 fibroblasts in vitro. *J. Biomater. Sci. Ed.* **11**, 439–457 (2000).
158. DeForest, C. A. & Anseth, K. S. Cytocompatible click-based hydrogels with dynamically tunable properties through orthogonal photocoupling and photodegradation reactions. *Nat. Chem.* **3**, 925–931 (2011).
159. Hoyle, C. E. & Bowman, C. N. Thiol-Ene Click Chemistry. *Angew. Chemie Int. Ed.* **49**, 1540–1573 (2010).
160. DeForest, C. A., Polizzotti, B. D. & Anseth, K. S. Sequential click reactions for synthesizing and patterning three-dimensional cell microenvironments. *Nat. Mater.* **8**, 659–664 (2009).
161. DeForest, C. A., Sims, E. A. & Anseth, K. S. Peptide-functionalized click hydrogels with independently tunable mechanics and chemical functionality for 3D cell culture. *Chem. Mater.* **22**, 4783–4790 (2010).
162. Sawicki, L. A. & Kloxin, A. M. Design of thiol-ene photoclick hydrogels using facile techniques for cell culture applications. *Biomater Sci* **2**, 1612–1626 (2014).
163. Fairbanks, B. D. *et al.* A versatile synthetic extracellular matrix mimic via thiol-norbornene photopolymerization. *Adv. Mater.* **21**, 5005–5010 (2009).
164. Alge, D. L., Azagarsamy, M. A., Donohue, D. F. & Anseth, K. S. Synthetically Tractable Click Hydrogels for Three-Dimensional Cell Culture Formed Using Tetrazine-Norbornene Chemistry. *Biomacromolecules* **14**, 949–953 (2013).
165. Gramlich, W. M., Kim, I. L. & Burdick, J. A. Synthesis and orthogonal photopatterning of hyaluronic acid hydrogels with thiol-norbornene chemistry. *Biomaterials* **34**, 9803–11 (2013).
166. Wade, R. J., Bassin, E. J., Gramlich, W. M. & Burdick, J. A. Nanofibrous hydrogels with spatially patterned biochemical signals to control cell behavior. *Adv. Mater.* **27**, 1356–62 (2015).
167. Mosiewicz, K. A. *et al.* In situ cell manipulation through enzymatic hydrogel photopatterning. *Nat. Mater.* **12**, 1071–1077 (2013).
168. Griffin, D. R. *et al.* Hybrid Photopatterned Enzymatic Reaction (HyPER) for in Situ Cell Manipulation. *Chembiochem* **15**, 233–242 (2014).
169. Petersen, S. *et al.* Phototriggering of Cell Adhesion by Caged Cyclic RGD Peptides. *Angew. Chemie* **120**, 3236–3239 (2008).
170. Ohmuro-Matsuyama, Y. & Tatsu, Y. Photocontrolled cell adhesion on a surface functionalized with a caged arginine-glycine-aspartate peptide. *Angew. Chemie-International Ed.* **47**, 7527–7529 (2008).
171. Weis, S., Lee, T. T., del Campo, A. & García, A. J. Dynamic cell-adhesive microenvironments and their effect on myogenic differentiation. *Acta Biomater.* **9**, 8059–8066 (2013).
172. Lee, T. T. *et al.* Light-triggered in vivo activation of adhesive peptides regulates cell adhesion, inflammation and vascularization of biomaterials. *Nat. Mater.* **14**, 352–360

(2015).
173. Kloxin, A. M., Kasko, A. M., Salinas, C. N. & Anseth, K. S. Photodegradable Hydrogels for Dynamic Tuning of Physical and Chemical Properties. *Science* **324**, 59–63 (2009).
174. Griffin, D. R. & Kasko, A. M. Photodegradable macromers and hydrogels for live cell encapsulation and release. *J. Am. Chem. Soc.* **134**, 13103–7 (2012).
175. Azagarsamy, M. A. & Anseth, K. S. Wavelength-controlled photocleavage for the orthogonal and sequential release of multiple proteins. *Angew. Chemie - Int. Ed.* **52**, 13803–13807 (2013).
176. DeForest, C. A. & Anseth, K. S. Photoreversible Patterning of Biomolecules within Click-Based Hydrogels. *Angew. Chemie Int. Ed.* **51**, 1816–1819 (2011).
177. Gandavarapu, N. R., Azagarsamy, M. A. & Anseth, K. S. Photo-Click Living Strategy for Controlled, Reversible Exchange of Biochemical Ligands. *Adv. Mater.* **26**, 2521–2526 (2014).
178. DeForest, C. A. & Tirrell, D. A. A photoreversible protein-patterning approach for guiding stem cell fate in three-dimensional gels. *Nat Mater* **14**, 523–531 (2015).
179. Farahani, P. E., Adelmund, S. M., Shadish, J. A. & DeForest, C. A. Photomediated Oxime Ligation as a Bioorthogonal Tool for Spatiotemporally-Controlled Hydrogel Formation and Modification. *J. Mater. Chem. B* **5**, 4435–4442 (2017).
180. Engler, A. J., Sen, S., Sweeney, H. L. & Discher, D. E. Matrix elasticity directs stem cell lineage specification. *Cell* **126**, 677–689 (2006).
181. Reilly, G. C. & Engler, A. J. Intrinsic extracellular matrix properties regulate stem cell differentiation. *J. Biomech.* **43**, 55–62 (2010).
182. Janmey, P. A. & Miller, R. T. Mechanisms of mechanical signaling in development and disease. *J. Cell Sci.* **124**, 9–18 (2011).
183. Nemir, S., Hayenga, H. N. & West, J. L. PEGDA hydrogels with patterned elasticity: Novel tools for the study of cell response to substrate rigidity. *Biotechnol. Bioeng.* **105**, 636–644 (2010).
184. Guvendiren, M., Perepelyuk, M., Wells, R. G. & Burdick, J. A. Hydrogels with differential and patterned mechanics to study stiffness-mediated myofibroblastic differentiation of hepatic stellate cells. *J. Mech. Behav. Biomed. Mater.* **38**, 198–208 (2014).
185. Nowatzki, P. J., Franck, C., Maskarinec, S. A., Ravichandran, G. & Tirrell, D. A. Mechanically tunable thin films of photosensitive artificial proteins: Preparation and characterization by nanoindentation. *Macromolecules* **41**, 1839–1845 (2008).
186. Khetan, S., Katz, J. S. & Burdick, J. A. Sequential crosslinking to control cellular spreading in 3-dimensional hydrogels. *Soft Matter* **5**, 1601–1606 (2009).
187. Khetan, S. & Burdick, J. A. Patterning network structure to spatially control cellular remodeling and stem cell fate within 3-dimensional hydrogels. *Biomaterials* **31**, 8228–8234 (2010).
188. Khetan, S. *et al.* Degradation-mediated cellular traction directs stem cell fate in covalently crosslinked three-dimensional hydrogels. *Nat Mater* **12**, 458–465 (2013).
189. Liu, Z. *et al.* Spatiotemporally Controllable and Cytocompatible Approach Builds 3D Cell Culture Matrix by Photo-Uncaged-Thiol Michael Addition Reaction. *Adv. Mater.* **26**, 3912–3917 (2014).
190. Mosiewicz, K. A., Kolb, L., Van Der Vlies, A. J. & Lutolf, M. P. Microscale patterning of hydrogel stiffness through light-triggered uncaging of thiols. *Biomater Sci* **2**, 1640–1651 (2014).

191. Cui, J., Wang, M., Zheng, Y., Rodríguez Muñiz, G. M. & del Campo, A. Light-Triggered Cross-Linking of Alginates with Caged Ca $^{2+}$. *Biomacromolecules* **14**, 1251–1256 (2013).
192. Stowers, R. S., Allen, S. C. & Suggs, L. J. Dynamic phototuning of 3D hydrogel stiffness. *Proc. Natl. Acad. Sci.* **112**, 1953–1958 (2015).
193. Brandenberg, N. & Lutolf, M. P. In Situ Patterning of Microfluidic Networks in 3D Cell-Laden Hydrogels. *Adv. Mater.* **28**, 7450–7456 (2016).
194. Heintz, K. A. *et al.* Fabrication of 3D Biomimetic Microfluidic Networks in Hydrogels. *Adv. Healthc. Mater.* **5**, 2153–2160 (2016).
195. Berkovitch, Y., Yelin, D. & Seliktar, D. Photo-patterning PEG-based Hydrogels for Neuronal Engineering. *Eur. Polym. J.* **72**, 473–483 (2015).
196. Johnson, J. A., Finn, M. G., Koberstein, J. T. & Turro, N. J. Synthesis of photocleavable linear macromonomers by ATRP and star macromonomers by a tandem ATRP-click reaction: Precursors to photodegradable model networks. *Macromolecules* **40**, 3589–3598 (2007).
197. Kloxin, A. M., Tibbitt, M. W. & Anseth, K. S. Synthesis of photodegradable hydrogels as dynamically tunable cell culture platforms. *Nat. Protoc.* **5**, 1867–1887 (2010).
198. Johnson, J. A., Baskin, J. M., Bertozzi, C. R., Koberstein, J. T. & Turro, N. J. Copper-free click chemistry for the in situ crosslinking of photodegradable star polymers. *Chem. Commun.* **0**, 3064–3066 (2008).
199. Wong, D. Y., Griffin, D. R., Reed, J. & Kasko, A. M. Photodegradable Hydrogels to Generate Positive and Negative Features over Multiple Length Scales. *Macromolecules* **43**, 2824–2831 (2010).
200. Frey, M. T. & Wang, Y. L. A photo-modulatable material for probing cellular responses to substrate rigidity. *Soft Matter* **5**, 1918–1924 (2009).
201. Tsang, K. M. C. *et al.* Facile One-Step Micropatterning Using Photodegradable Gelatin Hydrogels for Improved Cardiomyocyte Organization and Alignment. *Adv. Funct. Mater.* **25**, 977–986 (2015).
202. Kirschner, C. M. & Anseth, K. S. In situ control of cell substrate microtopographies using photolabile hydrogels. *Small* **9**, 578–584 (2013).
203. Kloxin, A. M., Tibbitt, M. W., Kasko, A. M., Fairbairn, J. a & Anseth, K. S. Tunable hydrogels for external manipulation of cellular microenvironments through controlled photodegradation. *Adv. Mater.* **22**, 61–6 (2010).
204. Tibbitt, M. W., Kloxin, A. M., Dyamenahalli, K. U. & Anseth, K. S. Controlled two-photon photodegradation of PEG hydrogels to study and manipulate subcellular interactions on soft materials. *Soft Matter* **6**, 5100–5108 (2010).
205. Kloxin, A. M., Benton, J. A. & Anseth, K. S. In situ elasticity modulation with dynamic substrates to direct cell phenotype. *Biomaterials* **31**, 1–8 (2010).
206. Wang, H., Haeger, S. M., Kloxin, A. M., Leinwand, L. A. & Anseth, K. S. Redirecting Valvular Myofibroblasts into Dormant Fibroblasts through Light-mediated Reduction in Substrate Modulus. *PLoS One* **7**, e39969 (2012).
207. Yang, C., Tibbitt, M. W., Basta, L. & Anseth, K. S. Mechanical memory and dosing influence stem cell fate. *Nat. Mater.* **13**, 645–652 (2014).
208. Tibbitt, M. W., Kloxin, A. M., Sawicki, L. A. & Anseth, K. S. Mechanical Properties and Degradation of Chain and Step-Polymerized Photodegradable Hydrogels. *Macromolecules* **46**, 2785–2792 (2013).
209. McKinnon, D. D., Brown, T. E., Kyburz, K. A., Kiyotake, E. & Anseth, K. S. Design and

Characterization of a Synthetically Accessible, Photodegradable Hydrogel for User-Directed Formation of Neural Networks. *Biomacromolecules* **15**, 2808–2816 (2014).
210. Arakawa, C. K., Badeau, B. A., Zheng, Y. & DeForest, C. A. Multicellular Vascularized Engineered Tissues through User-Programmable Biomaterial Photodegradation. *Adv. Mater.* **29**, 1703156 (2017).
211. Bernard, A. B., Lin, C.-C. C. & Anseth, K. S. A Microwell Cell Culture Platform for the Aggregation of Pancreatic beta-Cells. *Tissue Eng. Part C-Methods* **18**, 583–592 (2012).
212. Lewis, K. J. R. *et al.* In vitro model alveoli from photodegradable microsphere templates. *Biomater Sci* **3**, 821–832 (2015).
213. Kloxin, A. M. *et al.* Responsive culture platform to examine the influence of microenvironmental geometry on cell function in 3D. *Integr. Biol.* **4**, 1540–1549 (2012).
214. Fairbanks, B. D., Singh, S. P., Bowman, C. N. & Anseth, K. S. Photodegradable, Photoadaptable Hydrogels via Radical-Mediated Disulfide Fragmentation Reaction. *Macromolecules* **44**, 2444–2450 (2011).
215. Tamura, M. *et al.* Optical cell separation from three-dimensional environment in photodegradable hydrogels for pure culture techniques. *Sci. Rep.* **4**, 4793 (2014).
216. Truong, V. X. *et al.* Photodegradable Gelatin-Based Hydrogels Prepared by Bioorthogonal Click Chemistry for Cell Encapsulation and Release. *Biomacromolecules* **16**, 2246–2253 (2015).
217. Ki, C. S., Shih, H. & Lin, C. C. Facile preparation of photodegradable hydrogels by photopolymerization. *Polym.* **54**, 2115–2122 (2013).
218. Zhu, C. C. & Bettinger, C. J. Light-induced remodeling of physically crosslinked hydrogels using near-IR wavelengths. *J. Mater. Chem. B* **2**, 1613–1618 (2014).
219. Azagarsamy, M. A., McKinnon, D. D., Age, D. L. & Anseth, K. S. Coumarin-Based Photodegradable Hydrogel: Design, Synthesis, Gelation, and Degradation Kinetics. *ACS Macro Lett.* **3**, 515–519 (2014).
220. Andreopoulos, F. M. *et al.* Photoscissable hydrogel synthesis via rapid photopolymerization of novel PEG-based polymers in the absence of photoinitiators. *J. Am. Chem. Soc.* **118**, 6235–6240 (1996).
221. Andreopoulos, F. M., Beckman, E. J. & Russell, A. J. Light-induced tailoring of PEG-hydrogel properties. *Biomaterials* **19**, 1343–1352 (1998).
222. Andreopoulos, F. M., Beckman, E. J. & Russell, A. J. Photoswitchable PEG-CA hydrogels and factors that affect their photosensitivity. *J. Polym. Sci. Part A Polym. Chem.* **38**, 1466–1476 (2000).
223. Zheng, Y. *et al.* A novel photoscissile poly(ethylene glycol)-based hydrogel. *Adv. Funtional Mater.* **11**, 37–40 (2001).
224. Zheng, Y. J. *et al.* PEG-based hydrogel synthesis via the photodimerization of anthracene groups. *Macromolecules* **35**, 5228–5234 (2002).
225. Sako, Y. & Takaguchi, Y. A photo-responsive hydrogelator having gluconamides at its peripheral branches. *Org. Biomol. Chem.* **6**, 3843–3847 (2008).
226. Chen, Y. & Geh, J. L. Copolymers derived from 7-acryloyloxy-4-methylcoumarin and acrylates: 2. Reversible photocrosslinking and photocleavage. *Polymer (Guildf).* **37**, 4481–4486 (1996).
227. Maddipatla, M. V. S. N. *et al.* Photoresponsive Coumarin Polyesters That Exhibit Cross-Linking and Chain Scission Properties. *Macromolecules* **46**, 5133–5140 (2013).
228. Tamesue, S., Takashima, Y., Yamaguchi, H., Shinkai, S. & Harada, A. Photoswitchable

supramolecular hydrogels formed by cyclodextrins and azobenzene polymers. *Angew. Chem. Int. Ed. Engl.* **49**, 7461–4 (2010).
229. Rosales, A. M., Mabry, K. M., Nehls, E. M. & Anseth, K. S. Photoresponsive elastic properties of azobenzene-containing poly(ethylene-glycol)-based hydrogels. *Biomacromolecules* **16**, 798–806 (2015).
230. Rape, A. D., Zibinsky, M., Murthy, N. & Kumar, S. A synthetic hydrogel for the high-throughput study of cell–ECM interactions. *Nat. Commun.* **6**, 8129 (2015).
231. Smith, D. J. *et al.* A multiphase transitioning peptide hydrogel for suturing ultrasmall vessels. *Nat. Nanotechnol.* **11**, 95–102 (2016).
232. Sharma, B. *et al.* Human Cartilage Repair with a Photoreactive Adhesive-Hydrogel Composite. *Sci. Transl. Med.* **5**, 167ra6 (2013).
233. San Miguel, V., Bochet, C. G. & del Campo, A. Wavelength-Selective Caged Surfaces: How Many Functional Levels Are Possible? *J. Am. Chem. Soc.* **133**, 5380–5388 (2011).
234. Brown, T. E., Marozas, I. A. & Anseth, K. S. Amplified Photodegradation of Cell-Laden Hydrogels via an Addition-Fragmentation Chain Transfer Reaction. *Adv. Mater.* **29**, 1605001 (2017).
235. Zhao, Y.-L. & Stoddart, J. F. Azobenzene-Based Light-Responsive Hydrogel System. *Langmuir* **25**, 8442–8446 (2009).
236. Wang, D., Wagner, M., Butt, H.-J. & Wu, S. Supramolecular hydrogels constructed by red-light-responsive host–guest interactions for photo-controlled protein release in deep tissue. *Soft Matter* **11**, 7656–7662 (2015).
237. Schindler, S. E. *et al.* Photo-activatable Cre recombinase regulates gene expression in vivo. *Sci. Rep.* **5**, 13627 (2015).
238. Kawano, F., Okazaki, R., Yazawa, M. & Sato, M. A photoactivatable Cre–loxP recombination system for optogenetic genome engineering. *Nat. Chem. Biol.* **12**, 1059–1064 (2016).
239. Nihongaki, Y., Kawano, F., Nakajima, T. & Sato, M. Photoactivatable CRISPR-Cas9 for optogenetic genome editing. *Nat. Biotechnol.* **33**, 755–760 (2015).
240. Nihongaki, Y., Furuhata, Y., Otabe, T., Hasegawa, Saki Yoshimoto, K. & Sato, M. CRISPR-Cas9-based photoactivatable transcription systems to induce neuronal differentiation. *Nat. Methods* **14**, 963–966 (2017).
241. Shadish, J. A. & DeForest, C. A. Site-Selective Protein Modification: From Functionalized Proteins to Functional Biomaterials. *Matter* vol. 2 50–77 (2020).
242. Pakulska, M. M., Miersch, S. & Shoichet, M. S. Designer protein delivery: From natural to engineered affinity-controlled release systems. *Science* **351**, aac4750 (2016).
243. Sakiyama-Elbert, S. E. & Hubbell, J. A. Development of fibrin derivatives for controlled release of heparin-binding growth factors. *J. Control. Release* **65**, 389–402 (2000).
244. Sakiyama-Elbert, S. E. & Hubbell, J. A. Controlled release of nerve growth factor from a heparin-containing fibrin-based cell ingrowth matrix. *J. Control. Release* **69**, 149–158 (2000).
245. Tae, G., Scatena, M., Stayton, P. S. & Hoffman, A. S. PEG-cross-linked heparin is an affinity hydrogel for sustained release of vascular endothelial growth factor. *J. Biomater. Sci. Polym. Ed.* **17**, 187–197 (2006).
246. Hettiaratchi, M. H. *et al.* Competitive Protein Binding Influences Heparin-Based Modulation of Spatial Growth Factor Delivery for Bone Regeneration. *Tissue Eng. - Part A* **23**, 683–695 (2017).

247. Vulic, K. & Shoichet, M. S. Tunable growth factor delivery from injectable hydrogels for tissue engineering. *J. Am. Chem. Soc.* **134**, 882–885 (2012).
248. Savoca, M. P., Tonoli, E., Atobatele, A. G. & Verderio, E. A. M. Biocatalysis by transglutaminases: A review of biotechnological applications. *Micromachines* **9**, 562 (2018).
249. Davis, N. E., Ding, S., Forster, R. E., Pinkas, D. M. & Barron, A. E. Modular enzymatically crosslinked protein polymer hydrogels for in situ gelation. *Biomaterials* **31**, 7288–7297 (2010).
250. Jones, M. E. R. & Messersmith, P. B. Facile coupling of synthetic peptides and peptide–polymer conjugates to cartilage via transglutaminase enzyme. *Biomaterials* **28**, 5215–5224 (2007).
251. Schense, J. C. & Hubbell, J. A. Cross-Linking Exogenous Bifunctional Peptides into Fibrin Gels with Factor XIIIa. *Bioconjug. Chem.* **10**, 75–81 (1999).
252. Ehrbar, M. *et al.* Biomolecular hydrogels formed and degraded via site-specific enzymatic reactions. *Biomacromolecules* **8**, 3000–3007 (2007).
253. Griffin, D. R., Weaver, W. M., Scumpia, P. O., Di Carlo, D. & Segura, T. Accelerated wound healing by injectable microporous gel scaffolds assembled from annealed building blocks. *Nat. Mater.* **14**, 737–744 (2015).
254. Broguiere, N., Isenmann, L. & Zenobi-Wong, M. Novel enzymatically cross-linked hyaluronan hydrogels support the formation of 3D neuronal networks. *Biomaterials* **99**, 47–55 (2016).
255. Broguiere, N., Cavalli, E., Salzmann, G. M., Applegate, L. A. & Zenobi-Wong, M. Factor XIII Cross-Linked Hyaluronan Hydrogels for Cartilage Tissue Engineering. *ACS Biomater. Sci. Eng.* **2**, 2176–2184 (2016).
256. Dai, X., Böker, A. & Glebe, U. Broadening the scope of sortagging. *RSC Advances* vol. 9 4700–4721 (2019).
257. Mazmanian, S. K. *et al.* Staphylococcus aureus sortase, an enzyme that anchors surface proteins to the cell wall. *Science* **285**, 760–763 (1999).
258. Parthasarathy, R., Subramanian, S. & Boder, E. T. Sortase A as a novel molecular 'stapler' for sequence-specific protein conjugation. *Bioconjug. Chem.* **18**, 469–476 (2007).
259. Arkenberg, M. R. & Lin, C. C. Orthogonal enzymatic reactions for rapid crosslinking and dynamic tuning of PEG-peptide hydrogels. *Biomater. Sci.* **5**, 2231–2240 (2017).
260. Arkenberg, M. R., Moore, D. M. & Lin, C. C. Dynamic control of hydrogel crosslinking via sortase-mediated reversible transpeptidation. *Acta Biomater.* **83**, 83–95 (2019).
261. Valdez, J. *et al.* On-demand dissolution of modular, synthetic extracellular matrix reveals local epithelial-stromal communication networks. *Biomaterials* **130**, 90–103 (2017).
262. Lee, U. N. *et al.* Layer-by-layer fabrication of 3D hydrogel structures using open microfluidics. *Lab Chip* (2020) doi:10.1039/C9LC00621D.
263. Cambria, E. *et al.* Covalent Modification of Synthetic Hydrogels with Bioactive Proteins via Sortase-Mediated Ligation. *Biomacromolecules* **16**, 2316–2326 (2015).
264. Broguiere, N. *et al.* Morphogenesis guided by 3D patterning of growth factors in biological matrices. *bioRxiv* (2019) doi:10.1101/828947.
265. Warden-Rothman, R., Caturegli, I., Popik, V. & Tsourkas, A. Sortase-Tag Expressed Protein Ligation: Combining Protein Purification and Site-Specific Bioconjugation into a Single Step. *Anal. Chem.* **85**, 11090–11097 (2013).
266. Liu, L. *et al.* Cyclic Stiffness Modulation of Cell-Laden Protein – Polymer Hydrogels in

Response to User-Specified Stimuli Including Light. *Adv. Biosyst.* **2**, 1–9 (2018).
267. Gawade, P. M., Shadish, J. A., Badeau, B. A. & DeForest, C. A. Logic-Based Delivery of Site-Specifically Modified Proteins from Environmentally Responsive Hydrogel Biomaterials. *Adv. Mater.* **31**, 1902462 (2019).
268. Shadish, J. A., Benuska, G. M. & DeForest, C. A. Bioactive site-specifically modified proteins for 4D patterning of gel biomaterials. *Nat. Mater.* **18**, 1005–1014 (2019).
269. Antos, J. M., Truttmann, M. C. & Ploegh, H. L. Recent advances in sortase-catalyzed ligation methodology. *Curr. Opin. Struct. Biol.* **38**, 111–118 (2016).
270. Zakeri, B. *et al.* Peptide tag forming a rapid covalent bond to a protein, through engineering a bacterial adhesin. *Proc. Natl. Acad. Sci.* **109**, E690-7 (2012).
271. Hatlem, D., Trunk, T., Linke, D. & Leo, J. C. Catching a SPY: Using the SpyCatcher-SpyTag and related systems for labeling and localizing bacterial proteins. *Int. J. Mol. Sci.* **20**, (2019).
272. Sun, F., Zhang, W.-B. B., Mahdavi, A., Arnold, F. H. & Tirrell, D. A. Synthesis of bioactive protein hydrogels by genetically encoded SpyTag-SpyCatcher chemistry. *Proc Natl Acad Sci U S A* **111**, 11269–11274 (2014).
273. Gao, X., Lyu, S. & Li, H. Decorating a Blank Slate Protein Hydrogel: A General and Robust Approach for Functionalizing Protein Hydrogels. *Biomacromolecules* **18**, 3726–3732 (2017).
274. Liu, X. *et al.* Versatile Engineered Protein Hydrogels Enabling Decoupled Mechanical and Biochemical Tuning for Cell Adhesion and Neurite Growth. *ACS Appl. Nano Mater.* **1**, 1579–1585 (2018).
275. Wu, W.-H., Wei, J. & Zhang, W.-B. Controlling SpyTag/SpyCatcher Reactivity via Redox-Gated Conformational Restriction. *ACS Macro Lett.* **7**, 1388–1393 (2018).
276. Hammer, J. A., Ruta, A., Therien, A. M. & West, J. L. Cell-Compatible, Site-Specific Covalent Modification of Hydrogel Scaffolds Enables User-Defined Control over Cell–Material Interactions. *Biomacromolecules* **20**, 2486–2493 (2019).
277. Veggiani, G. *et al.* Programmable polyproteams built using twin peptide superglues. *Proc. Natl. Acad. Sci.* **113**, 1202–7 (2016).
278. Wieduwild, R. & Howarth, M. Assembling and decorating hyaluronan hydrogels with twin protein superglues to mimic cell-cell interactions. *Biomaterials* **180**, 253–264 (2018).
279. Thrane, S. *et al.* Bacterial superglue enables easy development of efficient virus-like particle based vaccines. *J. Nanobiotechnology* **14**, 30 (2016).
280. Brune, K. D. *et al.* Plug-and-Display: decoration of Virus-Like Particles via isopeptide bonds for modular immunization. *Sci. Rep.* **6**, (2016).
281. Guo, Y., Wang, J.-X., Zhang, H.-L. & Fan, X.-W. Recent Advances of Butelase 1 in Peptide/Protein Ligations. *Curr. Org. Chem.* **22**, 780–788 (2018).
282. Weeks, A. M. & Wells, J. A. Subtiligase-Catalyzed Peptide Ligation. *Chem. Rev.* acs.chemrev.9b00372 (2019) doi:10.1021/acs.chemrev.9b00372.
283. Nakamura, H. *et al.* Intracellular production of hydrogels and synthetic RNA granules by multivalent molecular interactions. *Nat. Mater.* **17**, 79–88 (2018).
284. Gübeli, R. J. *et al.* Pharmacologically triggered hydrogel for scheduling hepatitis B vaccine administration. *Sci. Rep.* **3**, (2013).
285. Nele, V. *et al.* Ultrasound-Triggered Enzymatic Gelation. *Adv. Mater.* 1905914 (2020) doi:10.1002/adma.201905914.
286. Lyu, S. *et al.* Optically controlled reversible protein hydrogels based on photoswitchable

fluorescent protein Dronpa. *Chem. Commun.* **53**, 13375–13378 (2017).
287. Wang, R., Yang, Z., Luo, J., Hsing, I. M. & Sun, F. B12-dependent photoresponsive protein hydrogels for controlled stem cell/protein release. *Proc. Natl. Acad. Sci.* **114**, 5912–5917 (2017).
288. Yang, Z. *et al.* Dynamically Tunable, Macroscopic Molecular Networks Enabled by Cellular Synthesis of 4-Arm Star-like Proteins. *Matter* **2**, 233–249 (2019).
289. Hammer, J. A., Ruta, A. & West, J. L. Using Tools from Optogenetics to Create Light-Responsive Biomaterials: LOVTRAP-PEG Hydrogels for Dynamic Peptide Immobilization. *Ann. Biomed. Eng.* (2019) doi:10.1007/s10439-019-02407-w.
290. Shadish, J. A., Strange, A. C. & DeForest, C. A. Genetically Encoded Photocleavable Linkers for Patterned Protein Release from Biomaterials. *J. Am. Chem. Soc.* **141**, 15619–15625 (2019).
291. Rost, B. R., Schneider-Warme, F., Schmitz, D. & Hegemann, P. Optogenetic Tools for Subcellular Applications in Neuroscience. *Neuron* vol. 96 572–603 (2017).
292. Riggsbee, C. W. & Deiters, A. Recent advances in the photochemical control of protein function. *Trends in Biotechnology* vol. 28 468–475 (2010).
293. Kennedy, M. J. *et al.* Rapid blue-light-mediated induction of protein interactions in living cells. *Nat. Methods* **7**, 973–975 (2010).
294. Kaberniuk, A., Shemetov, A. A. & Verkhusha, V. V. A bacterial phytochrome-based optogenetic system controllable with near-infrared light. *Nat. Methods* **13**, 591–597 (2016).
295. Spiltoir, J. I. & Tucker, C. L. Photodimerization systems for regulating protein-protein interactions with light. *Curr. Opin. Struct. Biol.* **57**, 1–8 (2019).
296. Kinjo, T. *et al.* FRET-assisted photoactivation of flavoproteins for in vivo two-photon optogenetics. *Nat. Methods* **16**, 1029–1036 (2019).
297. Nihongaki, Y., Kawano, F., Nakajima, T. & Sato, M. Photoactivatable CRISPR-Cas9 for optogenetic genome editing. *Nat. Biotechnol.* **33**, 755–60 (2015).
298. Nihongaki, Y., Otabe, T., Ueda, Y. & Sato, M. A split CRISPR–Cpf1 platform for inducible genome editing and gene activation. *Nat. Chem. Biol.* **15**, 882–888 (2019).
299. Weinberg, B. H. *et al.* High-performance chemical- and light-inducible recombinases in mammalian cells and mice. *Nat. Commun.* **10**, (2019).
300. Yu, D. *et al.* Optogenetic activation of intracellular antibodies for direct modulation of endogenous proteins. *Nat. Methods* **16**, 1095–1100 (2019).
301. Kawano, F., Suzuki, H., Furuya, A. & Sato, M. Engineered pairs of distinct photoswitches for optogenetic control of cellular proteins. *Nat. Commun.* **6**, (2015).
302. Chin, J. W. Expanding and reprogramming the genetic code. *Nature* vol. 550 53–60 (2017).
303. Baumann, T. *et al.* Computational aminoacyl-tRNA synthetase library design for photocaged tyrosine. *Int. J. Mol. Sci.* **20**, (2019).
304. Courtney, T. & Deiters, A. Recent advances in the optical control of protein function through genetic code expansion. *Current Opinion in Chemical Biology* vol. 46 99–107 (2018).
305. Brown, W., Liu, J., Tsang, M. & Deiters, A. Cell-Lineage Tracing in Zebrafish Embryos with an Expanded Genetic Code. *ChemBioChem* **19**, 1244–1249 (2018).

Chapter 2: DISSERTATION AIMS

The biological microenvironment is a complex, constantly changing space featuring varying levels of a multitude of cell-secreted signaling molecules that serve as the communicatory elements of biology. This communication between cells both within and across tissues is necessary to ensure proper growth, function, and survival of the organism, and relies on multifaceted protein-based signaling pathways to inhibit and promote specific cellular fates. By better understanding how well-defined combinations of individual proteins work in (a)synchrony to direct cellular and integrated tissue function, we can begin to unravel the irregularities within diseased systems and utilize this information to engineer therapies that promote healthy recovery. In this regard, photoresponsive biomaterials have proven to be viable platforms to resolve such 4D biological intricacies by providing user-defined biochemical and biophysical control of a tissue-like *in vitro* system.

While the application of photochemistries within biomaterials continues to rise, there is exceptionally limited knowledge of how cells respond to the associated light treatments, most typically short periods of high-wavelength ultraviolet light. To address this void, in Chapter 3:, we will examine the effects of commonly employed UV light treatments on cell function by quantifying post-irradiative growth, apoptotic events, and proteomic response. Building on the concepts of photoresponsive biomaterials, in Chapter 4:, we will expand the capabilities of "smart" biomaterials to allow complex combinations of environmental and external inputs to trigger the release of small molecules. We aim to establish a highly modular design such that the system can be easily programmed to respond to collections of user-defined inputs (e.g., light, cell-secreted enzymes, reductants), enabling therapeutic targeting to specific bodily locations that present unique biomarker combinations.

Just as photochemistry has proven an essential tool to alter the extracellular environment with spatiotemporal control, these types of reactions have been utilized to direct protein-protein interactions (PPIs) and protein function inside single cells. However, all photoresponsive systems offering control of PPIs reported to date have been limited by their transient and reversible nature, thereby requiring repetitive light doses to maintain the interaction and restricting applications. In Chapter 5:A Genetically Encoded Protein-Protein Photoligation through Light-Activated SpyCatcher**Error! Reference source not found.**, we seek to establish the first genetically encoded strategy to irreversibly promote specific protein binding, PPIs, and function using light. Exploiting genetic code expansion to photocage a critical lysine residue required for spontaneous isopeptide bond formation between two protein pairs, we attempt to gain photocontrol over the SpyCatcher/Tag ligation and to demonstrate the system's utility for optogenetic regulation of cell fate.

Finally, we conclude and offer forward-looking commentary on the implications of this work. In Chapter 6:, we will present unique methods to expand the accessibility and increase applications of techniques posed here. We envision this work will be valuable in probing complex questions of biological function and fate.

Chapter 3: PROTEOME-WIDE ANALYSIS OF CELLULAR RESPONSE TO ULTRAVIOLET LIGHT

As published: Ruskowitz, E.R., DeForest, C.A. Proteome-wide Analysis of Cellular Response to Ultraviolet Light for Biomaterial Synthesis and Modification. *ACS Biomaterials Science & Engineering*, **5**, 2111-2116 (2019).

3.1 ABSTRACT

Though the biomaterials community has widely utilized near-ultraviolet (UV) light to make and modify scaffolds for 3D cell culture, thorough examination of the downstream effects of such light on cell function has not been performed. Here, we investigate the global effects of common light treatments on NIH3T3 fibroblasts and human mesenchymal stem cells (hMSCs), cell types regularly employed in tissue engineering (**Figure 3.1**). Unchanged proliferation rates, an absence of apoptotic induction, and an unaltered proteome following low-dose 365 nm light exposure are observed, implying that near-UV-based radical-free photochemistries can be exploited in biomaterial systems without deleteriously affecting cell fate.

Figure 3.1. Cellular response to varying doses of 365 and 254 nm ultraviolet light was determined through quantitative analysis of cell proliferation, apoptotic events, and proteomic shifts.

3.2 Cellular Response to Ultraviolet Light

Photochemistries uniquely enable spatiotemporal control over biomaterial formation and chemical/physical modification[1], providing powerful strategies to probe and direct dynamic bioprocesses *in vitro*[2]. Among many examples, light-induced reactions have been utilized to irreversibly degrade hydrogels[1], covalently decorate materials with proteins[3], and to activate immunomodulatory peptide presentation *in vivo*[4]. Photoreactions are unique in that they can be confined to specific 4D locations (i.e., 3D space and time) designated by when and where photons are delivered to the sample. Theoretically limited only by the wavelength of utilized light, photochemical patterning resolution (~1 μm) is much smaller than the size of a single cell (~10 μm), enabling reactions to be controlled over virtually all biologically relevant length scales[5,6].

For photochemically modulated biomaterial systems involving living cells, wavelength selection represents a careful balance of several factors: photons must possess high enough energy to induce the intended reactions but not so much to incur oxidative stress or DNA mutations[7]. Though a suite of chemistries efficiently react to middle-UV light (λ = 200 – 300 nm, typically 254 nm), exposure to these high-energy wavelengths are widely accepted to damage cells through the production of DNA lesions in the form of cyclobutane pyrimidine dimers and pyrimidine-pyrimidone (6-4) photoproducts[7]. As such, the biomaterials community has gravitated towards using near-UV light (λ = 300 – 400 nm, most commonly 365 nm) to initiate reactions in the presence of living cells. Despite this regular utilization, there is lingering concern that such near-UV light exposure may induce damage through generation of reactive oxygen species (ROS)[8,9] or DNA oxidation[10]. Such long-term mutagenic effects can potentially be mitigated through cell cycle arrest and repair pathways through excision and replacement of damaged DNA prior to further replication[11]. Given the cell's endogenous propensity to repair possible UV-induced damage, in-

depth analyses of the functional state of cells downstream of treatment is necessary to understand the long-term effects of near-UV light exposure, particularly in a biomaterials' context.

Though some information is known about light's wavelength-dependent effects on DNA chemistry, perhaps more important is how such possible changes carry forward and manifest throughout transcription and translational processes. Although mRNA is directly translated into proteins, regulatory and post-translational processes hinder direct correlation between gene and protein abundance, necessitating measures of the key communicatory space – the proteome[12]. Current high-throughput proteomic tools permit quantitative, in-depth investigations into cell response downstream of stimuli. These techniques can provide a highly precise understanding of proteomic shifts in response to environmental perturbations or well-defined treatments with no prior prediction of the mechanisms of action. One such technique, pulsed stable isotope labeling by amino acids in cell culture (pSILAC), provides quantitative, comparative information between treated and untreated populations by incorporating isotopically heavy labels into newly translated proteins. Relative label abundance within each protein species, as determined through liquid chromatography coupled to tandem mass spectrometry (LC-MS/MS), offers a high-throughput approach to understanding how treatment globally influences protein production. Such experiments provide deeper insight into common practices that may otherwise bias experimental results. This manuscript highlights new findings on the proteomic response of multiple cell lines to UV light at dosages highly relevant in the synthesis and modification of biomaterials.

Even with its frequent utilization in biomaterials, studies investigating the cellular response to narrow band-pass, near-UV light are limited. Cytocompatibility has primarily been determined through simple proliferation assays at conditions common within biomaterials (λ = 365 nm, ~10 mW cm^{-2}, 10 min)[13,14]. More recently, the Kasko group investigated the effects of low-dose, near-

UV light on hMSC function and found no significant change in global gene expression after multiple exposures totaling 25 min at λ = 300 – 425 nm (3.5 mW cm^{-2})[15]; though this was a substantial finding, the broad-range light exposures and repetitive dosing does not mimic the most common photoconditions used to modify biomaterials, leaving open questions concerning the effects of more typical treatments on cell fate.

Herein, we sought to examine the downstream effects on cellular phenotype after exposure to UV light using global quantitative proteomic techniques. NIH3T3 mouse fibroblasts and hMSCs, two highly utilized cell types in 3D cell culture and material development that differ in proliferation rate and sensitivity, were maintained at 37 °C and 5% CO_2 on tissue-culture polystyrene T-75 flask (Genesee Scientific). NIH3T3s were cultured in Dulbecco's Modified Eagle Media (Thermo Fisher Scientific) containing glucose (4.5 g L^{-1}) supplemented with fetal bovine serum (FBS, 10%, Corning) and penicillin/streptomycin (PS, 1%, Corning), while hMSCs were maintained in complete MesenPRO RS medium (Thermo Fisher Scientific). Cells were seeded on six-well tissue culture polystyrene plates (Genessee Scientific) for 24 h prior to exchanging media with Dulbecco's phosphate-buffered saline containing magnesium and calcium (DPBS, Corning) and subsequent light treatment. Cells were exposed to collimated near-UV light (λ = 365 nm; 10 min at 1, 5, 10, and 20 mW cm^{-2}; Omnicure 1500) equipped with a 360 nm cut-off filter (Omega Optical Inc.) or middle-UV (λ = 254 nm, 0.5 min at 0.3 mW cm^{-2}, UVP Mineralight UVGL-25) before swapping back to complete media. The addition of a 360 nm cutoff filter acts as an engineered control to eliminate lower wavelengths due to possible light-source filter degradation or the natural bell-curve emission spectra of a mercury lamp.

To determine if light exposures altered cellular growth rate, proliferation was quantified (PicoGreen Assay, Molecular Probes) 24 h after light exposure. No significant changes in

proliferation were found after 365 nm light treatments (10 min at 1, 5, 10, and 20 mW cm^{-2}) in either NIH3T3s or hMSCs (**Figure 3.2A**) as compared with unexposed controls. In contrast, 254 nm treatments (0.5 min at 0.3 mW cm^{-2}) significantly decreased proliferation in both cell types, suggesting that middle-UV yielded irreparable DNA damage resulting in cell death or cell-cycle arrest. To further investigate an acceptable threshold of exposure of near-UV light, studies were extended to larger dosages (λ = 365 nm, 10 – 90 min at 10 and 20 mW cm^{-2}). Experiments revealed that hMSC proliferation is not affected with statistical significance ($p < 0.01$) until being exposed to near-UV light at 20 mW cm^{-2} for ≥ 90 min; NIH3T3 proliferation decreased slightly after ≥ 60 minutes of exposure (**Figure 3.2B**). These findings imply that the short exposures traditionally employed to photochemically control biomaterial properties do not affect cell function, though the decreased proliferation observed with very high light dosages motivates a deeper analysis of intracellular response under more typical exposure conditions.

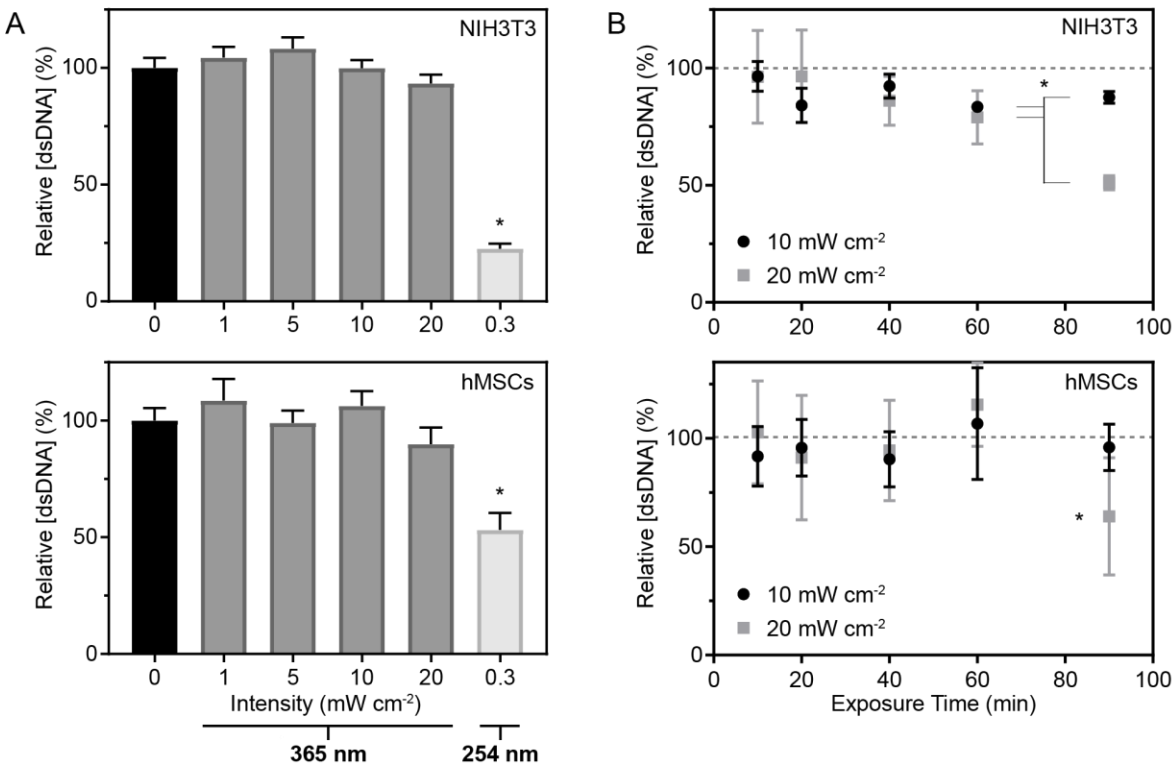

Figure 3.2. Cell proliferation was quantified 24 h after light treatment, **A**, (10 min for λ = 365 nm or 0.5 min for λ = 254 nm) at varied intensities (0 – 20 mW cm^{-2}) for (top) NIH3T3s and (bottom) hMSCs using the PicoGreen Assay. **B**, Similarly, the effects of prolonged near-UV exposure (10 – 90 min for λ = 365 nm at 10 and 20 mW cm^{-2}) on proliferation of NIH3T3s (top) and hMSCs (bottom) was quantified. * corresponds to statistically significant differences in observed values ($p < 0.01$, t-test) relative to unexposed controls. Error bars correspond to ±1 standard deviation about the mean for n≥4 biological replicates.

UV light is known to initiate pro-apoptotic pathways after the production of DNA photoproducts and in response to UV-induced oxidative stress[16]. Apoptotic pathways converge to the activation of downstream executioner caspases-3, -6, and -7 prior to programmed cell death[17]. To determine if apoptotic damage accompanied the selected treatments (λ = 365 nm, 10 min at 1, 5, 10, and 20 mW cm^{-2}; λ = 254 nm, 0.5 min at 0.3 mW cm^{-2}), we quantified caspase-3/7 activation 24 h after UV exposure by determining the percentage of activated cells (CellEvent, green) relative to total cell count (Hoechst 33342, blue) after staining and fluorescent imaging (**Figure 3.3**). In agreement with results from proliferation assays, NIH3T3s and hMSCs exhibited a quantitative

increase in caspase activation following 254 nm light treatment while cells treated with 365 nm light were statistically indistinguishable from unexposed controls ($p < 0.01$). These findings indicate that light-induced apoptosis occurs in a wavelength-dependent manner, further emphasizing the importance of appropriately selecting light treatments when working with photoresponsive biomaterials.

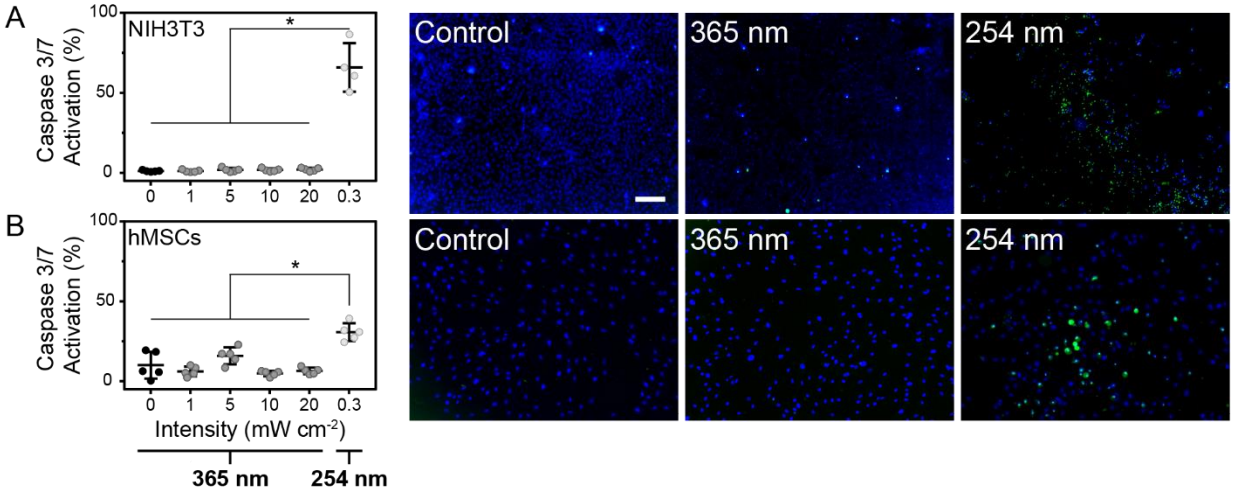

Figure 3.3. Apoptotic activation of **A**, NIH3T3s and **B**, hMSCs 24 h after light treatment (10 min for λ = 365 nm or 0.5 min for λ = 254 nm) at varied intensities (0 – 20 mW cm^{-2}). Activation was quantified through co-labeling with CellEvent Caspase-3/7 (green) and Hoechst 33342 nuclear stain (blue). Percent activation was calculated as the ratio of Caspase-3/7-positive cells (green) relative to the total number of cells (blue). Representative fluorescent images highlight significant activation following 254 nm light exposure (0.3 mW cm^{-2}, 0.5 min), as well as a lack of apoptosis in 365 nm-treated (10 mW cm^{-2}, 10 min) and unexposed control samples (p-value < 0.01). Error bars in column scatter plots correspond to ±1 standard deviation about the mean for n≥4 biological replicates. Scale bar = 250 μm.

With constant proliferation rates and an absence of apoptosis in either cell type, we employed high-throughput pSILAC to provide an in-depth analysis of global cell response of NIH3T3s and hMSCs to UV light. pSILAC offers quantification of all newly synthesized proteins, yielding insight into the processes occurring downstream of stimulation (**Figure 3.4A**)[18]. Based on protein concentrations (BCA assay, ThermoFisher), two protein samples generated using different isotopic labels are combined at a 1:1 ratio to quantify variations in protein synthesis after

light treatment. Here, we incorporated a lysine isotope into the proteome by swapping the growth medium to that containing either a "medium heavy" (D4-L-lysine, Cambridge Isotope Laboratories) or "heavy" ($^{13}C_6{}^{15}N_2$-L-lysine, Cambridge Isotope Laboratories) L-lysine hydrochloride (146 mg L^{-1} equivalents) for 24 h after exposure to either 365 nm light at 10 mW cm^{-2} or 254 nm light at 0.3 mW cm^{-2} (**Figure 3.4A**). Three biological replicates, including label-swap experiments, were collected for each treatment condition. Proteins were further purified and digested with the endopeptidase LysC (Wako Chemicals) to produce singly labeled peptides for quantification through LC-MS/MS (Supporting Information).

Acquired raw data were processed using the MaxQuant[19]/Andromeda[20] platform (v.1.5.3.30) under default settings (Supporting Information) to provide quantitative results reported here as treated/control (H/M or M/H) or fold change. Further data interpretation was performed on the normalized protein ratios, which accounts for unequal mixing or loading, in Perseus (v.1.6.1.2), a software platform to analyze quantitative proteomic data[21]. First, data was filtered for false detections, contaminants, and proteins detected by a single site. Stringent filtering for proteins detected in less than 70% of the replicates were then removed leaving 383 and 153 unique proteins in the NIH3T3 and hMSC datasets, respectively. Filtered data was then $\log_2$ transformed to center fold changes in protein expression around 0 (**Figure 3.S1**). Representative NIH3T3 biological replicates (**Figure 3.4B**) from the control and 365 nm groups clustered primarily around 0 while 254 nm samples correlated highly (average Pearson value of 0.90). In contrast to 254 nm light where changes were reproducibly detected, these trends indicate that 365 nm UV light exposure does not substantially shift protein production or alter the proteome.

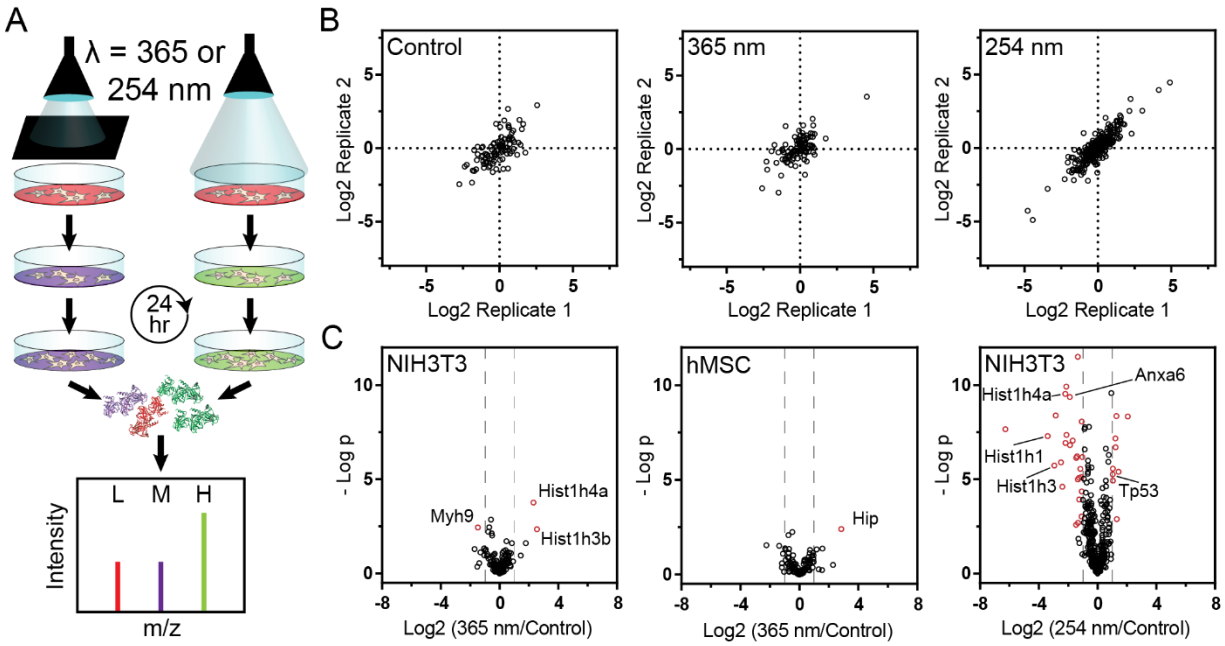

Figure 3.4. Quantification of the global proteomic response to UV light in cell culture. **A**, Pulsed stable isotopic labeling by amino acids in cell culture (pSILAC) permitted quantification of newly synthesized proteins after treatment with 254 nm (0.3 mW cm^{-2}, 0.5 min) or 365 nm light (10 mW cm^{-2}, 10 min). Relative protein expression was determined by combining treated samples with an unexposed control sample, digesting proteins into peptide fragments, and processing LC-MS/MS spectra. **B**, Representative correlations of the relative protein expression (log_2 treated/untreated) demonstrate consistent response in NIH3T3 label-swapped biological replicates. **C**, Treated samples were compared to controls to determine statistically significant differences in newly expressed proteins. Proteins with ratios significantly different (two-sided *t*-test with a false discovery rate of 0.01) from 1 are indicated by red circles. Vertical dashed lines indicate a protein ratio of ± 2.

Datasets were further analyzed for differentially regulated proteins after light exposure. To determine statistical significance, treatment replicates were grouped and compared to control samples using a two-sided *t*-test with the false discovery rate set to 0.01 (**Figure 3.4C**). Proteins resulting in a two-fold change in expression following treatment were considered significant. In NIH3T3s, only three proteins exhibited differential expression values after exposure to 365 nm light: the Myosin-9 motor-protein and potential marker of metastasis[22] was downregulated 2.8-fold, while histones-H3.2 and -H4 were upregulated 6.1- and 13.9-fold, respectively. These core

histones are structural proteins essential in nucleosomes that have shown fluctuation in gene expression correlating to cell-cycle phases[23]. While specific function of these histones is extremely dependent on post-translational modifications, UV-induced DNA damage (254 nm) initiates chromatin relaxation and localized H4 reduction within minutes to facilitate repair pathways[24–26]. As no up-regulation in key downstream markers associated with UV-induced DNA damage was detected for 365 nm exposure, we attribute the observed upregulation to slight differences in cell phase. For hMSCs, a single chaperone protein, heat-shock protein-70 interacting protein (Hip), was found to be upregulated 6.9-fold following 365 nm treatment (**Figure 3.4C**). Although Hip may take part in regulation of proliferation and apoptosis, very little experimental data exists to correlate expression changes to physiologic changes and proliferation and apoptosis rates matched control samples (**Figure 3.2** & **Figure 3.3B**)[27]. As these data indicate that near-UV 365 nm light does not induce significant proteomic shifts or activation of specific pathways, it can be considered cytocompatible.

In agreement with proliferation and apoptosis assays, middle-UV 254 nm light treatment significantly shifted protein expression in NIH3T3 cells (**Figure 3.4C**). 40 proteins were differentially expressed 24 h after 254 nm light (**Table 3.4.2S1**). Included in this list were histones-H1.2, -H2A, -H3.2, and -H4, which were found to be significantly down-regulated, and cellular tumor protein p53 which was among the 10 up-regulated proteins. DNA damage induced by ionizing radiation represses histone expression in a p53-dependent manner[28]. Additionally, further analysis using the STRING functional protein association network database[29] suggests its significant downregulation in metabolic pathways ($p < 0.005$). These results corroborate expected damage caused by 254 nm light.

The unique ability to direct light exposure near-instantaneously in 4D has enabled the development of materials for triggered drug delivery and advanced cell culture. To fully translate these systems into biological settings, complete knowledge of the biological impact of each of its element, including light dosage, is essential. Here, we provide a vital investigation of the biological impact of low-dose UV light treatments regularly used to control photochemistries in biomaterials. Proliferation rates remained unchanged and apoptosis was not induced after exposure to varied intensities of 365 nm light in two cell types; meanwhile, cells were significantly altered by exposure to lower wavelength UV light. Using pSILAC, we looked deeper for initiation of common repair pathways or any signal of cellular damage following treatment through analysis of the proteome and again found no significant changes in response to 365 nm light. Combined, low doses of 365 nm light are safe for application in a biological setting. However, the varied response to 254 nm light between NIH3T3s and hMSCs suggests a cell-line dependent sensitivity. This work gives credence to the further utilization of radical-free near-UV photochemistry in creation and modification of biomaterial systems without deleteriously affecting cell fate.

3.3 REFERENCES

1. Kloxin, A. M., Kasko, A. M., Salinas, C. N. & Anseth, K. S. Photodegradable Hydrogels for Dynamic Tuning of Physical and Chemical Properties. *Science* **324**, 59–63 (2009).
2. Ruskowitz, E. R. & DeForest, C. A. Photoresponsive biomaterials for targeted drug delivery and 4D cell culture. *Nat. Rev. Mater.* **3**, 17087 (2018).
3. DeForest, C. A. & Tirrell, D. A. A photoreversible protein-patterning approach for guiding stem cell fate in three-dimensional gels. *Nat Mater* **14**, 523–531 (2015).
4. Lee, T. T. *et al.* Light-triggered in vivo activation of adhesive peptides regulates cell adhesion, inflammation and vascularization of biomaterials. *Nat. Mater.* **14**, 352–360 (2015).
5. Arakawa, C. K., Badeau, B. A., Zheng, Y. & DeForest, C. A. Multicellular Vascularized Engineered Tissues through User-Programmable Biomaterial Photodegradation. *Adv. Mater.* **29**, 1703156 (2017).
6. Adelmund, S. M., Ruskowitz, E. R., Farahani, P. E., Wolfe, J. V. & DeForest, C. A. Light-Activated Proteomic Labeling via Photocaged Bioorthogonal Non-Canonical Amino Acids. *ACS Chem. Biol.* **13**, 573–577 (2018).

7. Pfeifer, G. P., You, Y.-H. & Besaratinia, A. Mutations induced by ultraviolet light. *Mutat. Res. Mol. Mech. Mutagen.* **571**, 19–31 (2005).
8. Cadet, J., Sage, E. & Douki, T. Ultraviolet radiation-mediated damage to cellular DNA. *Mutat. Res. Mol. Mech. Mutagen.* **571**, 3–17 (2005).
9. Lawrence, K. P. *et al.* The UV/Visible Radiation Boundary Region (385–405 nm) Damages Skin Cells and Induces "dark" Cyclobutane Pyrimidine Dimers in Human Skin in vivo. *Sci. Rep.* **8**, 12722 (2018).
10. Kozmin, S. *et al.* UVA radiation is highly mutagenic in cells that are unable to repair 7,8-dihydro-8-oxoguanine in Saccharomyces cerevisiae. *Proc. Natl. Acad. Sci.* **102**, 13538–43 (2005).
11. Dunkern, T. R., Fritz, G. & Kaina, B. Ultraviolet light-induced DNA damage triggers apoptosis in nucleotide excision repair-deficient cells via Bcl-2 decline and caspase-3/-8 activation. *Oncogene* **20**, 6026–6038 (2001).
12. Vogel, C. & Marcotte, E. M. Insights into the regulation of protein abundance from proteomic and transcriptomic analyses. *Nat. Rev. Genet.* **13**, 227–232 (2012).
13. Bryant, S. J., Nuttelman, C. R. & Anseth, K. S. Cytocompatibility of UV and visible light photoinitiating systems on cultured NIH/3T3 fibroblasts in vitro. *J. Biomater. Sci. Ed.* **11**, 439–457 (2000).
14. Gerecht, S. *et al.* Hyaluronic acid hydrogel for controlled self-renewal and differentiation of human embryonic stem cells. *Proc. Natl. Acad. Sci.* **104**, 11298–303 (2007).
15. Wong, D. Y., Ranganath, T. & Kasko, A. M. Low-Dose, Long-Wave UV Light Does Not Affect Gene Expression of Human Mesenchymal Stem Cells. *PLoS One* **10**, e0139307 (2015).
16. Ikehata, H. *et al.* UVA1 Genotoxicity Is Mediated Not by Oxidative Damage but by Cyclobutane Pyrimidine Dimers in Normal Mouse Skin. *J. Invest. Dermatol.* **128**, 2289–2296 (2008).
17. Budihardjo, I., Oliver, H., Lutter, M., Luo, X. & Wang, X. Biochemical Pathways of Caspase Activation During Apoptosis. *Annu. Rev. Cell Dev. Biol.* **15**, 269–290 (1999).
18. Schwanhäusser, B., Gossen, M., Dittmar, G. & Selbach, M. Global analysis of cellular protein translation by pulsed SILAC. *Proteomics* **9**, 205–209 (2009).
19. Cox, J. & Mann, M. MaxQuant enables high peptide identification rates, individualized p.p.b.-range mass accuracies and proteome-wide protein quantification. *Nat. Biotechnol.* **26**, 1367–1372 (2008).
20. Cox, J. *et al.* Andromeda: A Peptide Search Engine Integrated into the MaxQuant Environment. *J. Proteome Res.* **10**, 1794–1805 (2011).
21. Tyanova, S. *et al.* The Perseus computational platform for comprehensive analysis of (prote)omics data. *Nat. Methods* **13**, 731–740 (2016).
22. Lund, R. R. *et al.* Quantitative proteomics of primary tumors with varying metastatic capabilities using stable isotope-labeled proteins of multiple histogenic origins. *Proteomics* **12**, 2139–2148 (2012).
23. Chrysogelos, S., Riley, D. E., Stein, G. & Stein, J. A human histone H4 gene exhibits cell cycle-dependent changes in chromatin structure that correlate with its expression. *Proc. Natl. Acad. Sci.* **82**, 7535–9 (1985).
24. Hauer, M. H. & Gasser, S. M. Chromatin and nucleosome dynamics in DNA damage and repair. *Genes Dev.* **31**, 2204–2221 (2017).
25. Luijsterburg, M. S. *et al.* DDB2 promotes chromatin decondensation at UV-induced DNA

damage. *J. Cell Biol.* **197**, 267–81 (2012).
26. Adam, S. *et al.* Real-Time Tracking of Parental Histones Reveals Their Contribution to Chromatin Integrity Following DNA Damage. *Mol. Cell* **64**, 65–78 (2016).
27. Shi, Z., Zhang, J. & Zheng, S. What we know about ST13, a co-factor of heat shock protein, or a tumor suppressor? *J. Zhejiang Univ. Sci. B* **8**, 170–6 (2007).
28. Su, C. *et al.* DNA damage induces downregulation of histone gene expression through the G1 checkpoint pathway. *EMBO J.* **23**, 1133–43 (2004).

3.4 SUPPORTING INFORMATION

3.4.1 *Methods*

Proliferation Assay

Cell proliferation was measured as a function the concentration of double-stranded DNA (dsDNA), as quantified with Quant-iT PicoGreen reagent (Invitrogen), 24 h after light treatment. Cells were grown in white 96-well plates with clear bottoms (Falcon) for 24 h before light treatment. Cultures were washed twice with phosphate-buffered saline (PBS) before lysing by pipet mixing with Triton-X (0.1%) in Tris-EDTA buffer (TE, 0.1 mM EDTA, 10 mM Tris, pH 7.8). Lysates were then diluted 1:1 in TE buffer and then diluted 1:1 with PicoGreen reagent (1x). dsDNA was quantified using a SpectraMax M5 spectrometer with excitation set to 480 nm and emission to 520 nm.

Caspase Assay

Cells were treated identical to proliferative experiments; however, 24 h after treatment, Caspase reagent (6 μM) and Hoechst 33342 (1 μg mL^{-1}) were added to cultures. After 30 min incubation, apoptotic cells were quantified by counting positive detections relative to cell count in fluorescent images acquired on a Nikon Eclipse TE2000-U fluorescent microscope of at least 4 biological replicates.

Pulsed Stable Isotopic Labeling by Amino Acids in Cell Culture (pSILAC)

High-glucose DMEM depleted of L-arginine, L-glutamine, L-lysine, and L-methionine (Caisson Laboratories) was supplemented with dialyzed fetal bovine serum (10%), Penicillin/Steptromycin (1%), L-arginine HCl (84.0 mg L^{-1}), L-glutamine (584.0 mg L^{-1}), L-methionine (30 mg L^{-1}), and L-lysine (146.0 mg L^{-1}) equivalents of D4-L-lysine ("medium heavy") or $^{12}C_4{}^{15}N_2$-L-Lysine ("heavy"). NIH3T3s and StemPro bone marrow-hMSCs (Gibco) at passage 2 were seeded the day prior to treatments. Cells were washed twice then topped with PBS containing magnesium and calcium (Corning) for the duration of light treatments. Then, cultures were swapped to "medium heavy" or "heavy" DMEM and incubated for 24 h. Cell lysate (8 M urea, 50 mM tris at pH 8.2) was briefly boiled at 95 °C before proteins were reduced over 45 min at 56 °C by addition of dithiothreitol at a final concentration of 5 mM and alkylated in the dark with iodoacetamide (14 mM final concentration, 30 min). Proteins were then digested overnight at 37 °C with the endopeptidase LysC (Wako) at a 1:50 enzyme-to-substrate ratio. Peptides were desalted on C18 ZipTips (EMD Millipore) and vacuum concentrated before resuspending in water (1% acetic acid, 0.1% formic acid).

Mass spectrometry experiments were performed using a Waters Ultra Performance Liquid Chromatographic instrument coupled to an LTQ Orbitrap XL (Thermo Scientific). Peptides were loaded onto an in-house packed (ProntoSil 5 µm C18, pore size = 200 Å) trapping column (IntegraFrit, 3 cm, 100µm ID) and eluted during a 90 min gradient (5% to 40% ACN with 1% formic acid, 0.3 µL min^{-1}). Separation occurred across an in-house packed (ProntoSil 5 µm C18, pore size = 120 Å) flexible fused silica capillary column (Polymicro Tech, 30 cm, 75 µm ID). Peptides were analyzed in data-dependent mode, acquiring mass spectra across 400 – 2000 m/z at a resolution of 60,000. For identification and quantification, raw files were processed in

MaxQuant[1] equipped with the Andromeda search engine[2] under default settings with Lys4 and Lys8 selected as the "Light" and "Heavy" labels, respectively and LysC selected as the digestion enzyme. Peptides were identified against the *mus musculus* (UniProt, UP000000589) or *homo sapiens* (UniProt, UP000005640) database[3]. Further data analysis was performed in the Perseus suite following the published protocol[4].

3.4.2 *Supporting Figures*

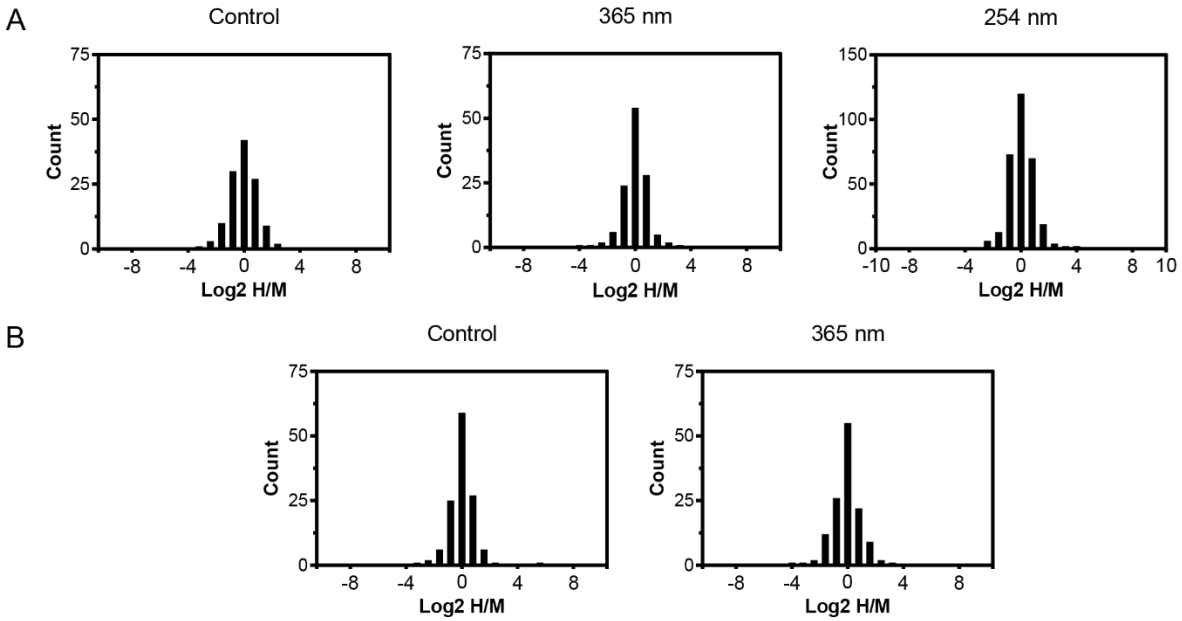

Figure 3.S1. Representative distributions of protein expression of **A**, NIH3T3s and **B**, hMSCs with or without light treatment. Data were normally distributed around Log_2 H/M = 0 or equal expression between treated and control samples.

Table 3.S1. Statistically differentially regulated proteins 24 h after NIH3T3s were treated with light (λ = 254 nm, 0.5 min at 0.3 mW cm^{-2}).

Protein name	Gene name	Difference
ATP-citrate synthase	Acly	-1.34
Fructose-bisphosphate aldolase A;Fructose-bisphosphate aldolase	Aldoa	-1.40
Annexin;Annexin A6	Anxa6	-1.89
Calumenin	Calu	-1.10
F-actin-capping protein subunit alpha-1	Capza1	-1.33
Collagen alpha-1(I) chain	Col1a1	-6.27
Dihydropyrimidinase-related protein 2	Dpysl2	-1.25
Fatty acid synthase;[Acyl-carrier-protein] S-acetyltransferase	Fasn	-1.04
Farnesyl pyrophosphate synthase	Fdps	-2.84
Fibronectin;Anastellin	Fn1	-2.49
Rab GDP dissociation inhibitor alpha	Gdi1	-1.73
Glutathione S-transferase Mu 1	Gstm1	-1.08
Histone H1.2	Hist1h1c	-3.39
Histone H2B	Hist1h2br	-1.23
Histone H3.2	Hist1h3b	-2.95
Histone H4	Hist1h4a	-2.20
Histone H2A type 2	Hist2h2ac	-1.69
Hydroxymethylglutaryl-CoA synthase, cytoplasmic	Hmgcs1	-2.39
Endoplasmin	Hsp90b1	-1.34
Isopentenyl-diphosphate Delta-isomerase 1	Idi1	-1.88
L-lactate dehydrogenase	Ldha	-2.11
Myristoylated alanine-rich C-kinase substrate	Marcks	-2.18
DNA helicase;DNA replication licensing factor MCM6	Mcm6	-1.16
Obg-like ATPase 1	Ola1	-1.03
Prolyl 4-hydroxylase subunit alpha-1	P4ha1	-1.30
Protein disulfide-isomerase A4	Pdia4	-1.26
40S ribosomal protein S5;40S ribosomal protein S5, N-terminally processed	Rps5	-1.46
Serpin H1	Serpinh1	-1.08
Staphylococcal nuclease domain-containing protein 1	Snd1	-2.13
Stathmin	Stmn1	-1.07
Triosephosphate isomerase	Tpi1	-1.44
Neuroblast differentiation-associated protein AHNAK	Ahnak	1.29
Glutathione S-transferase omega-1	Gsto1	2.06
Hypoxanthine-guanine phosphoribosyltransferase	Hprt1	1.31
Cellular tumor antigen p53	Trp53	1.03

Aldose reductase	Akr1b1	1.24
DnaJ homolog subfamily A member 1	Dnaja1	1.43
Complement component 1 Q subcomponent-binding protein, mitochondrial	C1qbp	1.04
Filamin-C	Flnc	1.22
Peptidyl-prolyl cis-trans isomerase D	Ppid	1.04

3.4.3 *Supporting References*

1. Cox, J. & Mann, M. MaxQuant enables high peptide identification rates, individualized p.p.b.-range mass accuracies and proteome-wide protein quantification. *Nat. Biotechnol.* **26**, 1367–1372 (2008).
2. Cox, J. *et al.* Andromeda: A Peptide Search Engine Integrated into the MaxQuant Environment. *J. Proteome Res.* **10**, 1794–1805 (2011).
3. The UniProt Consortium. UniProt: the universal protein knowledgebase. *Nucleic Acids Res.* **45**, D158–D169 (2017).
4. Tyanova, S. & Cox, J. Perseus: A Bioinformatics Platform for Integrative Analysis of Proteomics Data in Cancer Research. in *Cancer Systems Biology: Methods and Protocols* (ed. von Stechow, L.) 133–148 (Springer New York, 2018).

Chapter 4: LOGICAL STIMULI-TRIGGERED DELIVERY OF SMALL MOLECULES FROM HYDROGEL BIOMATERIALS

As published: Ruskowitz, E.R.*, Comerford M.P.*, Badeau B.A., DeForest C.A. Logical Stimuli-Triggered Delivery of Small Molecules from Hydrogel Biomaterials. *Biomaterials Science*, **7**, 542-546 (2019) *indicates equal authorship.

4.1 ABSTRACT

Stimuli-responsive biomaterials are useful platforms for environmentally triggered drug delivery. By varying the molecular architecture of orthogonal stimuli-labile linkages between small molecules and non-degradable materials, we demonstrate the Boolean logic-based release of model therapeutics from gels. Programmable responses are demonstrated for materials sensitive to input combinations involving enzymes, chemical reductants, and light via YES, OR, and AND logic gates.

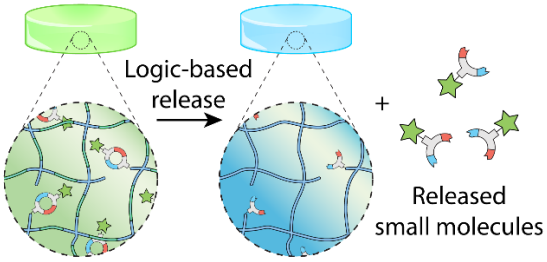

Figure 4.1. Triggered release of small molecule model therapeutics from hydrogel biomaterials is governed by user-programmable Boolean logic.

4.2 LOGICAL STIMULI-TRIGGERED RELEASE OF SMALL MOLECULES

Disease dynamics and the vast benefits of localized therapeutic activity necessitate development of smart drug delivery platforms with biologically defined release profiles. Stimuli-responsive hydrogels provide an isolated aqueous environment that can protect and stabilize its

payload until liberation is triggered[1–4]. Delivery of cargo larger than the mesh size of the hydrogel network (e.g., cells, proteins) can be obtained through physical entrapment within biodegradable constructs[5–7]. As unbound small molecules freely diffuse through the hydrogel mesh, their controlled release can be achieved through tethering to non-degradable hydrogels via scissile bonds[8,9]. While hydrolysable linkers can extend delivery from gels, smart material systems whose cargo release is triggered by specific environmental stimuli may provide new opportunities in personalized medicine[10–15].

Towards the advancement of intelligent drug delivery platforms, we recently introduced a modular synthetic strategy to formulate biomaterials that degrade in response to precise combinations of user-defined inputs following Boolean logic[16]. In this approach, stimuli sensitivity is programmed into materials by specifying the molecular architecture and arrangement of orthogonal degradable groups within hydrogel crosslinkers. Here, we extend this biocomputational approach to govern the logic-based release of pendant small molecule cargos from non-degradable gels through molecularly defined stimuli-degradable linkers (**Figure 4.2**).

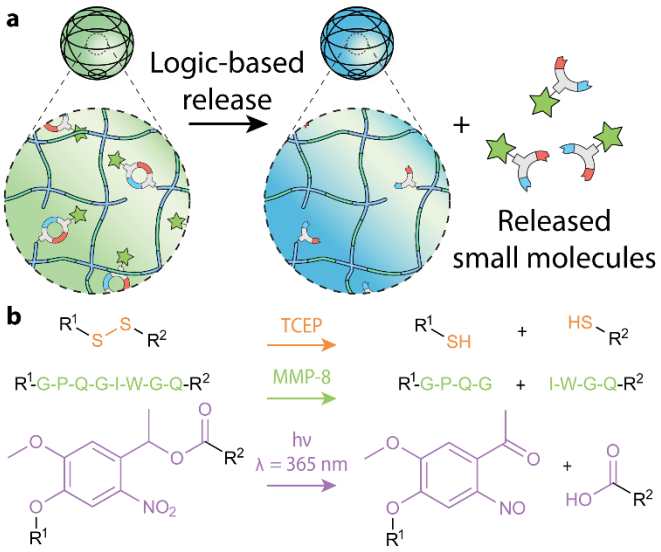

Figure 4.2. (a) Small molecules conjugated to hydrogel biomaterials through degradable linkages of defined molecular architecture undergo triggered release in response to precise combinations of environmental inputs following Boolean logic. (b) Disulfide-, –GPQGIWGQ– peptide-, and *ortho*-

nitrobenzyl ester-containing linkers are cleaved in response to TCEP, MMP-8, and light, respectively.

Non-degradable hydrogels were formed through a strain-promoted azide-alkyne cycloaddition (SPAAC) between a four-arm poly(ethylene glycol) (PEG) tetra-bicyclononyne (M_n ~ 20 kDa, 2 mM) and a linear PEG di-azide (M_n ~ 3.5 kDa, 4 mM, Appendix A) in phosphate-buffered saline (PBS, pH = 7.4). The copper-free SPAAC click chemistry[17–19] enables uniform hydrogels to be formed rapidly and in a bioorthogonal fashion[20–25], permitting encapsulation of living cells and bioactive therapeutics. Monofunctional azides present at low concentrations during gelation are stochastically incorporated as pendants with minimal impact on final network structure and mechanics, enabling logically releasable small molecules to be tethered into materials at user-specified concentrations.

Owing to its similar size and hydrophobicity to many common small molecule therapeutics[26], fluorescein (FAM) was chosen as a model cargo for logic-based release. The inherent fluorescence of FAM ($\lambda_{excitation}$ = 495 nm, $\lambda_{emission}$ = 530 nm) increases monotonically over a wide range of concentrations, permitting the quantification of pendant release from gels by measuring the fluorescence of the supernatant.

To enable the environmentally triggered release of small molecules from non-degradable biomaterials, we introduce stimuli-labile bonds between the gel-anchoring azide and the cargo (**Figure 4.2**). The controlled connectivity of multiple degradable groups gives rise to pendants whose release is governed by Boolean logic. Though any orthogonal combination of stimuli-labile moieties could be utilized, here we exploit those susceptible to three distinct reaction classes: (1) disulfide linkages that are chemically cleaved by reducing agents, (2) the –GPQG↓IWGQ– peptide sequence which is enzymatically degraded by matrix metalloproteinase-8 (MMP-8)[6,27,28], and (3) an *ortho*-nitrobenzyl ester (*o*NB) that undergoes photolysis upon exposure to UV light (λ = 365

nm)[29–32]. By combining Fmoc solid-phase peptide synthesis with subsequent chemical modifications, we created pendants containing FAM linked to an azide through at least one degradable bond.

Gels (10 μL formed in 1.5 mL microcentrifuge tubes) each containing one of the various releasable FAM pendants (25 μM) were washed with and maintained in buffer that supports MMP activity (100 μL, 200 mM sodium chloride, 50 mM tris, 5 mM calcium chloride, 1 μM zinc chloride, pH = 7.5). Samples receiving the reductive input ($_R$) were treated with tris(2-carboxyethyl)phosphine (TCEP, 2 mM) and incubated overnight at 37 °C. To quench any unreacted TCEP, these samples were further treated with hydroxyethyl disulfide (5 mM in buffer) prior to incubation (4 hr, 37 °C). Gels receiving the enzyme input ($_E$) were subsequently treated with recombinant MMP-8 (12.5 ng/μL, 20 hr, 37 °C). Samples receiving the light input ($_P$) were subsequently exposed to UV light (λ = 365 nm, 20 mW cm^{-2}, 10 min). All pendants were treated in triplicate in each of the eight possible input combinations (i.e., $_E$, $_P$, $_R$, $_{EP}$, $_{ER}$, $_{RP}$, $_{ERP}$, $_N$ for no treatment). Following treatments, gels were incubated for three days prior to fluorescence analysis of the gel supernatant. To account for differences in initial pendant concentrations and variations in their non-specific release (typically 5-20% of the formulated FAM), extent of release was normalized between 0% (corresponding to no treatment condition) and 100% (corresponding to treatment with highest release) for each pendant.

When a single degradable moiety is incorporated between the azide and the small molecule, FAM release is governed as a simple YES gate (**Figure 4.3**). In the presence of the proper stimulus, this linkage is severed to permit free diffusion of the cargo from the gel. We synthesized and tested YES-type pendants to deliver FAM in response to UV light, MMP-8 enzyme, and chemical reductants, respectively denoted as FAM-P, FAM-E, and FAM-R (Appendix A). These FAM

pendants behaved as expected, where YES-gated release occurred only when the relevant cue was present. The high triggered release specificity demonstrates orthogonality of the employed degradation chemistries.

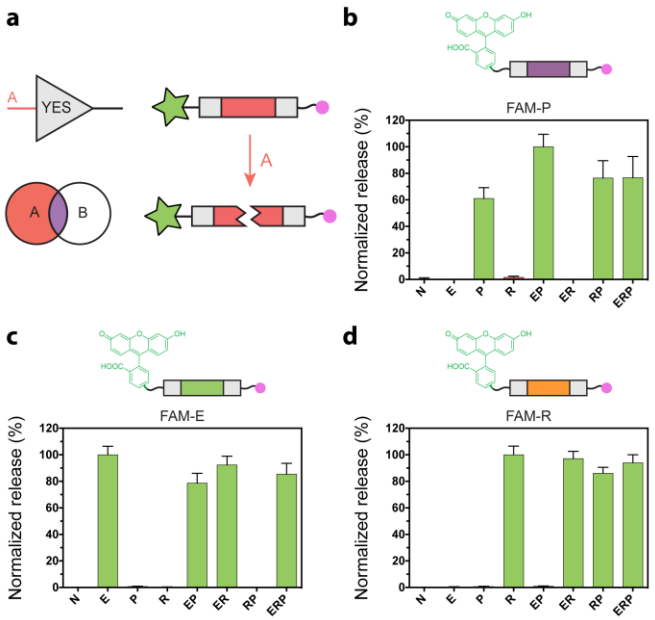

Figure 4.3. (a) Boolean YES-responsiveness is achieved through inclusion of a single degradable moiety between gel (pink circle) and small molecule (green star). Fluorescein is selectively released from gels for conditions involving (b) light, (c) MMP-8 enzyme, or (d) reductant. X-axis labels indicate material treatment conditions ($_N$ indicates no treatment, $_E$ is MMP enzyme, $_R$ is a chemical reductant, $_P$ is UV light). The extent of release was normalized between 0% (corresponding to $_N$) and 100% (in treatment with highest release) for each pendant. Green bars signify conditions expected to result in release; red bars indicate conditions expected not to yield release. Error bars correspond to ±1 standard deviation about the mean with propagated uncertainties for n = 3 experimental replicates.

Two degradable linkers connected in series between the azide and the small molecule cargo forms the basis of a Boolean OR gate (denoted with logic symbol ∨) (**Figure 4.4**). In this case, cleavage of either of the degradable bonds will each result in small molecule dissociation and release from the gel. We created and tested OR-type pendants that release FAM in response to enzyme OR reductant (FAM-E∨R) as well as enzyme OR reductant OR light (FAM-E∨R∨P) (Appendix A). In each case, small molecule release accompanied gel treatment with any of the

programmed inputs. Differences in apparent release are partially attributed to FAM's environmental sensitivity[33], where solution conditions and substituents can affect fluorescence.

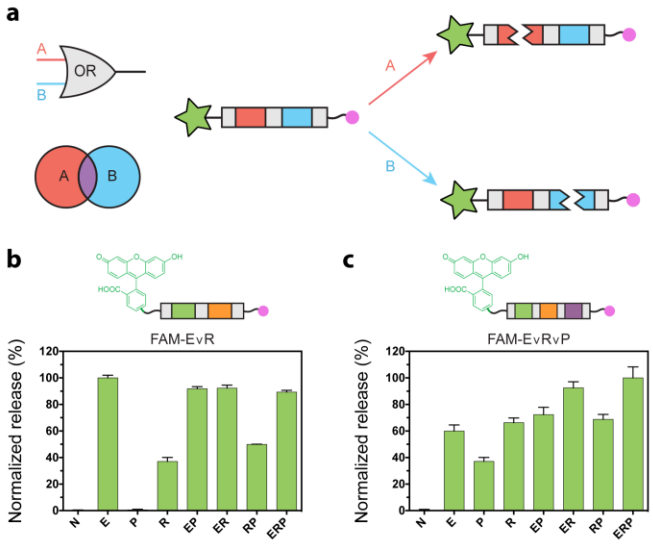

Figure 4.4. (a) Boolean OR-responsiveness is achieved through inclusion of two degradable moieties in series between gel (pink circle) and small molecule (green star). FAM is selectively released from gels for conditions involving (b) enzyme OR reductant, or (c) enzyme OR reductant OR light. X-axis labels indicating treatment conditions, release normalization criteria, histogram bar color, and error bar format match that described in **Figure 4.3**.

A Boolean AND gate (denoted with logic symbol ∧) is obtained when multiple stimuli-labile bonds connect the material and the small molecule payload in a parallel fashion (**Figure 4.5**). In these systems, the cleavage of both degradable groups is required for cargo release. We synthesized and analyzed FAM release from AND-type pendants that respond to enzyme AND reductant (FAM-E∧R) or to light AND reductant (FAM-P∧R) (Appendix A). In each case, small molecule release was enhanced in treatment conditions involving both programmed inputs. While FAM-P∧R exhibited modest undesired release when treated with either P or R, FAM-E∧R behaved fully as expected by cleaving only in response to treatments including both E and R.

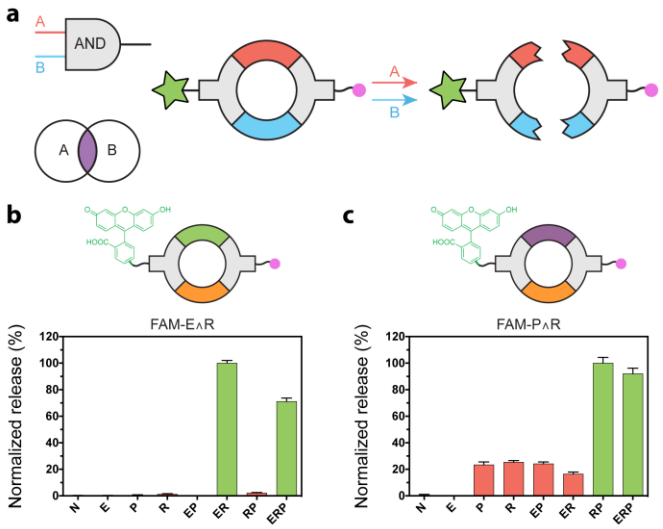

Figure 4.5. (a) Boolean AND-responsiveness is achieved through inclusion of two degradable moieties in parallel between gel (pink circle) and small molecule (green star). FAM is selectively released from gels for conditions involving (b) enzyme AND reductant, or (c) light AND reductant. X-axis labels indicating treatment conditions, release normalization criteria, histogram bar color, and error bar format match that described in **Figure 4.3**.

To demonstrate that logic-based responsive pendants could be utilized to obtain sequentially triggered release in response to staggered inputs, we synthesized and functionalized gels with FAM-R∨P (Appendix A), which is released upon exposure to reductant OR light (**Figure 4.6**). Cylindrical gels (10 μL) of uniform thickness (0.5 mm) were first exposed to collimated light (P) through a chrome mask containing an array of closed squares (edge length = 250 μm, interspacing = 250 μm), creating a mask-defined pattern through selective FAM release. Gels were subsequently treated with TCEP (R), resulting in complete programmed release of all remaining pendant from the material. Gels were fluorescently imaged before and after each treatment, and results matched expectations based on the pendant's programmed response. Furthermore, small molecule release from gels containing FAM-R∨P accompanied reductive or light treatment, as expected (Appendix A). Such sequential delivery strategies may improve disease treatment by providing additional control over complex small molecule release.

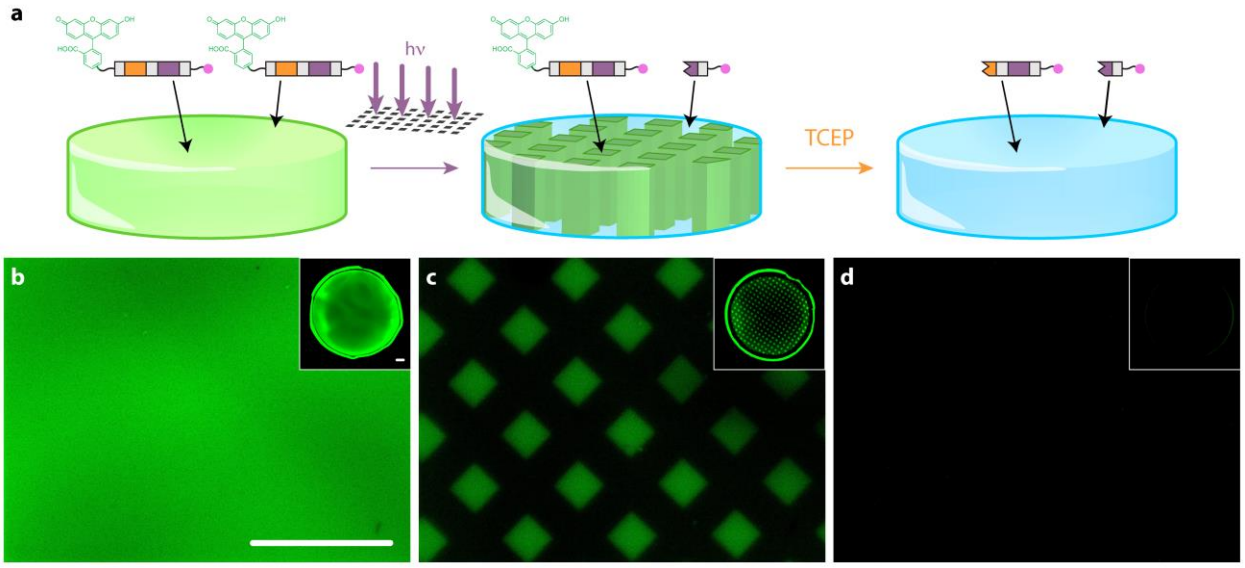

Figure 4.6. (a) Gels containing FAM-RVP exhibit sequentially triggered release in response to masked light followed by reductive treatment. Fluorescent images of gels (b) prior to treatment ($_N$), after (c) exposure to photomasked light ($_P$), and (d) successive incubation with TCEP ($_R$). Insets depict full hydrogel imaged on a Typhoon gel scanner. Scale bars = 1 mm.

4.3 CONCLUSIONS

In this work, we have introduced the first modular strategy to release tethered prodrugs in response to precise combinations of user-defined environmental inputs. By varying the molecular architecture and connectivity of multiple stimuli-labile moieties between materials and small molecule cargos, we have constructed a suite of smart biomaterials that perform biocomputation to release model therapeutics following Boolean logic. OR-gated response enables multiple characteristics of complex tissue disorders to be exploited for therapeutic delivery. AND-gated systems can increase target specificity by requiring the presence of multiple disease hallmarks. We expect that the introduced platforms sensitive to MMP-8 and/or chemical reductants will be useful in targeting the tumor microenvironment, where each cue is overexpressed. Photoresponsive systems can be externally triggered to provide spatiotemporal control over small molecule release.

Though our efforts have focused on polymeric hydrogels sensitive to input combinations of enzymes, chemical reductants, and light, the modularity of the approach – whereby overall

response is dictated by the identity and connectivity of various stimuli labile bonds – should enable the creation of a near-infinite number of responsive materials that sense a wide variety of inputs (e.g., pH, alternative enzymes, small molecules). We anticipate that these platforms will be highly applicable in targeted drug delivery, molecular diagnostics, and tissue engineering.

4.4 REFERENCES

1. Bajpai, A. K., Shukla, S. K., Bhanu, S. & Kankane, S. Responsive polymers in controlled drug delivery. *Prog. Polym. Sci.* **33**, 1088–1118 (2008).
2. Koetting, M. C., Peters, J. T., Steichen, S. D. & Peppas, N. A. Stimulus-responsive hydrogels: Theory, modern advances, and applications. *Mater. Sci. Eng. R Reports* **93**, 1–49 (2015).
3. Li, J. & Mooney, D. J. Designing hydrogels for controlled drug delivery. *Nat. Rev. Mater.* **1**, (2016).
4. Ruskowitz, E. R. & DeForest, C. A. Photoresponsive biomaterials for targeted drug delivery and 4D cell culture. *Nat. Rev. Mater.* **3**, 17087 (2018).
5. Hoare, T. R. & Kohane, D. S. Hydrogels in drug delivery: Progress and challenges. *Polymer (Guildf).* **49**, 1993–2007 (2008).
6. Lutolf, M. P. *et al.* Synthetic matrix metalloproteinase-sensitive hydrogels for the conduction of tissue regeneration: Engineering cell-invasion characteristics. *Proc. Natl. Acad. Sci.* **100**, 5413–5418 (2003).
7. Griffin, D. R. & Kasko, A. M. Photodegradable Macromers and Hydrogels for Live Cell Encapsulation and Release. *J. Am. Chem. Soc.* **134**, 13103–7 (2012).
8. Lin, C.-C. & Anseth, K. S. PEG Hydrogels for the Controlled Release of Biomolecules in Regenerative Medicine. *Pharm. Res.* **26**, 631–643 (2009).
9. Griffin, D. R. & Kasko, A. M. Photoselective Delivery of Model Therapeutics from Hydrogels. *ACS Macro Lett.* **1**, 1330–1334 (2012).
10. Qiu, Y. & Park, K. Environment-sensitive hydrogels for drug delivery. *Adv. Drug Deliv. Rev.* **53**, 321–339 (2001).
11. Liechty, W. B., Kryscio, D. R., Slaughter, B. V. & Peppas, N. A. Polymers for Drug Delivery Systems. *Annu. Rev. Chem. Biomol. Eng.* **1**, 149–173 (2010).
12. Larson, N. & Ghandehari, H. Polymeric Conjugates for Drug Delivery. *Chem. Mater.* **24**, 840–853 (2012).
13. Hoffman, A. S. Stimuli-responsive polymers: Biomedical applications and challenges for clinical translation. *Adv. Drug Deliv. Rev.* **65**, 10–16 (2013).
14. Knipe, J. M. & Peppas, N. A. *Multi-responsive hydrogels for drug delivery and tissue engineering applications*. vol. 1 (2014).
15. Lu, Y., Aimetti, A. A., Langer, R. & Gu, Z. Bioresponsive materials. *Nat. Rev. Mater.* **2**, (2016).
16. Badeau, B. A., Comerford, M. P., Arakawa, C. K., Shadish, J. A. & DeForest, C. A. Engineered modular biomaterial logic gates for environmentally triggered therapeutic delivery. *Nat. Chem.* **10**, 251–258 (2018).

17. Sletten, E. M. & Bertozzi, C. R. Bioorthogonal chemistry: fishing for selectivity in a sea of functionality. *Angew. Chemie Int. Ed.* **48**, 6974–6998 (2009).
18. Debets, M. F. *et al.* Bioconjugation with Strained Alkenes and Alkynes. *Acc. Chem. Res.* **44**, 805–815 (2011).
19. Dommerholt, J. *et al.* Readily Accessible Bicyclononynes for Bioorthogonal Labeling and Three-Dimensional Imaging of Living Cells. *Angew. Chemie-International Ed.* **49**, 9422–9425 (2010).
20. DeForest, C. A., Polizzotti, B. D. & Anseth, K. S. Sequential click reactions for synthesizing and patterning three-dimensional cell microenvironments. *Nat. Mater.* **8**, 659–664 (2009).
21. DeForest, C. A. & Tirrell, D. A. A photoreversible protein-patterning approach for guiding stem cell fate in three-dimensional gels. *Nat Mater* **14**, 523–531 (2015).
22. Madl, C. M., Katz, L. M. & Heilshorn, S. C. Bio-Orthogonally Crosslinked, Engineered Protein Hydrogels with Tunable Mechanics and Biochemistry for Cell Encapsulation. *Adv. Funct. Mater.* **26**, 3612–3620 (2016).
23. Hodgson, S. M., Bakaic, E., Stewart, S. A., Hoare, T. & Adronov, A. Properties of Poly(ethylene glycol) Hydrogels Cross-Linked via Strain-Promoted Alkyne–Azide Cycloaddition (SPAAC). *Biomacromolecules* **17**, 1093–1100 (2016).
24. Arakawa, C. K., Badeau, B. A., Zheng, Y. & DeForest, C. A. Multicellular Vascularized Engineered Tissues through User-Programmable Biomaterial Photodegradation. *Adv. Mater.* **29**, 1703156 (2017).
25. Liu, L. *et al.* Cyclic Stiffness Modulation of Cell-Laden Protein – Polymer Hydrogels in Response to User-Specified Stimuli Including Light. *Adv. Biosyst.* **2**, 1–9 (2018).
26. Schoener, C. A., Hutson, H. N. & Peppas, N. A. pH-Responsive Hydrogels with Dispersed Hydrophobic Nanoparticles for the Delivery of Hydrophobic Therapeutic Agents. *Polym. Int.* **61**, 874–879 (2012).
27. Nagase, H. & Fields, G. B. Human matrix metalloproteinase specificity studies using collagen sequence-based synthetic peptides. *Biopolymers* **40**, 399–416 (1996).
28. Raeber, G. P., Lutolf, M. P. & Hubbell, J. A. Molecularly engineered PEG hydrogels: A novel model system for proteolytically mediated cell migration. *Biophys. J.* **89**, 1374–1388 (2005).
29. Kloxin, A. M., Kasko, A. M., Salinas, C. N. & Anseth, K. S. Photodegradable Hydrogels for Dynamic Tuning of Physical and Chemical Properties. *Science* **324**, 59–63 (2009).
30. DeForest, C. A. & Anseth, K. S. Cytocompatible click-based hydrogels with dynamically tunable properties through orthogonal photocoupling and photodegradation reactions. *Nat. Chem.* **3**, 925–931 (2011).
31. Tomatsu, I., Peng, K. & Kros, A. Photoresponsive hydrogels for biomedical applications. *Adv. Drug Deliv. Rev.* **63**, 1257–1266 (2011).
32. Bao, C., Zhu, L., Lin, Q. & Tian, H. Building Biomedical Materials using Photochemical Bond Cleavage. *Adv. Mater.* **27**, 1647–1662 (2015).
33. Smart, P. L. & Laidlaw, I. M. S. An evaluation of some fluorescent dyes for water tracing. *Water Resour. Res.* **13**, 15–33 (1977).

Chapter 5: A GENETICALLY ENCODED PROTEIN-PROTEIN PHOTOLIGATION THROUGH LIGHT-ACTIVATED SPYCATCHER

5.1 ABSTRACT

Protein-protein interactions (PPIs) are the primary mechanism of executing cellular processes across biology. Eliciting spatiotemporal control over these processes by forcing PPIs can permit user-guided cell fate and function on a single/sub-cellular level. However, current chemistries rely on photoresponsive proteins that disassociate in the dark. Here, we present a new protein-protein photoligation through a transamidation reaction between genetically encoded, Cloaked-SpyCatcher (cSC) and its binding partner, SpyTag. Using genetic code expansion, we site-specifically mutate the critical lysine of SpyCatcher to an Nε-(*o*-nitrobenzyloxycarbonyl)-L-lysine to inhibit SpyCatcher-SpyTag ligation until photoactivation, a reaction termed laSC. Using laSC, we biochemically pattern 3D hydrogels with full-length proteins by activating immobilized cSC – a technique only requiring a 13-amino acid SpyTag modification to proteins of interest. Further, we irreversibly control intracellular association of split-protein fragments through *in vitro* cSC activation. We expect laSC will have far-reaching applications in diverse fields including biomaterials, tissue engineering, and optogenetics.

5.2 INTRODUCTION

Biology is comprised of a series of well-orchestrated chemical reactions, precisely controlled in time and space. Proteins act as the key conductors of these reactions through interactions with other biomolecules, e.g., small molecules, DNA, and proteins. Protein-protein interactions (PPIs) represent the primary mechanism of cellular regulation, dictating complex biological processes including cell growth and migration, cell-matrix interactions and diseases

including Alzheimer's. Since PPI govern nearly all cellular activities, there is tremendous interest to precisely control when and where such reactions occur. This, however, is a tall order, as the biological environment is characterized by fluctuating solution conditions from varying pH, presence of reductive/oxidative species, and a staggeringly complex milieu of functional reactive groups. Performing additive chemistry in this space requires highly specific and "unsensitive" reactions that do not rely on damaging/cross-reactive species such as radical-based chemistries.

Spontaneous ligation chemistries which utilize bioorthogonal functionalities can be used to control biologic function by forcing specific PPIs to occur. Complementary reactive handles (e.g., azide/alkyne, aldehyde/ketone) are typically introduced exogenously with little specificity (e.g., NHS-chemistry) or metabolically with single-residue or single-site precision[1]. Perfect amino acid specificity can be achieved through genetic code expansion, a technique that relies on unnatural tRNA/tRNA synthetase (tRNArs) pairs engineered to insert a non-canonical amino acid at amber stop codon sites (TAG)[2]. By overriding this rarely used codon, a bioorthogonal reactive moiety can be site-specifically incorporated during protein translation avoiding further modification. Installing reactive groups that do not naturally exist in living systems affords high reaction specificity.

More recently, spontaneous ligation of naturally derived reactive protein partners presented a genetically encoded means to achieve precise control over PPIs. SpyCatcher (SC)[3], SnoopCatcher[4] and SdyCatcher[5] ligations, proceeding through isopeptide covalent bond formation between split-protein fragments upon re-association, leads to long-term binding. Since these strategies are bioorthogonal, fast, and genetically encodable, there have been an explosion of applications in the few short years since their development including intracellular protein localization, biomaterial functionalization, and modular vaccine development[6].

Though spontaneous ligation strategies afford reaction specificity, tremendous benefit comes from being able to externally trigger when and where biological reactions occur. PPIs can be temporally controlled through exogenous addition of small molecule[7–9]. However, spatially selective activation requires localization of the stimuli to a region of interest like local heating, sonication, or light. Unlike other triggers, light is unique in that it can be controlled in both time and space without disrupting cellular function[10], offering specification to when, where, and to what extent reaction occurs. Naturally occurring photoresponsive protein systems (e.g., Magnets, PhyB-PIF, Dropna) have been developed in recent years by the optogenetic community as a handle for triggering PPI in individual cells[11]. These photoresponsive proteins are a genetically encodable approach to achieving spatial control of PPIs by photoactivating protein multimerization[12]. Though such reactions have found great utility in optogenetic regulation of intracellular signaling, reactions are non-covalent and reversible, placing limitations on their potential applications.

In this work, we sought to overcome these limitations by developing a versatile protein-protein binding reaction scheme that is (1) highly specific, (2) genetically encoded, (3) phototriggered, and (4) irreversible. High reaction specificity permits reactivity within a biological context without concern of cross-reactions leading to cellular impairment. Constraining the scheme to genetically encoded chemistries enables scalable synthesis of reactive components through conventional fermentation processes. Further, reactions can be performed *in vitro* and *in vivo* by expressing components within the system in study. Light-activated chemistries afford cytocompatible and spatiotemporal control over the extent of interaction by manipulating dosages. Finally, reaction irreversibility ensures long-term, stable interactions independent of solution conditions.

Towards this, we introduce a strategy to photocontrol the SC ligation to spatiotemporally direct PPIs. Since this reaction proceeds through amide bond formation between a critical lysine residue on SC with an aspartic acid residue on the complementary SpyTag (ST)[3], the reaction in amenable to photocaging methodologies. Through genetic code expansion, a single photocaged lysine is site-specifically incorporated at the critical lysine of SC to generate a caged, inactive species – Cloaked-SpyCatcher (cSC) (**Figure 5.1a,b**). We hypothesized that cSC would not react with ST until user-directed light exposure generates uncaged-SpyCatcher (uSC), the native species capable of undergoing spontaneous ligation (**Figure 5.1c,d**). Here, we demonstrate this predicted response to control PPIs between purified species in solution. Then, we show the broad applicability of this light-activated SpyCatcher (laSC) reaction in biological systems by patterning the biochemical landscape of 3D hydrogels and directing PPIs inside living cells.

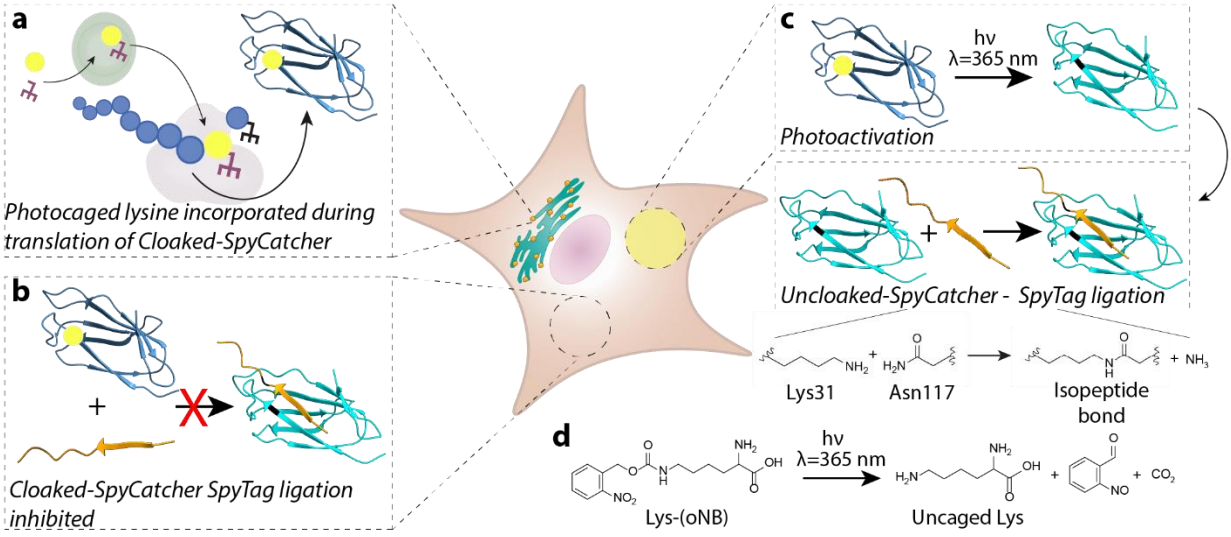

Figure 5.1. Light-activated SpyCatcher (laSC)-SpyTag ligation affords externally initiated protein-protein interactions. **a**, A photocaged lysine is site-specifically incorporated within the active site of SpyCatcher during protein translation via an unnatural tRNA/tRNA synthetase pair, giving Cloaked-SpyCatcher (cSC). **b**, cSC remains inactive, and unable to interact with its binding partner, SpyTag, due to the presence of a bulky aromatic photocage. **c**, With user-directed light exposure, the critical lysine is uncaged to liberate Uncloaked-SpyCatcher (uSC), an active species capable of spontaneously forming an isopeptide bond between Lys31 and Asn117 of SpyTag. **d**, Photoactivation is imparted through an *ortho*-nitrobenzyloxycarbonyl (*o*NB) installed on the ε-amine of lysine, such that light exposure restores the native species.

5.3 RESULTS

5.3.1 *Synthesis of a genetically encoded Cloaked-SpyCatcher*

Creating a reaction scheme as outlined above requires chemistries that proceed in a bioorthogonal manner and appropriately photocage the critical lysine of SC until light-activation. We chose to employ an Nε-(*o*-nitrobenzyloxycarbonyl)-L-lysine [Lys(*o*NB), Supporting Information] which offers quick kinetics to tracelessly and spatiotemporally generate a functional protein by restoring the native amine upon photodegradation (**Figure 5.1c,d**). This photocage can be efficiently cleaved with cytocompatible single and multiphoton (λ = 365 nm and 730 nm, respectively) excitation to restore the native amine enabling bulk 2D and precise 3D patterning. Through in-solution photolysis studies tracking expected shifts in the absorbance profile of Lys(*o*NB) (**Figure 5.S1**), the first-order degradation rate constant was found to be 2.78×10^{-3} s^{-1} with a half-life of 4.16 min under aqueous conditions (λ = 365 nm at 10 mW cm^{-2}) in agreement with published values[13] and within a cytocompatible range of exposure[10].

Genetic code expansion techniques rely on the orthogonality of the mutant tRNA/tRNArs with canonical machinery. Orthogonality entails the tRNArs to only aminoacylate its cognate tRNA with the unnatural amino acid being used and not recognize canonical tRNAs or amino acids. Further, the charged tRNA must contain the anticodon CUA to land at the amber stop codon on the mRNA during translation to provide single residue specificity. Many tRNA/tRNArs pairs have been successfully optimized to insert a variety of unnatural amino acids including a mutant pyrrolysyl-tRNA synthetase (tRNArs) with a cognitive $tRNA_{CUA}^{Pyl}$ derived from *M. mazei*[14] (gifted from Peter Schultz). Its achaeal origin enables expression of caged proteins in *E. coli* and mammalian cells with a single plasmid containing the necessary tRNA/tRNArs machinery in conjunction with an expression vector. We generated the appropriate cSC vector by mutating the

critical lysine of SC to the amber stop codon (K31TAG) using site-directed mutagenesis. After transformation of *E. coli* with both plasmids, functional cSC (**Figure 5.2a**) was recombinantly expressed and purified using basic immobilized metal affinity chromatography (IMAC) techniques. As cSC only contains a single modification, we confirmed the presence of Lys(*o*NB) by detecting the expected mass shift relative to wildtype SC (m_{SC} + 179 Da) with whole-protein mass spectrometry (**Figure 5.2b**).

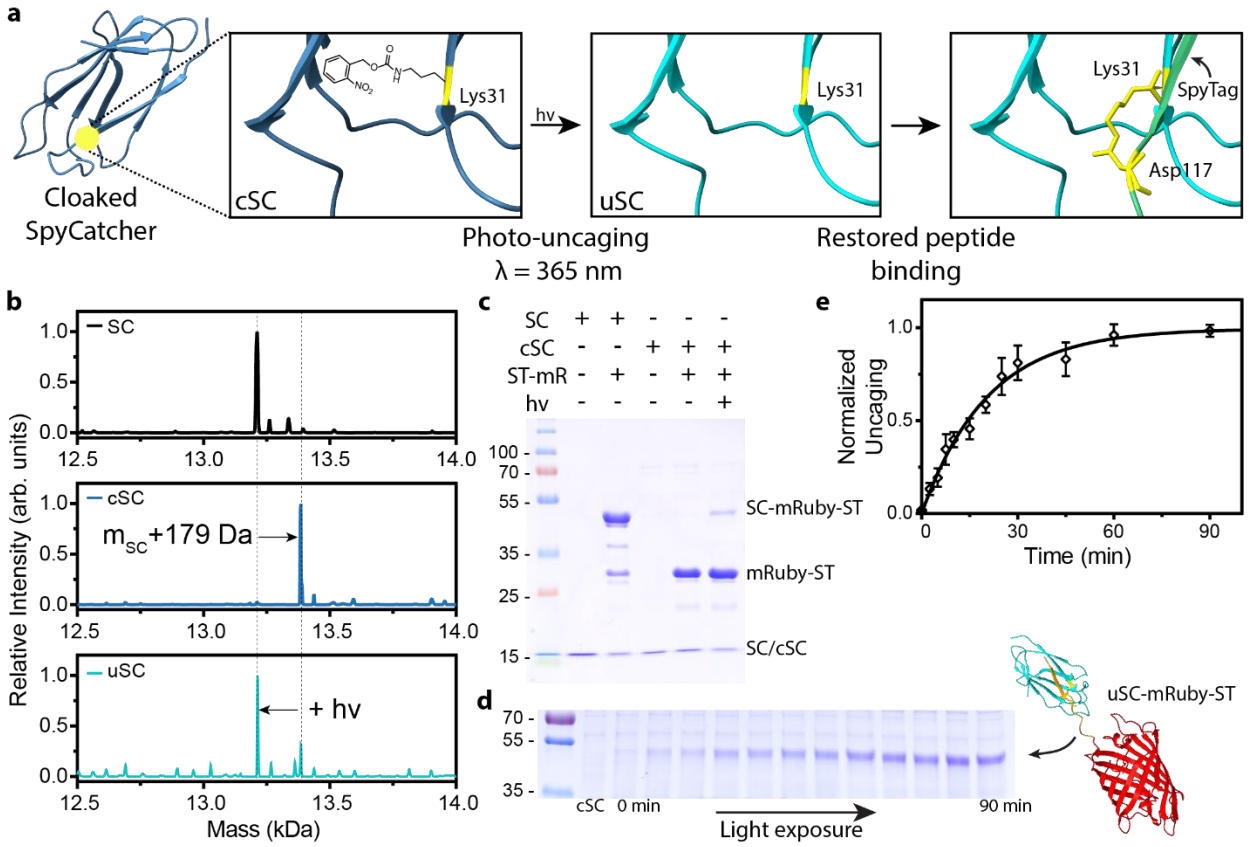

Figure 5.2. In-solution activity of recombinantly expressed cloaked-SpyCatcher (cSC). **a**, cSC remains inactive until light exposure cleaves the photocage to give uncloaked-SpyCatcher (uSC) This cleavage product undergoes spontaneous ligation to SpyTag. **b**, Whole-protein mass spectrometry indicates the presence of a single *ortho*-nitrobenzyl photocage on cSC which cleaves with light to give uSC of the same mass as wildtype SpyCatcher (SC). **c**, mRuby-SpyTag (mRuby-ST, 15 µM) overnight reaction with SC and cSC (10 µm) with and without light exposure (15 min, λ = 365 nm at 20 mW cm^{-2}) analyzed by SDS-PAGE demonstrated ligated product was only present after mixing SC or uncloaked-SpyCatcher (uSC). **d**,**e**, Photoactivation kinetics of cSC (10 µM) quantified by measuring total product formed with varying light exposure (0 - 90 min, λ = 365 nm at 10 mW cm^{-2}) through SDS-PAGE. **e**, Analysis of normalized band intensity yielded

first-order kinetics. Image in **d** corresponds to a representative gel. Solid curve is the best fit of data for 1st order kinetics. Error bars correspond to ±1 standard deviation of n = 4 experimental replicates.

5.3.2 *Evaluating cSC reactivity in-solution*

After expressing and purifying cSC (**Figure 5.S2**), we sought to demonstrate light-activated SC-ST binding (laSC-ST). Through extended light exposure (30 min, λ = 365 nm at 20 mW cm^{-2}), we generated uSC, the photocleaved product with a mass identical to SC^{WT} and thus confirmed photoliberation of the native protein (**Figure 5.2b**). Incubating cSC with a model fluorescent protein, mRuby, fused to the short 13 amino acid ST (mRuby-ST), led to no detectable amount of ligated product suggesting the presence of Lys(*o*NB) is sufficient to block isopeptide bond formation. However, incubating either uSC (15 min, λ = 365 nm at 20 mW cm^{-2}) or SC^{WT} with mRuby-ST yielded bound product (**Figure 5.2c**). Photouncaging the critical amine of Lys31 is necessary for ligation between cSC and ST.

As photodegradation of Lys(*o*NB) occurs in a dose-dependent manner, the extent of laSC-ST binding can be controlled by simply varying the exposure time. To determine uncaging kinetics of cSC in solution, we assessed product formation with electrophoretic techniques after a range of light treatment (0 - 90 min, λ = 365 nm at 10 mW cm^{-2}) (**Figure 5.2d**). Complete reaction was achieved with 90 min of exposure (**Figure 5.2e**). The difference in photodegradation kinetics between free and incorporate Lys(*o*NB) are suspected to be due to local environment conditions when incorporated within cSC.

While this successfully demonstrated photocontrol of product formation, the appeal of this reaction lies with the ability to perform both the uncaging and ligation in biological environments. To test the efficiency of laSC-ST binding in more complex solution conditions, we exogenously combined cSC and mRuby-ST in *E. coli* lysate before uncaging. uSC, successfully generated after

light exposure, spontaneously reconstituted with mRuby-ST in a dose-dependent manner (**Figure 5.S3**) further demonstrating the high specificity.

Critically, SC and ST are known to noncovalently associate with high affinity (K_d of 0.2 μM) prior to ligation[3]. In order to determine if the presence of Lys(*o*NB) was sufficient to inhibit this association in addition to covalent bond formation, the dissociation constant of cSC and uSC can be determined using techniques including bio-layer interferometry (BLI). We suspect the presence of Lys(*o*NB) will block the noncovalent association due to its bulky aromatic structure but further experimentation is necessary to evaluate this.

5.3.3 *Conjugation of cSC into biomaterials for 3D control*

After demonstrating activity in solution, we sought to emphasize the wide-reaching applicability of this new reaction. The complex conditions of the extracellular space created a growing desire to generate biomimetic cell culture platforms. Highly specific reactions that provide user-input to appropriately control the extracellular space without damaging sensitive biomolecules or cells are vital. As such, we sought to determine if by tethering cSC to a biomaterial, we could spatially dictate ST-protein binding (**Figure 5.3a**).

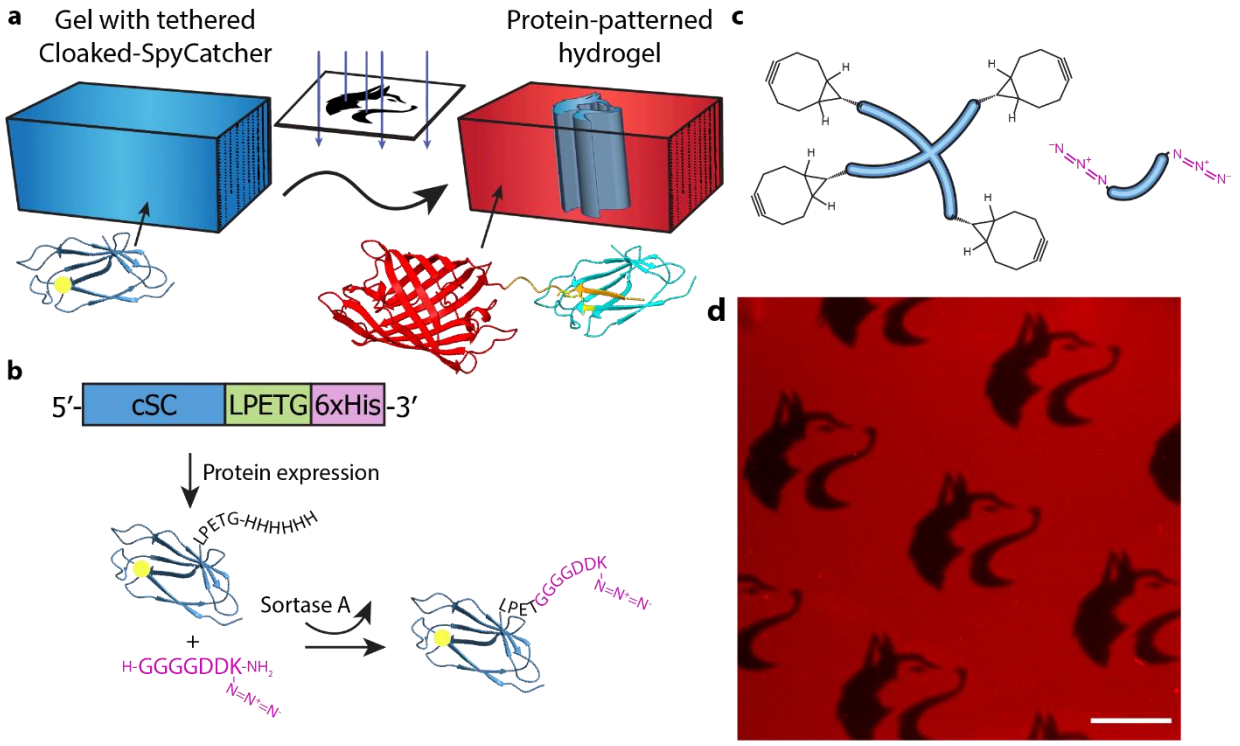

Figure 5.3. Application of cSC to biochemically pattern hydrogels. **a**, Spatially controlled light exposure selectively uncaged cSC to generate patterns of tethered ST-protein. **b**, cSC was modified with the Sortase A motif -LPETG- for post-translational transpeptidation to introduce a C-terminal azide moiety for gel immobilization. **c**, A four-arm PEG tetrabicyclononyne backbone crosslinked with a linear PEG diazide at off-stoichiometry ratios provided spare strained alkyne groups for cSC immobilization. **d**, Photolithography (λ = 365 nm at 10 mW cm^{-2}) afforded spatial control over mRuby-ST immobilization throughout the bulk of a gel. Scale bar represents 150 µm.

Due to the high specificity of laSC-ST binding and its flexibility to modifications to either termini without disrupting function, cSC is compatible with many advanced strategies for protein functionalization including enzymatic methodologies. Here, we employed the transpeptidase Sortase A which displaces the glycine of its recognition motif -LPETG- with any N-terminal polyglycine species, to install a single short, C-terminal azide-modified peptide (H-GGGG-DDK(N_3)-NH_2)[15]. By modifying the cSC fusion to encode -LPETG- just upstream of the histidine tag, we were able to azide functionalize cSC after purification to generate cSC-N_3 (**Figure 5.3b**). Through a strain-promoted azide-alkyne cycloaddition (SPAAC) click-reaction, we immobilized cSC-N_3 into poly(ethylene glycol) (PEG)-based hydrogels comprised of a four-arm PEG

tetrabicyclononyne backbone and a linear PEG diazide crosslinker (**Figure 5.3c**). These materials possess high biocompatibility for cellular encapsulation, offer a transparent platform to efficiently perform photochemistries or imaging based assays, and spontaneously undergo step-growth polymerization to form a nearly ideal network within minutes[15–17].

Exploiting mask-based photolithographic techniques, immobilized cSC was selectively uncaged (10 min, λ = 365 nm at 10 mW cm^{-2}) with spatial control to give uSC. Upon swelling mRuby-ST into the material, laSC-ST binding occurred in the pattern regions tethering mRuby-ST to the gel. Diffusing unconjugated protein out of the material generated a biochemically patterned gel (**Figure 5.3d**). The high contrast of the patterned and unpatterned regions further suggests that Lys(*o*NB) sufficiently blocks cSC and ST association. Through advanced exposure techniques, complex gradients and 3D patterns can be created with this system to further complete the applicability of laSC in biomaterials.

5.3.4 *Intracellular control of protein-protein interactions*

As the complexity of the intracellular space creates unique challenges for chemists, a genetically encoded, externally activatable chemistry to control PPIs is highly desired[12]. With the precise spatial control afforded by laSC-ST binding, we sought to demonstrate intracellular applicability by directing split-protein activity, functional proteins split into two fragments that gain activity when forced into proximity[18]. Recently, the green fluorescent protein UnaG was split into N- and C-terminal fragments (nUnaG and cUnaG, respecitvely) which show no association unless forced into proximity by interaction between fusion pairs[8]. We hypothesized that laSC-ST ligation would drive UnaG fragments together to generate fluorescence with spatiotemporal control. To demonstrate this, we fused nUnaG and cUnaG to cSC and ST, respectively, flanked the sequence with a fluorescent reporter, mCherry, and packaged these genes into a multicistronic

vector each separated by self-cleaving P2A sequences (**Figure 5.4a**). This vector was transiently co-transfected into HEK293-T cells with the relevant mammalian-optimized Lys(*o*NB) machinery[14]. Intracellular activation of UnaG after light treatment (15 min, λ = 365 nm at 10 mW cm^{-2}) was demonstrated through increased green fluorescence (**Figure 5.4b**). This preliminary result, for the first time, reveals irreversible photocontrol over PPIs inside living cells. We envision with further optimization and expansion to biologically relevant split proteins like Cre-recombinase[19], we will greatly improve upon the technique.

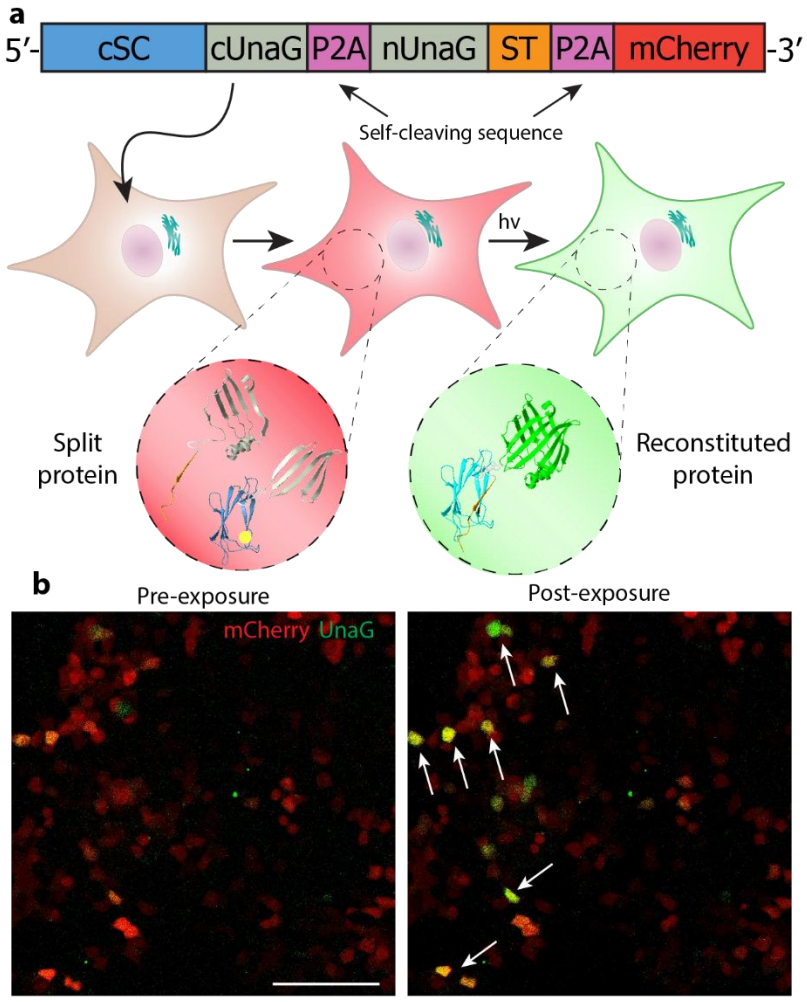

Figure 5.4. Intracellular protein activation laSC reconstitution. **a**, A multicistronic vector encoding cSC fused to the C-terminal fragment of split-UnaG, the N-terminal fragment fused to ST, and a red reporter mCherry each separated by a self-cleaving sequence, P2A, was used to express each component inside HEK293-T cells. With light exposure, uSC binds to ST bringing split-UnaG

fragments into proximity to generate green fluorescence. **b**, Cells imaged pre- and post-light exposure showed increased green fluorescence (white arrows). Scale bar represents 100 μm.

5.4 DISCUSSION

Here, we present a new class of protein-based chemistries which offer photoactivatable covalent binding through entirely genetically encoded means. While we have focused on demonstrating the applicability of this reaction in biomaterials and joining split proteins, this reaction has far reaching applications. As the first genetically encoded photoligation strategy, we envision this new chemical scheme to have significant impact in optogenetics and beyond.

Additionally, the approach used to develop laSC could be expanded to similar genetically encoded protein-peptide tags such as SnoopCatcher/SnoopTag which form an isopeptide bond between Asn and Lys[4], thereby expanding the catalog of protein-based photoligation chemistries. As this ligation is orthogonal to SC-ST binding, different PPIs could be controlled simultaneously. Interestingly, the development of a redshifted photocaged amino acid with a tRNA/tRNArs pair for genetic incorporation could be used to provide wavelength control over each interaction. This would vastly improve the current state of user-controlled PPIs.

While the application of cSC to pattern model proteins in biomaterials was presented, this system can be easily expanded to biologically relevant species. Benefitting from the small size of ST, there is great versatility in this regard. However, the current method lacks the reversibility characteristic of the complex, highly dynamic cellular niche. Future work in coupling cSC with genetically encoded labile chemistries will afford reversible control of protein immobilization greatly appealing to the biomaterials community.

We expanded the chemical repertoire of genetically encoded reactions to include photoactivatable, irreversible protein-protein binding with our development of cSC. Through the application of genetic code expansion, we demonstrated installation of an *o*NB photocage at the

critical lysine of SC prevents further reaction with ST and through user-directed light exposure, activity is restored. By exploiting the spatiotemporal control afford by light-activated chemistries, we created complex patterns of proteins within hydrogels and directed intracellular PPIs. As the beauty of this novel chemistry lies with its genetic encodability and high precision, laSC presents endless applications in better understanding PPIs, dictating protein localization, or guiding cell-matrix and cell-cell attachment. This novel chemistry offers an innovative approach to unraveling biological complexities of cell signaling.

5.5 REFERENCES

1. Shadish, J. A. & DeForest, C. A. Site-Selective Protein Modification: From Functionalized Proteins to Functional Biomaterials. *Matter* vol. 2 50–77 (2020).
2. Chin, J. W. Expanding and reprogramming the genetic code. *Nature* vol. 550 53–60 (2017).
3. Zakeri, B. *et al.* Peptide tag forming a rapid covalent bond to a protein, through engineering a bacterial adhesin. *Proc. Natl. Acad. Sci.* **109**, E690-7 (2012).
4. Veggiani, G. *et al.* Programmable polyproteams built using twin peptide superglues. *Proc. Natl. Acad. Sci.* **113**, 1202–7 (2016).
5. Tan, L. L., Hoon, S. S. & Wong, F. T. Kinetic Controlled Tag-Catcher Interactions for Directed Covalent Protein Assembly. *PLoS One* **11**, e0165074 (2016).
6. Hatlem, D., Trunk, T., Linke, D. & Leo, J. C. Catching a SPY: Using the SpyCatcher-SpyTag and related systems for labeling and localizing bacterial proteins. *Int. J. Mol. Sci.* **20**, (2019).
7. Kolos, J. M., Voll, A. M., Bauder, M. & Hausch, F. FKBP Ligands—Where We Are and Where to Go? *Front. Pharmacol.* **9**, 1425 (2018).
8. Ruskowitz, E. R. & DeForest, C. A. Proteome-wide Analysis of Cellular Response to Ultraviolet Light for Biomaterial Synthesis and Modification. *ACS Biomater. Sci. Eng.* **5**, 2111–2116 (2019).
9. Rost, B. R., Schneider-Warme, F., Schmitz, D. & Hegemann, P. Optogenetic Tools for Subcellular Applications in Neuroscience. *Neuron* vol. 96 572–603 (2017).
10. Wiens, M. D. & Campbell, R. E. Surveying the landscape of optogenetic methods for detection of protein–protein interactions. *Wiley Interdisciplinary Reviews: Systems Biology and Medicine* vol. 10 e1415 (2018).
11. DeForest, C. A. & Anseth, K. S. Cytocompatible click-based hydrogels with dynamically tunable properties through orthogonal photocoupling and photodegradation reactions. *Nat. Chem.* **3**, 925–931 (2011).
12. Chen, P. R. *et al.* A Facile System for Encoding Unnatural Amino Acids in Mammalian Cells. *Angew. Chemie Int. Ed.* **48**, 4052–4055 (2009).
13. Shadish, J. A., Benuska, G. M. & DeForest, C. A. Bioactive site-specifically modified proteins for 4D patterning of gel biomaterials. *Nat. Mater.* **18**, 1005–1014 (2019).

14. DeForest, C. A. & Tirrell, D. A. A photoreversible protein-patterning approach for guiding stem cell fate in three-dimensional gels. *Nat Mater* **14**, 523–531 (2015).
15. Arakawa, C. K., Badeau, B. A., Zheng, Y. & DeForest, C. A. Multicellular Vascularized Engineered Tissues through User-Programmable Biomaterial Photodegradation. *Adv. Mater.* **29**, 1703156 (2017).
16. Shekhawat, S. S. & Ghosh, I. Split-protein systems: Beyond binary protein-protein interactions. *Current Opinion in Chemical Biology* vol. 15 789–797 (2011).
17. To, T. L., Zhang, Q. & Shu, X. Structure-guided design of a reversible fluorogenic reporter of protein-protein interactions. *Protein Sci.* **25**, 748–753 (2016).
18. Hirrlinger, J. *et al.* Split-CreERT2: Temporal Control of DNA recombination mediated by split-cre protein Fragment Complementation. *PLoS One* **4**, (2009).

5.6 SUPPORTING INFORMATION

General synthetic information

Chemical reagents and solvents were supplied through either Sigma-Aldrich or Fisher Scientific. Solvents were removed under reduced pressure using a Buchi Rotovapor R-3 equipped with a V-700 vacuum pump and V-855 vacuum controller and a Welch 1400 DuoSeal Belt-Drive high vacuum pump. ^{1}H nuclear magnetic resonance (NMR) data was collected using Bruker instruments at 298 K and chemical shifts were determined relative to tetramethylsilane (TMS, δ=0). Synthesized species were lyophilized using the LABCONCO FreeZone 2.5 Plus with a LABCONCO rotary vane 117 vacuum pump. Small molecule mass spectrometry data was collected through direct-injection into a Thermo Linear Trap Quadrupole Orbitrap Xclaibur 2.0 DS. Whole-protein mass spectrometry was performed using a Waters Synapt – G2 QTOF. Light exposures were performed using a Lumen Dynamics OmniCure S1500 Spot UV Curing system with an internal 365 nm filter and an external 360 nm cut-on longpass filter. Light intensity was measured using a Cole-Parmer Series 9811-50 Radiometer (λ = 365 nm). Polymerase chain reaction (PCR) was achieved using a Bioer LifeECO thermo cycler. *E. coli* cultures were maintained in a Thermo Scientific MaxQ 4000 shaker incubator. Cell lysis was achieved with a Fisher Scientific Model 505 Soni Dismembrator equipped with a 1.27 cm diameter probe.

Synthesis of previously reported compounds used in this work

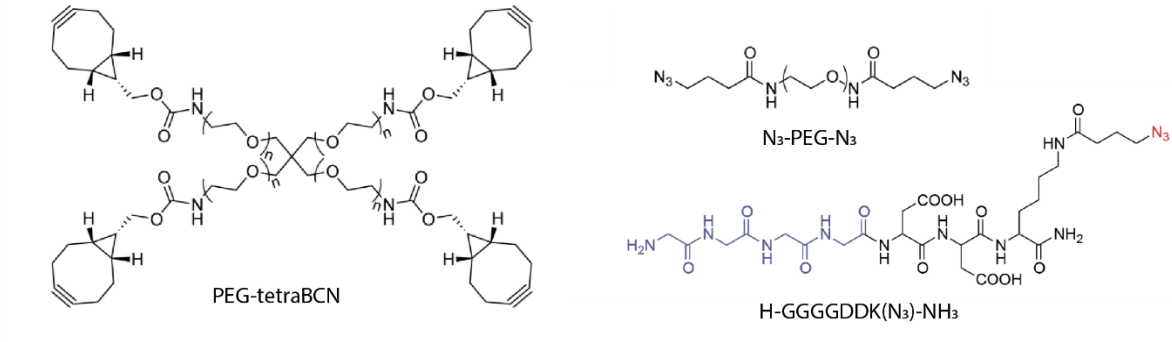

Poly(ethylene glycol) tetrabicyclononyne (PEG-tetraBCN, Mn ~ 20,000 Da), poly(ethylene glycol) diazide (N_3-PEG-N_3, Mn ~ 3,400 Da), and peptide H-GGGGDDK(N_3) were synthesized as previously reported[1,2].

Synthesis of Nε-(o-nitrobenzyloxycarbonyl)-L-lysine (Lys(oNB))

Synthesis of 2-nitrobenzyl-N-succinimidyl carbonate:

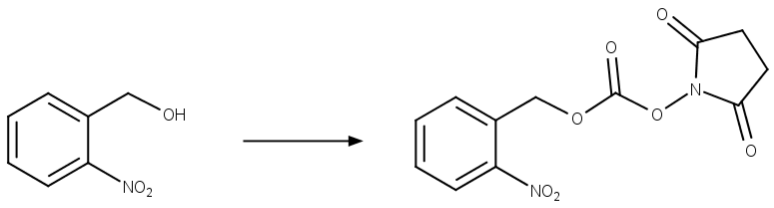

2-nitrobenzyl-N-succinimidyl carbonate was synthesized as previously reported[3] with minor modification. Disuccinimidyl carbonate (4.64 g, 18.1 mmol) was added to a mixture of 2-nitrobenzyl alcohol (2.5 g, 16.3 mmol) and triethylamine (3.4 mL, 24.5 mmol) in acetonitrile (80 mL) under nitrogen and stirred at room temperature for 30 min. The resulting reaction mixture was extracted with three washes of EtOAc with brine and water. The combined organic extracts were dried over Na_2SO_4 and concentrated under reduced pressure. Purification by column chromatography (Hexanes:EtOAc, 1:1) gave 2-nitrobenzyl-N-succinimidyl carbonate as a straw-colored oil (3.11 g, 65%).

Synthesis of Nε-(o-nitrobenzyloxycarbonyl)-L-lysine (Lys(oNB)):

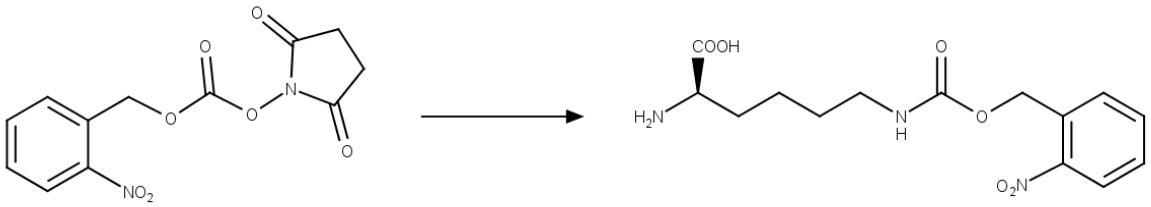

To a solution of 2-nitrobenzyl-N-succinimidyl carbonate (3.11g, 10.6 mmol) in DMF (50 mL) was added N_α-Boc-L-lysine (2.87 g, 11.7 mmol, Chem-Impex) and N,N-diisopropylethylamine (7.35 mL, 42.4 mmol) and stirred at room temperature overnight. The resulting reaction mixture was extracted with three washes of EtOAc with brine and water. The combined organic extracts were concentrated under reduced pressure, then purified by column chromatography (Hexanes:[EtOAc with 1% acetic acid], 1:1) to give Boc-protected Lys(*o*NB) as a light brown oil (3.08 g, 69%). The Boc-protected Lys(*o*NB) was dissolved in 3 mL 1,4-dioxane and 30 mL of 4 N HCl in 1,4-dioxane was added dropwise. The reaction was stirred at room temperature for 2.5 h, concentrated under reduced pressure, then subsequently triturated with 3 x 15 mL of diethyl ether to give Lys(*o*NB) (1.78 g, 51.4%) as a white solid. H^1 NMR (300 MHz, DMSO d6): δ = 1.28-1.33 (m, 1H), 1.42 (s, 3H), 1.67-1.81 (m, 2H), 2.99 (d, J = 6.0 Hz, 2H), 5.35 (s, 2H), 7.42 (t, J = 7.7 Hz, 1H), 7.58-7.65 (m, 2H), 7.80 (td, J = 7.7 Hz, 1H), 8.11 (dd, J = 7.9 Hz, 1H). MS (LTQ-MS): calculated for $C_{14}H_{20}N_3O_6$ ($[M+H]^+$): 326.1; found, 326.1. These spectral data matched those previously reported[4].

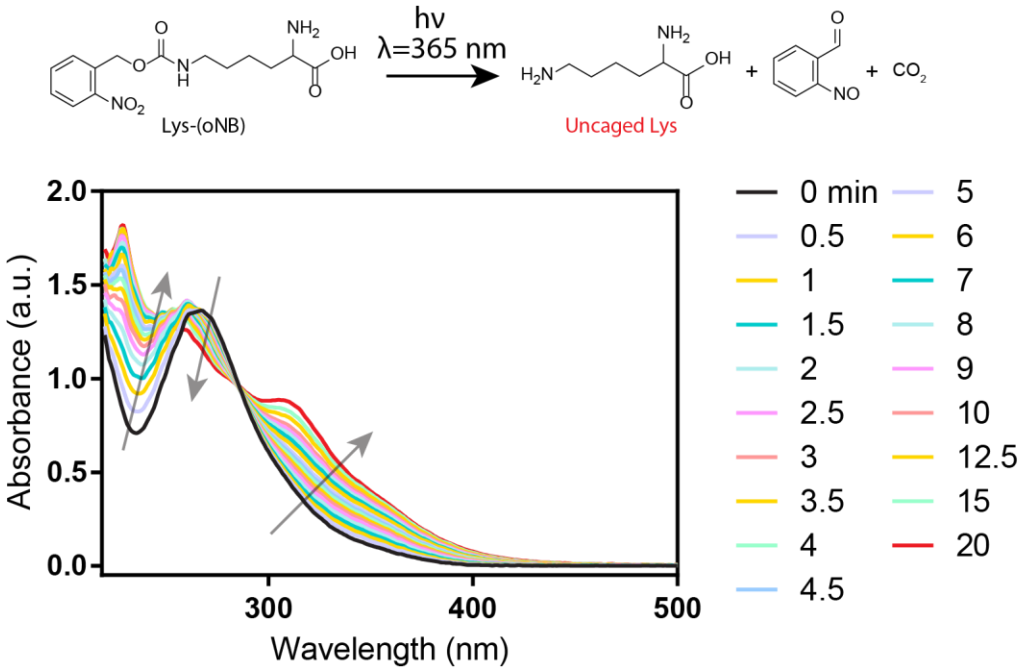

Figure 5.S1. Photodegradation of Lys(*o*NB). Lys(*o*NB) photolysis kinetics under aqueous conditions were determined by tracking absorbance profile shifts over increasing exposure times (0-20 min, λ = 365 nm at 10 mW cm^{-2}). Arrows indicate general shifts found over 20 min of exposure. Absorbance at λ = 365 nm was used to determine the kinetic constant associated with this first-order degradation to give 2.78×10^{-3} s^{-1}.

Plasmid construction for expression of Cloaked-SpyCatcher systems

Plasmid Construction

The SpyCatcher gene (Addgene, Plasmid #35044) was amplified through Polymerase Chain Reaction (PCR) using primers that included 5' NdeI and 3' XhoI restriction enzyme digestion sites (SpyCatcher-Forward and -Reverse). The amplified gene and pET21 expression plasmid (Novagen) were double digested with FastDigest™ NdeI and XhoI (Thermo Scientific) for 1 h at 37 C, separated using agarose gel electrophoresis (1% UltraPure Agarose, Thermo Scientific), and extracted with the QIAquick Gel Extraction Kit (Qiagen). SpyCatcher was ligated into the pET21 expression plasmid (T4 DNA ligase – New England Biolabs, overnight at 16 °C). Chemically competent Top10 *E. coli* (Thermo Scientific) were transformed with the ligation

product through heat shock (42 °C, 30 s), incubated in SOC media (1 h at 37 °C; 20 g L^{-1} tryptone, 5 g L^{-1} yeast extract, 0.5 g L^{-1} NaCl, 2.5 mM KCl, 10 mM $MgCl_2$, 10 mM $MgSO_4$, 20 mM glucose) and spread on agar plates (10 g L^{-1} tryptone, 5 g L^{-1} yeast extract, 10 g L^{-1} NaCl, 15 g L^{-1} agar) containing ampicillin (100 ug mL^{-1}) overnight. A single colony was grown overnight in 5 mL of LB (10 g L^{-1} tryptone, 5 g L^{-1} yeast extract, 10 g L^{-1} NaCl) and plasmid DNA was collected using the QIAprep Spin Miniprep Kit (Qiagen). DNA sequences were confirmed through Sanger Sequencing (GeneWiz) before transforming chemically competent BL21(DE3) *E. coli* (Promega) for protein expression as SC^{WT}.

The Cloaked-SpyCatcher (cSC) plasmid was constructed through site-directed mutagenesis at Lys31. The SC^{WT} plasmid generated above was mutated to the 'cloaked' variant by PCR amplification using overlapping forward and reverse primers each containing the amber stop codon TAG in-place of Lys (SpyCatcher-SDM-Forward and -Reverse). Remaining SC^{WT} plasmid was digested with DpnI (37 °C, 2 h) which was then heat inactivated (80 °C, 20 min) before transformation into chemically competent Top10 *E. coli*. The mutation was confirmed through Sanger Sequencing (GeneWiz).

An mRuby-SpyTag fusion was generated by double digesting a pET21 expression vector containing a 5' mRuby gene with a 3' HindIII and XhoI multiple cloning site with HindIII and XhoI restriction enzymes (37 °C overnight, New England Biolabs). The digest was purified as described above. Single-stranded forward and reverse DNA oligos encoding SpyTag with a 5' HindIII and 3' XhoI restriction site (Integrated DNA Technologies) such that oligos would anneal to generate sticky ends, were annealed by heating equimolar amounts of each oligo in annealing buffer (10 mM tris, pH 7.5, 50 mM NaCl, 1 mM EDTA) in a heat block (95 °C, Eppendorf) for 5 min before turning it off to cool to room temperature (1 h). The annealed oligos were used as is

for ligation into the digested pET21-mRuby vector which was subsequently transformed into chemically competent Top10 *E. coli*.

The SpyCatcher-UnaGc-P2A-UnaGn-SpyTag-P2A-mCherry system was received cloned into the pTwist CMV vector with the puromycin resistance gene designed for high levels of expression in mammalian cells (Twist Bioscience).

DNA Sequences

The primers used while cloning the desired plasmids are as described in Table S1. Listed below are the 5' to 3' open reading frames as confirmed by sequencing for expression of the proteins utilized here.

SpyCatcherWT-HHHHHH
ATGGTTGATACCTTATCAGGTTTATCAAGTGAGCAAGGTCAGTCCGGTGATATGACA
ATTGAAGAAGATAGTGCTACCCATATTAAATTCTCAAAACGTGATGAGGACGGCAA
AGAGTTAGCTGGTGCAACTATGGAGTTGCGTGATTCATCTGGTAAAACTATTAGTAC
ATGGATTTCAGATGGACAAGTGAAAGATTTCTACCTGTATCCAGGAAAATATACATT
TGTCGAAACCGCAGCACCAGACGGTTATGAGGTAGCAACTGCTATTACCTTTACAGT
TAATGAGCAAGGTCAGGTTACTGTAAATGGCAAAGCAACTAAAGGTGACGCTCATA
TTCTCGAGCACCACCACCACCACCACTGA

Cloaked SpyCatcher(TAG)-HHHHHH
ATGGTTGATACCTTATCAGGTTTATCAAGTGAGCAAGGTCAGTCCGGTGATATGACA
ATTGAAGAAGATAGTGCTACCCATATTAAATTCTCATAGCGTGATGAGGACGGCAA
AGAGTTAGCTGGTGCAACTATGGAGTTGCGTGATTCATCTGGTAAAACTATTAGTAC
ATGGATTTCAGATGGACAAGTGAAAGATTTCTACCTGTATCCAGGAAAATATACATT
TGTCGAAACCGCAGCACCAGACGGTTATGAGGTAGCAACTGCTATTACCTTTACAGT
TAATGAGCAAGGTCAGGTTACTGTAAATGGCAAAGCAACTAAAGGTGACGCTCATA
TTCTCGAGCACCACCACCACCACCACTGA

mRuby-SpyTag-HHHHHH
ATGGTTTCTAAAGGTGAAGAACTGATCAAAGAAAACATGCGTATGAAAGTTGTTAT
GGAAGGTTCTGTTAACGGTCACCAGTTCAAATGCACCGGTGAAGGTGAAGGTCGTC
CGTACGAAGGTGTTCAGACCATGCGTATCAAAGTTATCGAAGGTGGTCCGCTGCCGT
TCGCTTTCGACATCCTGGCTACCTCTTTCATGTACGGTTCTCGTACCTTCATCAAATA
CCCGGCTGACATCCCGGACTTCTTCAAACAGTCTTTCCCGGAAGGTTTCACCTGGGA
ACGTGTTACCCGTTACGAAGACGGTGGTGTTGTTACCGTTACCCAGGACACCTCTCT
GGAAGACGGTGAACTGGTTTACAACGTTAAAGTTCGTGGTGTTAACTTCCCGTCTAA
CGGTCCGGTTATGCAGAAAAAAACCAAAGGTTGGGAACCGAACACCGAAATGATGT
ACCCGGCTGACGGTGGTCTGCGTGGTTACACCGACATCGCTCTGAAAGTTGACGGTG

GTGGTCACCTGCACTGCAACTTCGTTACCACCTACCGTTCTAAAAAAACCGTTGGTA
ACATCAAAATGCCGGGTGTTCACGCTGTTGACCACCGTCTGGAACGTATCGAAGAAT
CTGACAACGAAACCTACGTTGTTCAGCGTGAAGTTGCTGTTGCTAAATACTCTAACC
TGGGTGGTGGTATGGACGAACTGTACAAAAAGCTTGCACACATAGTAATGGTAGAC
GCCTACAAGCCGACGAAGCTCGAGCACCACCACCACCACCACTGA

SpyCatcher-cUnaG-P2A-nUnaG-SpyTag-P2A-mCherry
ATGGTTGATACCTTATCAGGTTTATCAAGTGAGCAAGGTCAGTCCGGTGATATGACA
ATTGAAGAAGATAGTGCTACCCATATTAAATTCTCAAAACGTGATGAGGACGGCAA
AGAGTTAGCTGGTGCAACTATGGAGTTGCGTGATTCATCTGGTAAAACTATTAGTAC
ATGGATTTCAGATGGACAAGTGAAAGATTTCTACCTGTATCCAGGAAAATATACATT
TGTCGAAACCGCAGCACCAGACGGTTATGAGGTAGCAACTGCTATTACCTTTACAGT
TAATGAGCAAGGTCAGGTTACTGTAAATGGCAAAGCAACTAAAGGTGACGCTCATA
TTGGTGGCTCTGGAGGTGGATCTGGCGGTGTTAAATCCGTAGTCAACTTGGTCGGAG
AAAAACTCGTATATGTCCAAAAATGGGATGGCAAAGAGACAACCTACGTGCGTGAA
ATTAAAGACGGGAAACTGGTTGTGACGCTGACAATGGGCGACGTGGTGGCAGTGCG
CTCGTACCGGCGTGCAACCGAAGGAAGCGGTGCCACCAATTTCTCCCTCCTGAAGCA
GGCTGGGGACGTGGAGGAAAACCCTGGCCCCATGGTTGAAAAATTTGTTGGTACGT
GGAAAATAGCGGATTCTCATAATTTTGGCGAATATCTGAAGGCTATCGGGGCGCCTA
AAGAGCTGAGTGATGGAGGCGATGCCACGACTCCAACTCTGTATATTTCACAGAAG
GACGGTGATAAAATGACCGTTAAGATCGAGAATGGCCCGCCCACCTTCCTGGATAC
ACAGGTAAAGTTTAAACTTGGTGAAGAATTTGATGAGTTCCCGAGCGACAGACGCA
AAGGAGGCTCTGGTGGAGGCTCTGGAGGTGGCTCTGGAGCACACATAGTAATGGTA
GACGCCTACAAGCCGACGAAGGGAAGCGGAGCTACTAACTTCAGCCTGCTGAAGCA
GGCTGGAGACGTGGAGGAGAACCCTGGACCTGTGAGCAAGGGCGAGGAGGATAAC
ATGGCCATCATCAAGGAGTTCATGCGCTTCAAGGTGCACATGGAGGGCTCCGTGAA
CGGCCACGAGTTCGAGATCGAGGGCGAGGGCGAGGGCCGCCCCTACGAGGGCACCC
AGACCGCCAAGCTGAAGGTGACCAAGGGTGGCCCCCTGCCCTTCGCCTGGGACATC
CTGTCCCCTCAGTTCATGTACGGCTCCAAGGCCTACGTGAAGCACCCCGCCGACATC
CCCGACTACTTGAAGCTGTCCTTCCCCGAGGGCTTCAAGTGGGAGCGCGTGATGAAC
TTCGAGGACGGCGGCGTGGTGACCGTGACCCAGGACTCCTCCCTCCAGGACGGCGA
GTTCATCTACAAGGTGAAGCTGCGCGGCACCAACTTCCCCTCCGACGGCCCCGTAAT
GCAGAAGAAGACCATGGGCTGGGAGGCCTCCTCCGAGCGGATGTACCCCGAGGACG
GCGCCCTGAAGGGCGAGATCAAGCAGAGGCTGAAGCTGAAGGACGGCGGCCACTA
CGACGCTGAGGTCAAGACCACCTACAAGGCCAAGAAGCCCGTGCAGCTGCCCGGCG
CCTACAACGTCAACATCAAGTTGGACATCACCTCCCACAACGAGGACTACACCATC
GTGGAACAGTACGAACGCGCCGAGGGCCGCCACTCCACCGGCGGCATGGACGAGCT
GTACAAGTAA

Table 5.1. Primers used to generate desired expression vectors

Primer Name	*Sequence 5' -> 3'*
SpyCatcher-Forward	agatacgcatatggttgataccttatcaggtttatcaag
SpyCatcher-Reverse	cgtgcctcgagaatatgagcgtcacctttagttgc
SpyCatcher-SDM-Forward	attctcatagcgtgatgaggacggcaaagagttag
SpyCatcher-SDM-Reverse	catcacgctatgagaatttaatatgggtagcactatcttc
SpyTag Forward Oligo	agcttgcacacatagtaatggtagacgcctacaagccgacgaagc
SpyTag Reverse Oligo	tcgagcttcgtcggcttgtaggcgtctaccattactatgtgtgca

Protein Expression and Purification

cSC expression

BL21(DE3) cells were double transformed with the expression vector and the corresponding amber suppression machinery (pSUPAR-mmPyl-NBK1, generously gifted by Peter Schultz[4]). Cells were grown in overnight (37 °C agitated at 250 rev min^{-1}) in Terrific Broth (TB; 24 g L^{-1} yeast extract, 20 g L^{-1} tryptone, 4 mL L^{-1} glycerol, 0.017 M monopotassium phosphate, 0.072 M dipotassium phosphate) supplemented with ampicillin (100 µg mL^{-1}) and chloramphenicol (25 µg mL^{-1}). Large cultures (125 mL) were inoculated at a 1:25 and grown until reaching an optical density of 0.6 (λ = 600 nm). Lys(*o*NB) dissolved in 2 equivalents 0.5 M NaOH was added to a final concentration of 1 mM and cultures were wrapped with aluminum foil. After 30 min at 37 °C, cultures were induced by adding arabinose to 0.1% and IPTG (final concentration of 0.5 mM). Cultures were agitated overnight at 16 °C, then pelleted by centrifugation at 4,000 x g for 20 min at 4 °C. Cell pellets were resuspended in lysis buffer (40 mL, 20 mM Tris, 50 mM NaCl, 10 mM imidazole) supplemented with protease inhibitor cocktail (1 tablet, Pierce) and sonicated (0 °C, 6 x 3 min cycles at 30% amplitude, 33% duty cycle with 3 min rest). Cell lysate was clarified by centrifugation (4,000 x g, 20 min) before purification via immobilized metal affinity chromatography (IMAC) using Ni-NTA resin (2 mL). After discarding the flow-through, the resin was washed (4 mL three times, 20 mM Tris, 50 mM NaCl, 20 mM imidazole) and protein was eluted (20 mM Tris, 50 mM NaCl, 250 mM imidazole). Imidazole was removed through dialysis (ThermoFisher SnakeSkin MWCO 10 kDa Dialysis Tubing) against Tris buffer (20 mM Tris, 50 mM NaCl) and spin concentrated (Amicon® Ultra-15, MWCO 10 kDa). Proteins (~5-10 mg L^{-1} of culture) were stored at -20 °C in Tris buffer with 8% glycerol until use.

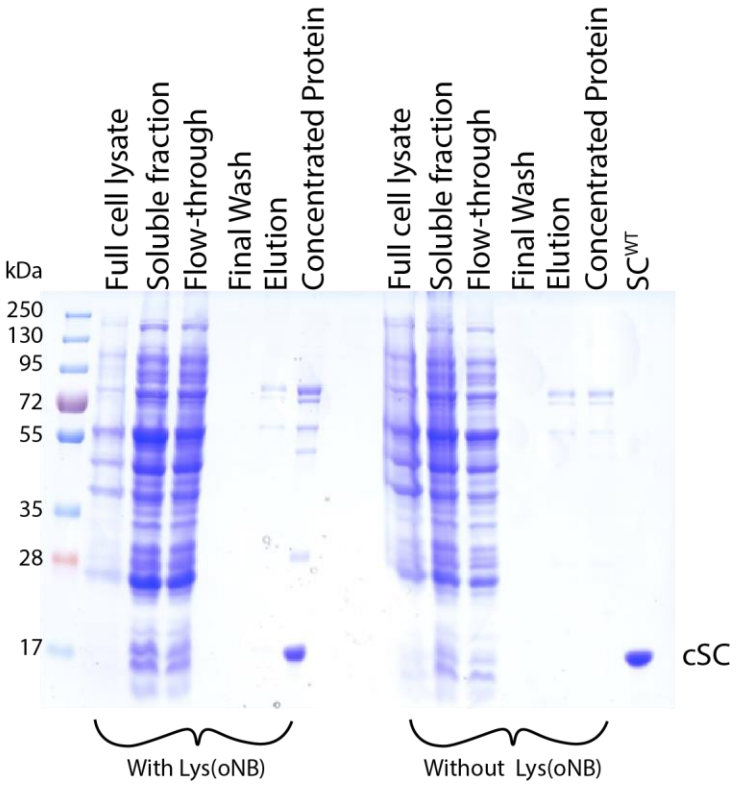

Figure 5.S2. Expression and purification of Cloaked-SpyCatcher. SDS-PAGE stained with Coomassie Brilliant Blue was used to analyze protein expression and verify protein purity. Expression and purification of cSC was depended upon addition of Lys(*o*NB) which confirms the orthogonality of the mutant tRNA/tRNA synthetase pair used for incorporation. Purified cSC aligned with recombinantly expressed wildtype SC.

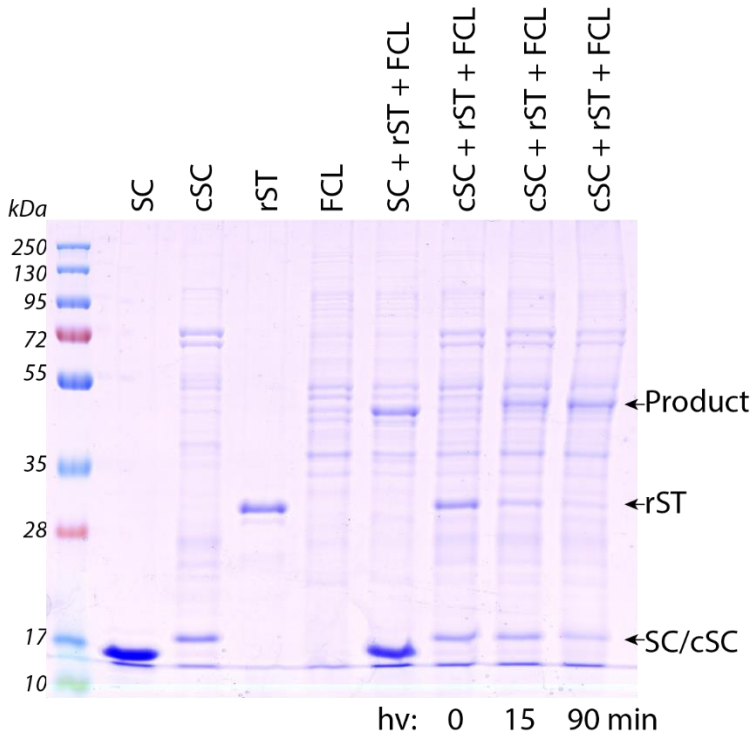

Figure 5.S3. laSC ligation proceeds under biologically complex solution conditions. SpyCatcher (SC, 40 µM) or irradiated (0, 15, or 90 min; λ = 365 nm at 10 mW cm^{-2}) Cloaked-SpyCatcher (cSC, 40 µM) were incubated with *E. coli* full cell lysate (FCL) and mRuby-SpyTag (rST, 10 µM) overnight prior analysis by SDS-PAGE stained with Coomassie. Product formation increased with extended light exposure demonstrating reactivity in biologically relevant conditions such as in the presence of full cell lysate.

User-guided cSC activation for 3D patterned protein immobilization in hydrogels

Purified cSC (100 µM) was prereacted with PEG-tetraBCN (4mM) in PBS overnight at 4 °C prior to reaction with N_3-PEG-N_3 (7.5 mm). Solutions were mixed well then aliquoted into 10 µL droplets on a Rain-X® coated glass slide with 0.5 µm silicone rubber spacers before placing a second glass slide on top. Cylindrical gels of controlled thickness were formed at room temperature over 1 h and were then stored in PBS overnight at 4 °C. Gels were then patterned with a repeated husky silhouette by photolithographic exposure (10 min, λ = 365 nm at 10 mW cm^{-2}). mRuby-ST (25 µL, 1.7 mg mL^{-1}) was swelled into the gel overnight before washing with PBS (3x) for 24 h at 25 °C. Gels were imaged on a Zeiss LSM 710 confocal microscope using a 10x dry objective.

Mammalian Cell Culture

HEK293T cells were maintained at 37 °C and 5% CO_2 in Dulbecco's minimal essential media (DMEM) supplemented with 10% Fetal bovine serum (FBS) and 1% penicillin/streptromycin (P/S). Cells were seeded at 50,000 cells cm^{-2} on 8-well chambered coverglass 24 h prior to transfection. At transfection, cells were swapped to complete DMEM with 1 mM Lys(*o*NB) made fresh. Equal molar amounts of cSC-UnaG expression vector and pCMV-NBK1 (generously gifted by Peter Schultz[4]) were co-transfected using Lipofectamine 2000 by following the supplied protocol. Media was replenished 12 h after transfection. Cells were imaged through confocal microscopy (Zeiss LSM 710) before replacing media with PBS with calcium and magnesium and treated with light (20 min, λ = 365 nm at 10 mW cm^{-2}). After light treatment, cells were stored in complete media for 15 min and then re-imaged.

Supporting References

1. DeForest, C. A. & Tirrell, D. A. A photoreversible protein-patterning approach for guiding stem cell fate in three-dimensional gels. *Nat Mater* **14**, 523–531 (2015).
2. Shadish, J. A., Strange, A. C. & DeForest, C. A. Genetically Encoded Photocleavable Linkers for Patterned Protein Release from Biomaterials. *J. Am. Chem. Soc.* **141**, 15619–15625 (2019).
3. Kawada, Y., Kodama, T., Miyashita, K., Imanishi, T. & Obika, S. Synthesis and evaluation of novel caged DNA alkylating agents bearing 3,4-epoxypiperidine structure. *Org. Biomol. Chem.* **10**, 5102–5108 (2012).
4. Chen, P. R. *et al.* A Facile System for Encoding Unnatural Amino Acids in Mammalian Cells. *Angew. Chemie Int. Ed.* **48**, 4052–4055 (2009).

Chapter 6: CONCLUSIONS AND FUTURE DIRECTIONS

Photoresponsive biomaterials present a promising platform for engineering tissues *in vitro* and localized drug delivery systems. The ability to precisely regulate biological complexity within these systems in a user-programmable manner has attracted scientists to apply these tools in a growing application space. In this dissertation, we have expanded upon the current capabilities of photoresponsive drug delivery systems and established a new genetically encodable protein photoligation reaction controllable with light conditions demonstrated here to be cytocompatible. This concluding chapter summarizes these advances and identifies opportunities arising from this work to further direct the field.

In Chapter 3:, we began by evaluating the bioorthogonality of ultraviolet (UV) light (λ = 365 nm, 10 mW cm^{-2}) typically used to activate small-molecule photochemistries in biomaterial systems. By quantifying cellular response to UV light through survival assays and global proteomic studies, we found low doses of near UV light to be cytocompatible across multiple cell types. By applying pulsed stable isotope labeling by amino acids in cell culture (pSILAC), we detected significant shifts in the global proteome with exposure to low wavelength, high energy light (λ = 254 nm, 0.5 mW cm^{-2}) which is known to be harmful to cells[1]. However, minimal changes were found in identical studies after near-visible UV light treatment (λ = 365 nm, 10 mW cm^{-2}). These results further justify the expansion and application of photoresponsive systems across biology.

In Chapter 4:, we utilized a small molecule photocleavable linker in combination with two additional orthogonally degradable chemistries for controlled delivery of small molecules from biomaterials. Through the implementation of Boolean logic-inspired chemical architectures linking externally degradable chemistries to a cargo of interest, delivery of therapeutics were

triggered by user-defined combinations of release factors. By selecting chemistries degradable to native and locally unique microenvironments in the body (e.g., enzymes, reductant) or an external stimulus such as light, release profiles and locations were demonstrated as tunable. Localizing release to specific sites can reduce therapeutic toxicity and increase potency, both desirable for improved patient outcome during treatment.

In Chapter 5:, we introduced light-activated SpyCatcher (laSC) as the first spatiotemporally controlled genetically encoded ligation chemistry, opening the door to newfound control over intra- and extracellular processes. We hypothesized the installation of a photocage on the key residue that participates in the isopeptide bond formation between SpyCatcher and SpyTag would inhibit SpyCatcher/SpyTag association until user-directed light exposure. Using genetic code expansion, SpyCatcher was site-specifically modified with an *o*-nitrobenzyl photocaged lysine [Lys(*o*NB)] at its key reactive site to create Cloaked-SpyCatcher (cSC). Through enzymatic modification with Sortase A, cSC was C-terminally modified with a reactive azide handle for immobilization in SPAAC-based biomaterials. cSC was selectively activated inside hydrogels to control biochemical cue patterning with 4D precision by expressing proteins of interest with the short, easily translatable SpyTag. Further exploiting the encodability of this chemistry, irreversible photocontrol of intracellular protein-protein interactions was demonstrated. The association, thus activity, of split proteins ranging from merely fluorescent to biologically active species, can be initiated by 4D selective uncaging of cSC, bring the split fragments into proximity through the covalent SpyCatcher/SpyTag linkage. laSC ligation has significant applications in optogenetics ranging from single cell tracking to genetic modification, in biomaterials and beyond.

Following on the successes reported in this thesis, our laboratory is currently expanding the laSC methodology so as to reversibly control the biochemical landscape of hydrogels. With

the goal of creating a fully genetically encoded system for reversible biomaterial modification such that it can be easily implemented across disciplines, cSC can be expressed with the N-terminal recognition sequence of N-myristoyltransferase (NMT), an enzyme that can install a fatty-acid azide during recombinant expression for conjugation. By fusing a genetically encoded photocleavable protein (PhoCl) between SpyTag and a protein of interest (PoI), PoIs can be patterned both into and out of hydrogels using two different wavelengths of light (λ = 365 nm and 405 nm, respectively) (**Figure 6.1**). Adding to the versatility of this system, the PoI can be purified using Spy&Go[2], a resin with an immobilized SpyCatcher mutant which noncovalently associates to SpyTag for increased purity over traditional IMAC strategies.

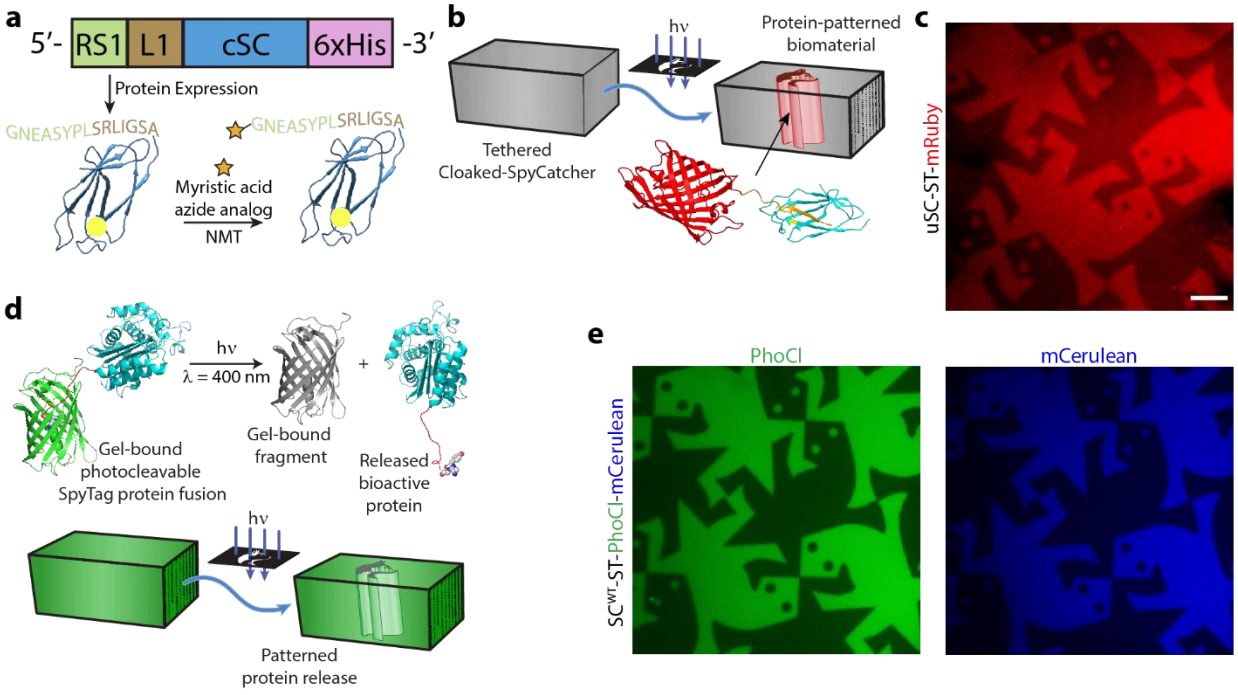

Figure 6.1. Coupling Cloaked-SpyCatcher (cSC) and a photocleavable protein (PhoCl) for a fully genetically encoded method to reversibly biochemically pattern hydrogels. **a**, N-myristoyltransferase (NMT) recognition sequence (RS1) and a flexible linker (L1) were included on the N-terminal of cSC and recombinantly expressed with NMT to install an azide-containing fatty acid on the N-terminal glycine during expression giving N_3-cSC. **b**, PEG-based hydrogels were cast homogenously containing N_3-cSC. Through user-guided light exposure, protein immobilization was spatially controlled. **c**, laSC binding was limited only to regions which received light (λ = 365 nm at 20 mW cm^{-2}) as demonstrated by ST-mRuby fluorescence. **d**, Using

a photocleavable protein (PhoCl) which cleaves under blue light, patterned protein release has been previously acheived[3]. **e**, By conjugating a PhoCl-mCerulean fusion through SC-ST binding, spatially controlled protein release is demonstrated (λ = 400 nm at 10 mW cm^{-2}). Coupling PhoCl and cSC will afford reversible control. Scale is 150 µm. **d** is adapted from previous work[3].

Additionally, laSC could provide user-control over protein-based hydrogel formation and on-demand crosslinking. Our initial design includes a gel formed through reaction of a cSC-SpyCatcher fusion linked by the unstructured hydrophilic protein XTEN[4] (cSC-X144-SC), uncaged variant (SC-X144-SC), as well as a tri-functional SpyTag-X144-SpyTag-X144-SpyTag crosslinker. Gelation will occur spontaneously through reaction between SC-X144-SC and the trifunction SpyTag; additional crosslinks in the material will be formed through laSC chemistry to subsequently photostiffen the material. By varying the ratio of cSC-X144-SC and SC-X144-SC, the initial mechanical properties of the gel and the magnitude of the change in stiffness could be tuned. The mechanical range could be further broadened by incorporating orthogonal ligation chemistry (e.g., SnoopCatcher/SnoopTag[5]) within each fusion to create a four-arm SpyCatcher-end-functionalized star protein polymer.

Signaling pathways can be triggered by minuscule concentrations of a signaling molecule and on sub-second timescales. However, during traditional biochemical patterning of gels with encapsulated cells, high concentrations of active protein are swollen into/out of the material over several hours all while cells can sense and respond to the signaling molecule. Through *in situ* activation in large, diffusion-limited materials such as hydrogels or tissues, protein activity and cellular response can more appropriately mimic biology by capturing these shorter timescales. Photocaged unnatural amino acids that appropriately hinder protein activity would allow proteins to furtively reach cells before user-directed activation initiates signaling. Work currently underway in the DeForest lab aims to apply the Lys(*o*NB) used here to activate luciferase (**Figure 6.2**) – a model luminescent protein – and erythropoietin (EPO) – a surface-active angiogenic and

neurotrophic protein – within biomaterials. Patterned EPO may have potential in designing new materials to improve healing and functional outcome in large peripheral nerve defects as the presence of EPO improves axonal nerve growth and the regeneration of myelinated nerve fibers after injury[6]. Further, controlling angiogenesis through selective EPO activation in 3D may aid in the guiding vascularization within tissue mimetics. However, this can be extended beyond these proteins. This approach offers the high precision of optogenetics without complicated transfection procedures or genetic modification of the cells of interest.

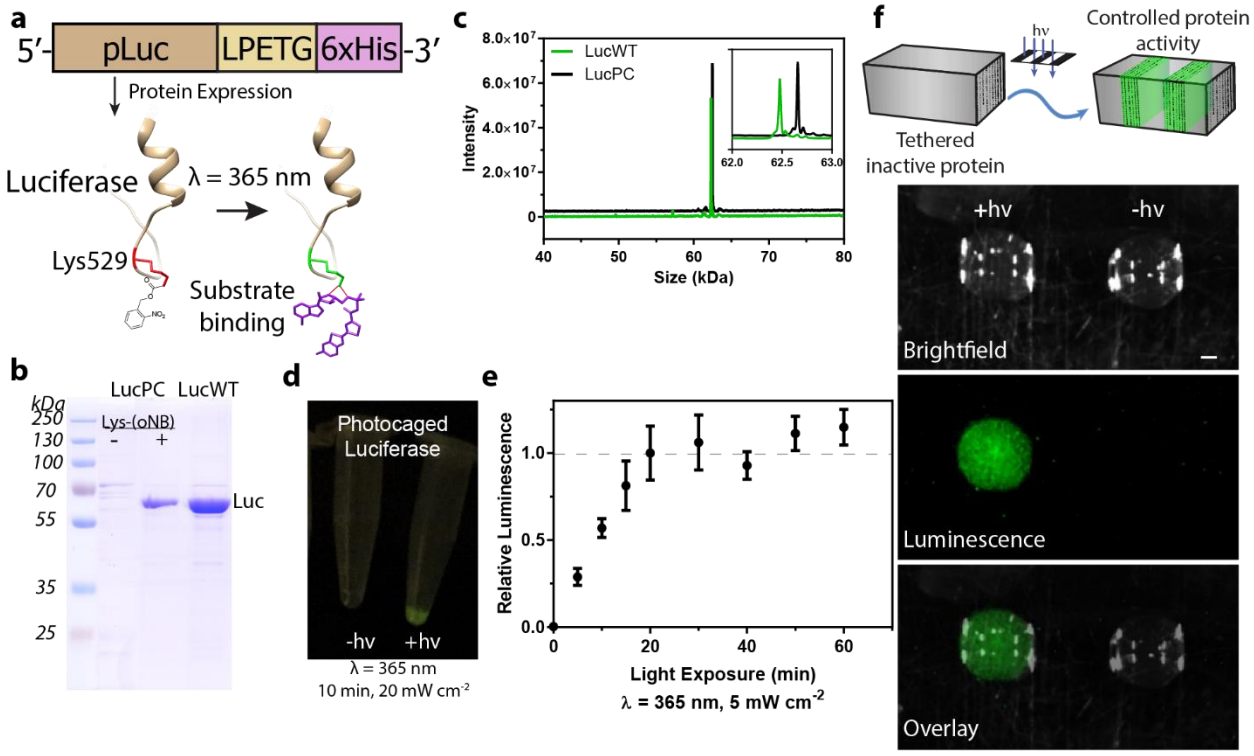

Figure 6.2. *In situ* protein activation overcomes diffusion limitations of current 3D platforms. **a**, a photocaged luciferase containing Lys(*o*NB) at K529 requires light exposure to restore a native lysine critical for substrate binding. Through photo-uncaging, LucPC regains bioluminescent activity. **b**, Highly pure LucPC was expressed only with the addition of Lys(*o*NB) and **c**, full-protein mass spectrometry confirmed the presence of a single mutated amino acid by a mass shift of the expected m_{WT} + 179 Da. **d**, Bioluminescence was restored with light exposure (λ = 365 nm at 20 mW cm^{-2}) and **e**, demonstrated dependence on total dosage of exposure meaning the effective concentration of active protein can be controlled. **f**, Immobilized LucPC required light treatment to restore activity and bioluminescence. Scale bar is 1 mm. Error bars indicate standard deviation for n=4 replicates.

A current limitation of the work involving generation of proteins with site-specifically photocaged functionalities is the comparatively low expression yields, owing to inefficiencies of the tRNA/tRNA synthetase pair optimized for incorporation of Lys(*o*NB). Recombinant expression yields could improve by utilizing alternative *E. coli* strains in which all genomic TAG amber stop codons have been changed to TAA (Addgene #48999), allowing for non-toxic knockout of the competing class I release factor (Addgene #48998)[7]. Additionally, orthogonal ribosomes/mRNAs that function independently from native machinery can increase non-canonical amino acid incorporation[8,9]. However, similar genomic mutants of mammalian cells that might be of interest like when controlling intracellular protein-protein interactions, as was reported in Chapter 5, are not yet available. Through increased collaborations with computational scientists or the application of phage-assisted continual evolution[10], improved efficiency of these key components may be possible.

Further, these techniques could greatly improve by implementing a more efficient single- and multi-photon responsive photocage. Coumarin-based cages offer improved kinetics compared to the *o*-nitrobenzyl group used here and an absorbance spectrum that extends into visible light. This class of cages, when conjugated to a lysine, have an evolved tRNA/tRNArs pair making the adoption feasible. This pair can incorporate three coumarin lysine variants with differing success suggesting that alternative coumarin cages might be translated without additional evolution of the synthetase[11]. By exploiting the blue light-responsive nature of coumarin cages, spatially controlled activation could be achieved using a 405 nm laser equipped on most confocal microscopes. The promiscuity of the tRNA/tRNArs pair may permit lysines caged with species such as 7-dicarboxymethylaminocoumarin (DCMAC)[12] which shows highly efficient multiphoton cleavage, to be translated. Increased multiphoton cleavage efficiency which helps minimize microscopy time

and potential for deleterious effects due to higher laser intensities would greatly improve intracellular applications of laSC.

An interesting spin-off of the SpyCatcher/SpyTag chemistry, coined SpyLigase, was developed by splitting the protein-peptide pair into a protein-peptide-peptide group each containing one component of the catalytic triad. This created an enzymatic peptide-peptide ligation reaction with extremely high specificity[13]. Like the significant applicability of SpyCatcher/SpyTag in biomaterials, SpyLigase offers unique potential applications to control both the biochemical and mechanical properties of hydrogels. Towards modulating the crosslinking density of gels, the peptide tags, modified to contain a photo-protecting group at the reactive Lys, could be incorporated within the backbone of a hydrogel and ligated in the presence of SpyLigase. Uniquely, the ligation does not require either peptide to be positioned as a pendent group which would increase the maximum gel moduli obtainable by the primary network structure. This design could be applied to synthetic networks by using solid-state peptide synthesis strategies to generate the relevant peptides or to protein-based networks by using an expanded genetic code as done in Chapter 5. Further, by incorporating the two-photon-responsive 3-(4,5-dimethoxy-2-nitrophenyl)-2-butyl (DMNPB) ester on the sidechain carboxylic acid of the reactive aspartic acid of SpyTag through synthetic strategies, the time needed to pattern gels would greatly decrease.

While reaction between SpyCatcher and SpyTag occurs on the order of tens of minutes, improved non-mutually exclusive mutants (e.g., SpyCatcher002/SpyTag002, SpyCatcher003/SpyTag003) demonstrate increased kinetics which can be particularly useful at low concentrations. A combination of the mutants could significantly improve the rate of binding intracellularly like when controlling protein-protein interactions (Chapter 5:). However, the photocage must disrupt the non-covalent association between SpyCatcher and SpyTag, so

association constants between the (photocaged) mutants would need to be closely examined if these new reactions were to be incorporated into the laSC methodologies.

Currently, multiphoton microscopy has proven quintessential to the 3D biomaterial patterning. However, the microscope must raster z-stacks of individual 2D planes to create complex patterns often shown in publications. While small features can be easily created, larger patterns can take hours of microscope time limiting feasibility for large scale patterning that would be required for tissue mimetics. Recent advances in multiphoton techniques pioneered by Prellis Biologics may help overcome this limitation. In one potential approach, the to-be-released Holograph X platform may be hacked to activate photochemistries in 3D. Advanced optogenetics have been demonstrated using computer-generated holography coupled with temporal focusing to simultaneously activate and image multiple points of interest using multiphoton light[14]. Porting these methodologies to biomaterial systems would revolutionize material patterning and tissue engineering through drastically increased processing speeds.

During the creation of Cloaked-SpyCatcher, the process of working with SpyCatcher/SpyTag was greatly simplified by the open and collaborative mindset of the Howarth group. After developing this ligation tool, their group began maintaining a "SpyBank" – a database of all uses of Spy- technologies, the amino acid sequences used, the expression system, and references to the work[15]. Additionally, the relevant plasmids needed to implement these technologies are deposited into the Addgene repository for easy access and useful information can be easily found on their lab website. This is a key demonstration of how to create widely accessible tools for the scientific community – something lacking in many other fields.

Here, strategies that offer unique control of (intra)cellular biochemical space and future applications were presented. We envision wide-reaching use of these technologies and hope they can increase accessibility across disciplines to help unravel the many intricacies of biology.

References

1. Pfeifer, G. P., You, Y.-H. & Besaratinia, A. Mutations induced by ultraviolet light. *Mutat. Res. Mol. Mech. Mutagen.* **571**, 19–31 (2005).
2. Khairil Anuar, I. N. A. *et al.* Spy&Go purification of SpyTag-proteins using pseudo-SpyCatcher to access an oligomerization toolbox. *Nat. Commun.* **10**, 1–13 (2019).
3. Shadish, J. A., Strange, A. C. & DeForest, C. A. Genetically Encoded Photocleavable Linkers for Patterned Protein Release from Biomaterials. *J. Am. Chem. Soc.* **141**, 15619–15625 (2019).
4. Podust, V. N. *et al.* Extension of in vivo half-life of biologically active molecules by XTEN protein polymers. *J. Control. Release* **240**, 52–66 (2016).
5. Veggiani, G. *et al.* Programmable polyproteams built using twin peptide superglues. *Proc. Natl. Acad. Sci.* **113**, 1202–7 (2016).
6. Yin, Z. S., Zhang, H. & Gao, W. Erythropoietin promotes functional recovery and enhances nerve regeneration after peripheral nerve injury in rats. *Am. J. Neuroradiol.* **31**, 509–515 (2010).
7. Smolskaya, S. & Andreev, Y. A. Site-specific incorporation of unnatural amino acids into escherichia coli recombinant protein: Methodology development and recent achievement. *Biomolecules* **9**, 255 (2019).
8. Wang, K., Neumann, H., Peak-Chew, S. Y. & Chin, J. W. Evolved orthogonal ribosomes enhance the efficiency of synthetic genetic code expansion. *Nat. Biotechnol.* **25**, 770–777 (2007).
9. Thyer, R., Filipovska, A. & Rackham, O. Engineered rRNA enhances the efficiency of selenocysteine incorporation during translation. *J. Am. Chem. Soc.* **135**, 2–5 (2013).
10. Bryson, D. I. *et al.* Continuous directed evolution of aminoacyl-tRNA synthetases. *Nat. Chem. Biol.* **13**, 1253–1260 (2017).
11. Luo, J. *et al.* Genetically encoded optochemical probes for simultaneous fluorescence reporting and light activation of protein function with two-photon excitation. *J. Am. Chem. Soc.* **136**, 15551–15558 (2014).
12. Broguiere, N. *et al.* Morphogenesis guided by 3D patterning of growth factors in biological matrices. *bioRxiv* (2019) doi:10.1101/828947.
13. Fierer, J. O., Veggiani, G. & Howarth, M. SpyLigase peptide-peptide ligation polymerizes affibodies to enhance magnetic cancer cell capture. *Proc. Natl. Acad. Sci.* **111**, E1176-81 (2014).
14. Pégard, N. C. *et al.* Three-dimensional scanless holographic optogenetics with temporal focusing (3D-SHOT). *Nat. Commun.* **8**, 1–14 (2017).
15. Hatlem, D., Trunk, T., Linke, D. & Leo, J. C. Catching a SPY: Using the SpyCatcher-SpyTag and related systems for labeling and localizing bacterial proteins. *Int. J. Mol. Sci.* **20**, (2019).

APPENDIX A

Supplementary Information for Chapter 4: Logical Stimuli-Triggered Delivery of Small Molecules from Hydrogel Biomaterials

General Synthetic Information

Chemical reagents and solvents were purchased from either Sigma-Aldrich or Fisher Scientific and used without further purification. Distilled water (dH_2O) was obtained from a U.S. Filter Corporation Reverse Osmosis system equipped with a desalination membrane. All chemical reactions were performed under inert nitrogen atmosphere in flame-dried glassware and were stirred with Teflon-coated magnetic stir bars. Solvent was removed under reduced pressure with a Buchi Rotovap R-3 by using either V-700 vacuum pump or Welch 1400 high vacuum pump. All peptides were synthesized using Fmoc-based, microwave-assisted, solid-phase methodologies on a CEM Liberty 1. All peptides were purified by semi-preparative reverse-phase high pressure liquid chromatography (RP-HPLC) performed on a Dionex Ultimate 3000 equipped with an RS multiple variable wavelength detector, an automated fraction collector, and a C18 column. Peptide characterization was performed by Matrix-assisted laser desorption/ionization time of flight (MALDI-TOF) analysis on a Bruker AutoFlex II. Lyophilization was performed on a Labconco FreeZone 2.5 Plus freeze-dryer equipped with Labconco rotary vane 117 vacuum pump. A Lumen Dynamics OmniCure S1500 Spot UV curing system was used for photochemical cleavage reactions, where light intensity was determined using a Cole-Palmer radiometer (Series 9811-50, λ = 365 nm). Fluorescence measurements were performed using a SpectraMax M5 spectrometer. Fluorescence imaging was performed on a Nikon Eclipse TE2000-U fluorescent microscope or a Typhoon FLA9000 fluorescent gel scanner.

Synthesis of Previously Reported Compounds Used in this Work

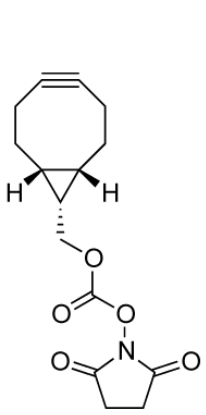

BCN-OSu

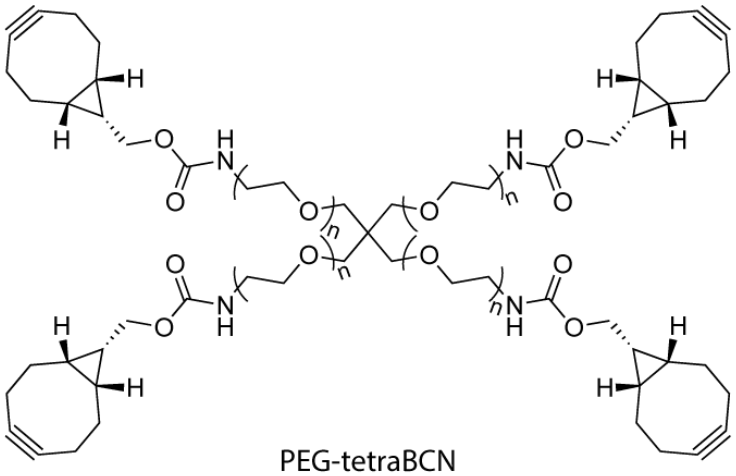

PEG-tetraBCN

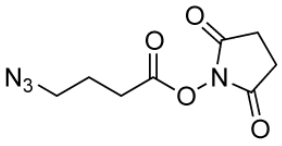

N_3-OSu

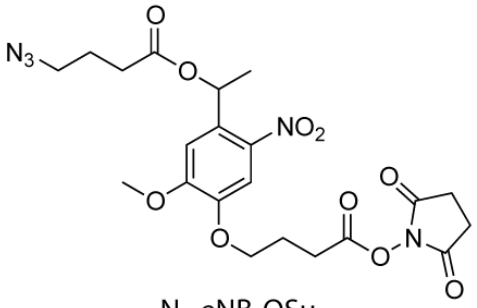

N_3-*o*NB-OSu

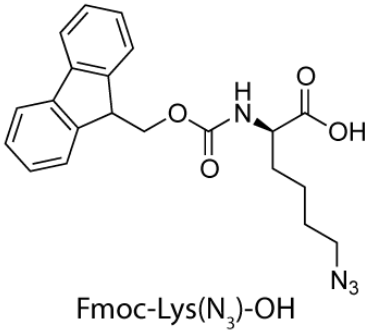

Fmoc-Lys(N_3)-OH

(1R,8S,9s)-bicyclo[6.1.0]non-4-yn-9-ylmethyl (2,5-dioxopyrrolidin-1-yl) carbonate (BCN-OSu), poly(ethylene glycol) tetrabicyclononyne (PEG-tetraBCN, M_n ~ 20,000 Da), 2,5-dioxopyrrolidin-1-yl 4-azidobutanoate (N_3-OSu), 2,5-dioxopyrrolidin-1-yl 4-(4-(1-((4-azidobutanoyl)oxy)ethyl)-2-methoxy-5-nitrophenoxy)butanoate (N_3-*o*NB-OSu), (*R*)-2-((((9H-fluoren-9-yl)methoxy)carbonyl)amino)-6-azidohexanoic acid (Fmoc-Lys(N_3)-OH), and recombinant MMP-8 were synthesized as previously reported[1–3].

Method S1: Synthesis of PEG-diazide (N_3-PEG-N_3)

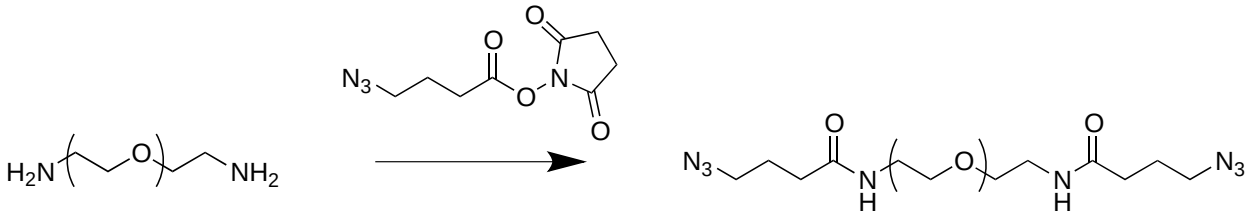

Linear poly(ethylene glycol) diamine (M_n ~ 3,500 Da, 1 g, 0.57 mmol NH_2, 1x, Jenkem) and N_3-OSu (194 mg, 0.86 mmol, 1.5x) were dissolved in dimethylformamide (5 mL). *N*,*N*-Diisopropylethylamine (398 µL, 294 mg, 2.28 mmol, 4x) was added to the mixture, and the reaction was stirred overnight, diluted in water (15 mL), dialyzed (MWCO ~ 2 kDa, SpectraPor), and lyophilized to yield a white powder (1.00 g, quantitative yield). ^{1}H NMR (500 MHz, $CDCl_3$) δ 3.75 (m, 4H), 3.65-3.61 (m, 318H), 3.28 (m, 4H), 2.35 (m, 4H), 1.86 (m, 4H). Functionalization was found to be >95% by comparing integral values for hydrogens introduced upon azide coupling (δ 3.28, 2.35, 1.86) with those from the PEG backbone (δ 3.60-3.42).

Method S2: Synthesis of FAM-P

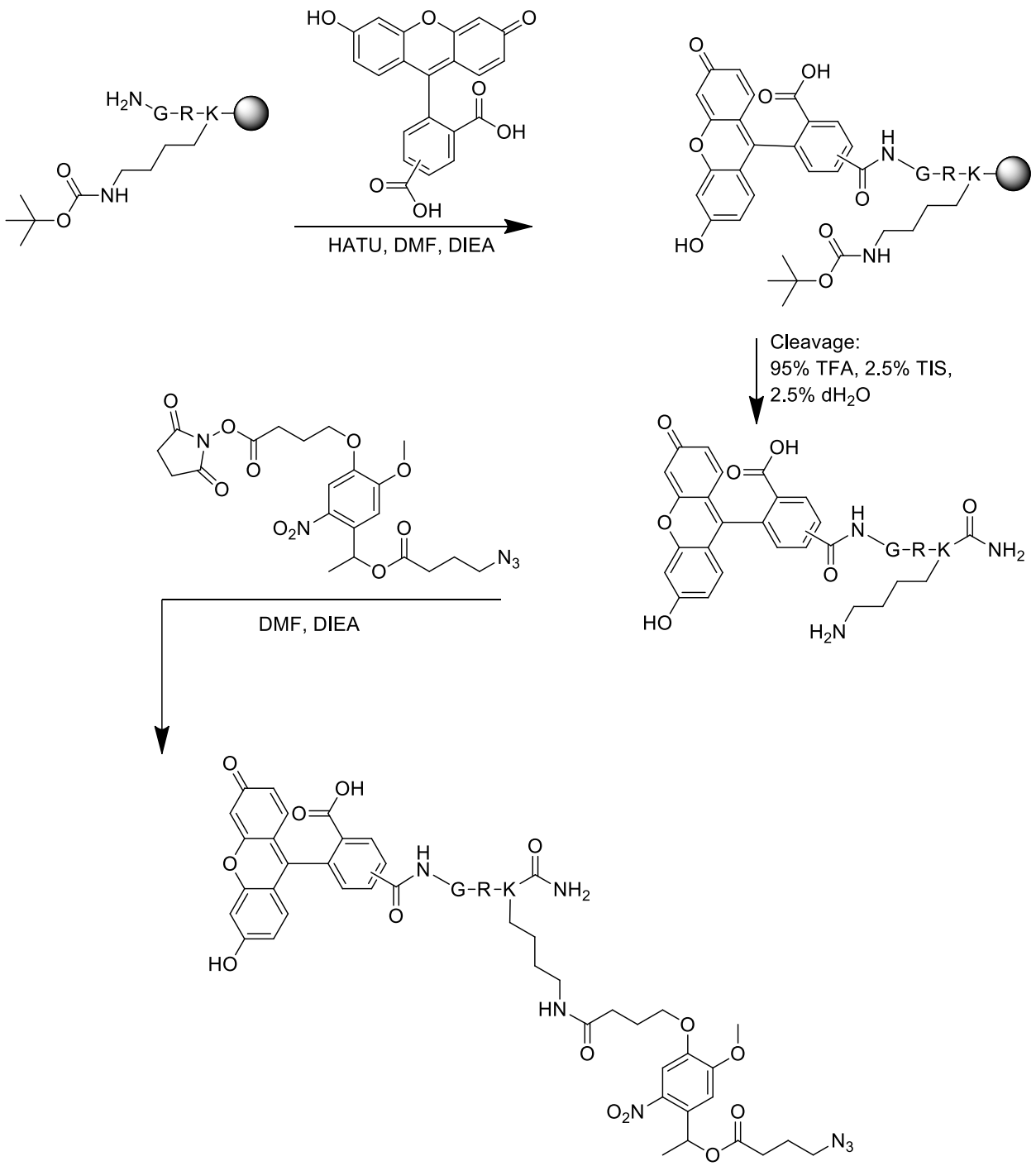

The base peptide H-GRK(Boc)-NH_2 was synthesized (0.25 mmol scale) on rink amide resin (ChemPep, loading capacity = 0.8 mmol/g) *via* standard microwave-assisted Fmoc solid-phase methodologies with HBTU activation. Microwave-assisted coupling of 5,6-Carboxyfluorescein (4x, 377 mg, Fisher) was conducted at 60 °C and 25W for 30 min on resin with HATU (3.9x, 371 mg) dissolved in minimal DMF containing DIEA (8x, 258.3 mg). Resin was treated with

trifluoroacetic acid/triisopropylsilane/water (95:2.5:2.5) for 2 h, and the crude peptide was precipitated in and washed (2x) with ice-cold diethyl ether. The crude peptide was purified by RP-HPLC using a 55-min linear gradient (5–100% of acetonitrile and 0.1% trifluoroacetic acid) and lyophilized to give the intermediate (FAM-GRK-NH_2) as a fluffy, yellow solid. N_3-*o*NB-OSu (53 mg, 0.105 mmol, 1.3x) was dissolved in minimal DMF containing DIEA (40 mg, 0.31 mmol, 4x) and added to the peptide to react overnight. The peptide was purified by RP-HPLC using a 55-min linear gradient (5–100% of acetonitrile and 0.1% trifluoroacetic acid) and lyophilized to give the product (FAM-GRK(*o*NB-N_3)-NH_2, denoted FAM-P) as a fluffy, yellow solid (11.0 mg, 0.01 mmol) with a yield of 4%. Peptide purity was confirmed with analytical RP-HPLC and matrix-assisted laser desorption-ionization time-of-flight mass spectrometry using α-cyano-4-hydroxycinnamic acid matrix: MALDI-TOF: calculated for $C_{52}H_{60}N_{12}O_{16}^{+}$ $[M + {}^{1}H]^{+}$, 1109.1; found 1109.3.

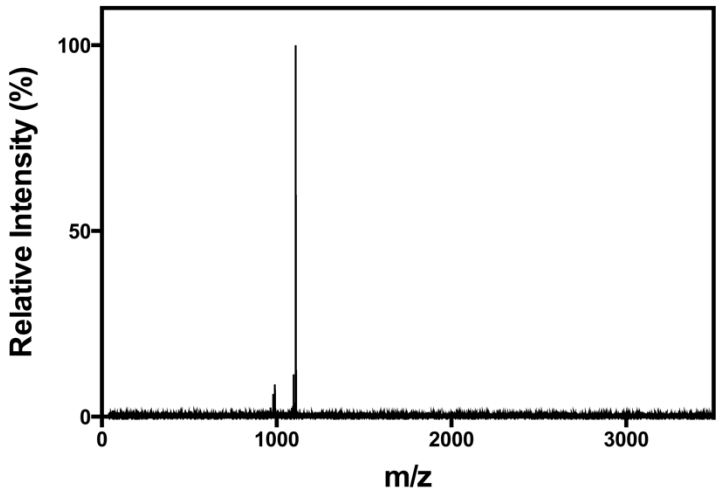

Method S3: Synthesis of FAM-E

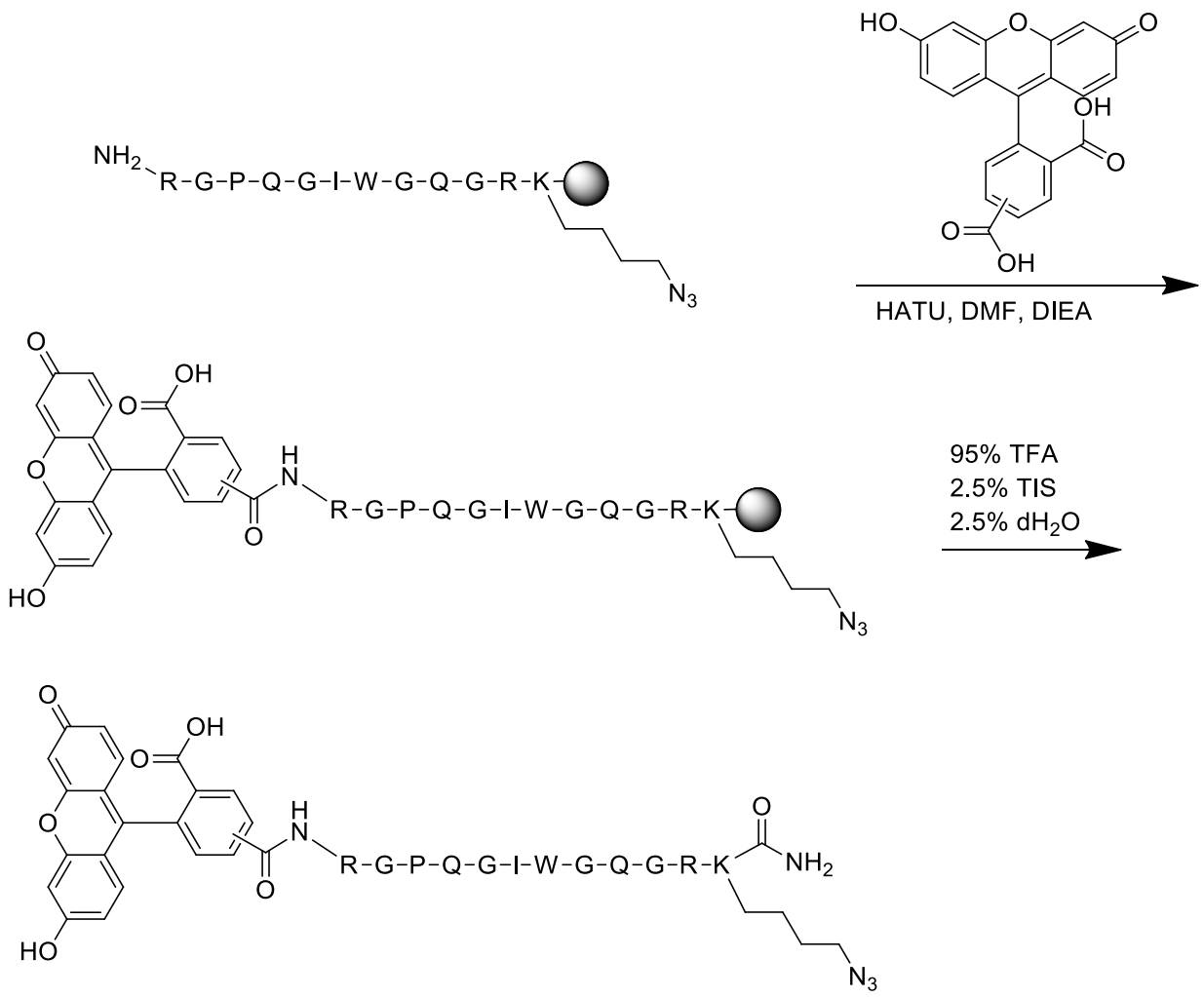

The base peptide H-RGPQGIWGQGRK(N_3)-NH_2 was synthesized (0.25 mmol scale) on rink amide resin (ChemPep, loading capacity = 0.8 mmol/g) *via* standard microwave-assisted Fmoc solid-phase methodologies with HBTU activation. 5,6-Carboxyfluorescein (4x, 376 mg, Fisher) was coupled at room temperature twice for 2 h on resin with HATU (3.9x, 370 mg) dissolved in minimal DMF containing DIEA (8x, 258 mg). Resin was treated with trifluoroacetic acid/triisopropylsilane/water (95:2.5:2.5) for 2 h, and the crude peptide was precipitated in and washed (2x) with ice-cold diethyl ether. The crude peptide was purified using semi-preparative reversed-phase high-performance liquid chromatography (RP-HPLC) using a 55-min linear gradient (5–100% of acetonitrile and 0.1% trifluoroacetic acid) and lyophilized to give the product (FAM-RGPQGIWGQGRK(N_3)-NH_2, denoted FAM-E) as a fluffy, yellow solid (56.2 mg, 32.6 µmol, 13% overall).

Peptide purity was confirmed with analytical RP-HPLC and matrix-assisted laser desorption-ionization time-of-flight mass spectrometry using α-cyano-4-hydroxycinnamic acid matrix: MALDI-TOF: calculated for $C_{79}H_{103}N_{25}O_{20}^{+}$ $[M + {}^{1}H]^{+}$, 1722.8; found 1722.6.

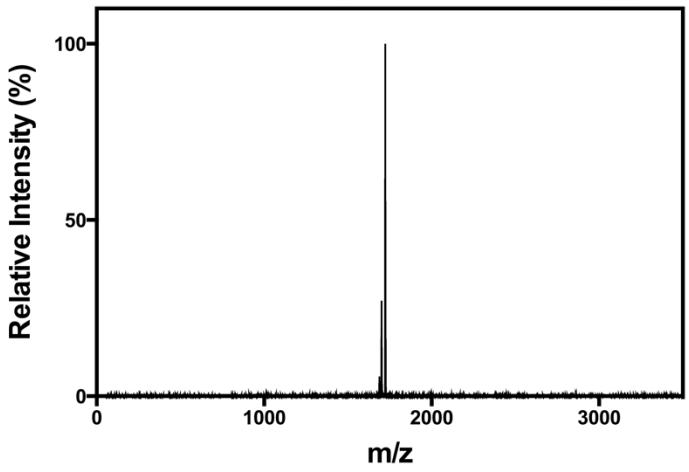

Method S4: Synthesis of FAM-R

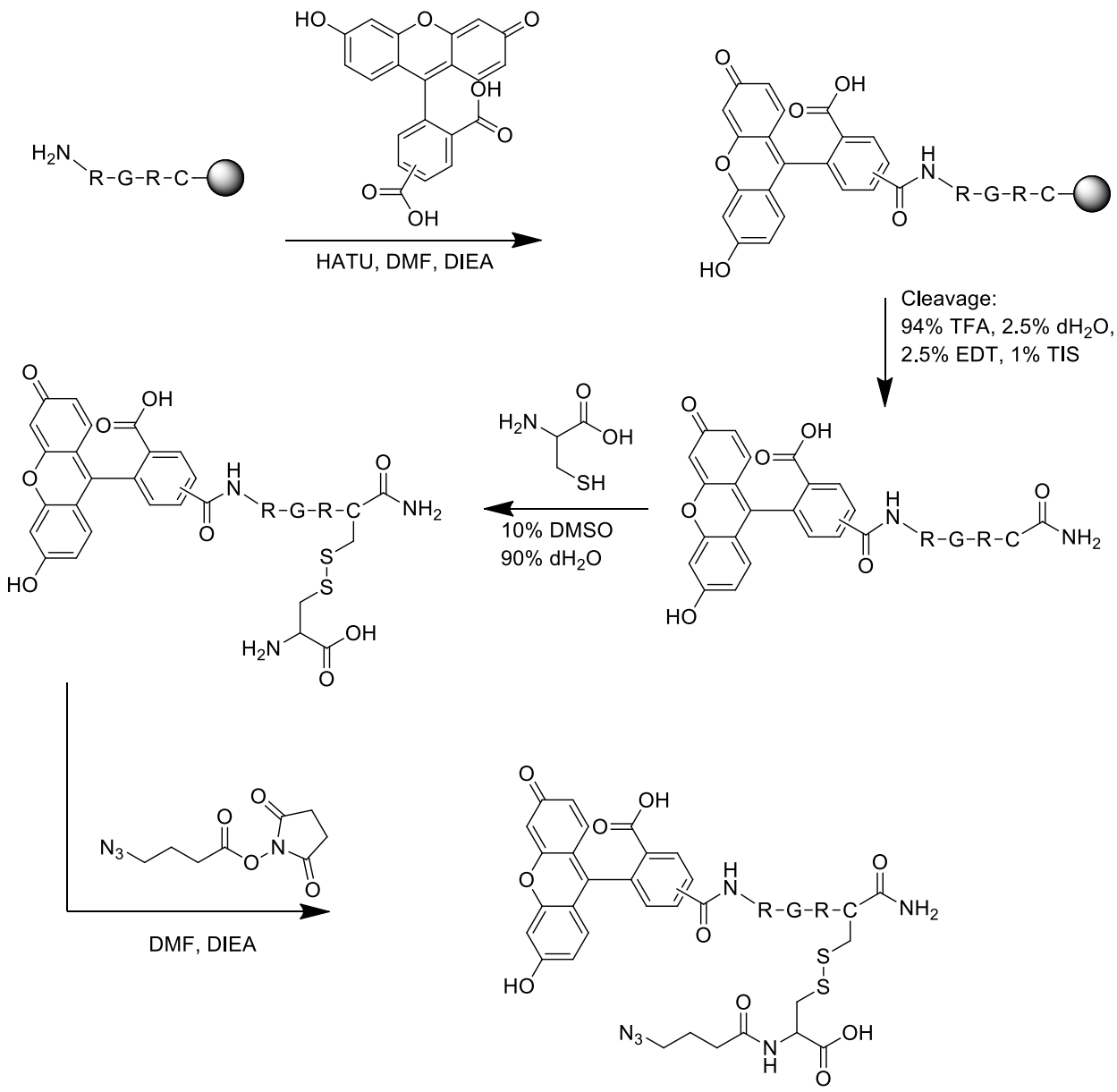

The base peptide H-RGRC-NH_2 was synthesized (0.25 mmol scale) on rink amide resin (ChemPep, loading capacity = 0.8 mmol/g) *via* standard microwave-assisted Fmoc solid-phase methodologies with HBTU activation. Microwave-assisted coupling of 5,6-Carboxyfluorescein (4x, 377 mg, Fisher) was conducted at 60 °C and 25 W for 30 min on resin with HATU (3.9x, 371 mg) dissolved in minimal DMF containing DIEA (8x, 258.3 mg). Resin was treated with trifluoroacetic acid/1,2-ethanedithiol/water/triisopropylsilane (94:2.5:2.5:1) for 2 h, and the crude peptide was precipitated in and washed (2x) with ice-cold diethyl ether. The crude peptide was purified by RP-HPLC using a 42-min linear gradient (20–100% of acetonitrile and 0.1% trifluoroacetic acid) and lyophilized to give the intermediate (FAM-RGRC-NH_2) as a fluffy, yellow solid. Cysteine (606 mg, 5 mmol, 20x) was codissolved with intermediate peptide in a

dH_2O/DMSO (90:10) solution (50 mL) and agitated for 24 h. Additional cysteine (606 mg, 5 mmol, 20x) was added to solution and reacted for 24 h while agitating at room temperature. Product was vacuum filtered and washed with dH_2O. The filtrate was frozen, lyophilized, and purified by RP-HPLC using a 42-min linear gradient (20–100% of acetonitrile and 0.1% trifluoroacetic acid); lyophilization afforded the purified intermediate (FAM-RGRC(C)-NH_2 linked *via* a cysteine-cysteine disulfide bridge) as a fluffy, yellow solid (104.4 mg, 0.10795 mmol). N_3-OSu (29.32 mg, 0.13 mmol, 1.2x) was coupled overnight with the peptide in minimal DMF containing DIEA (55.8 mg, 0.43 mmol, 4x). The crude peptide was purified by RP-HPLC using a 42-min linear gradient (20–100% of acetonitrile and 0.1% trifluoroacetic acid) and lyophilized to give the product (FAM-RGRC(C-N_3)-NH_2 linked *via* a cysteine-cysteine disulfide bridge, denoted FAM-R) as a fluffy, yellow solid (83.2 mg, 0.077 mmol) with a good overall yield (29.6%). Peptide purity was confirmed with analytical RP-HPLC and matrix-assisted laser desorption-ionization time-of-flight mass spectrometry using α-cyano-4-hydroxycinnamic acid matrix: MALDI-TOF: calculated for $C_{45}H_{56}N_{15}O_{13}S_2^+$ $[M + {}^1H]^+$, 1079.2; found 1079.3.

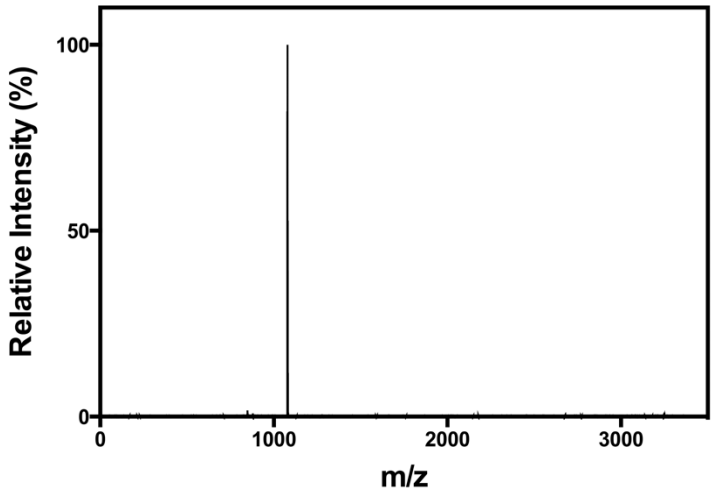

Method S5: Synthesis of FAM-EVR

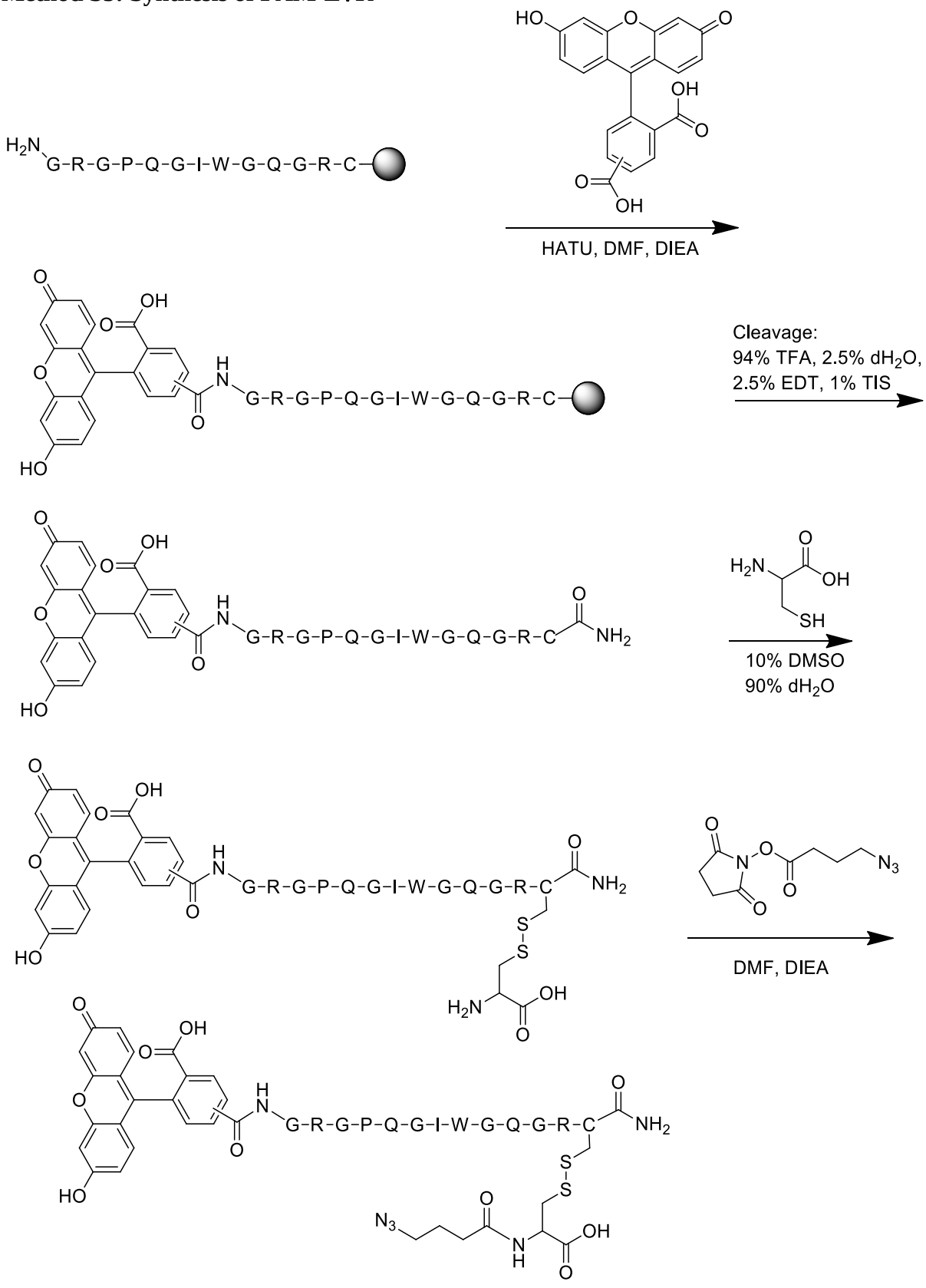

The base peptide H-GRGPQGIWGQGRC-NH_2 was synthesized (0.25 mmol scale) on rink amide resin (ChemPep, loading capacity = 0.8 mmol/g) *via* standard microwave-assisted Fmoc solid-phase methodologies with HBTU activation. Coupling of 5,6-Carboxyfluorescein (4x, 376 mg, Fisher) was conducted at room temperature overnight on resin with HATU (3.9x, 370 mg) dissolved in minimal DMF containing DIEA (8x, 258 mg). Resin was treated with trifluoroacetic acid/1,2-ethanedithiol/water/triisopropylsilane (94:2.5:2.5:1) for 2 h, and the crude peptide was precipitated in and washed (2x) with ice-cold diethyl ether. The crude peptide was purified by RP-HPLC using a 55-min linear gradient (5–100% of acetonitrile and 0.1% trifluoroacetic acid) and lyophilized to give the intermediate (FAM-GRGPQGIWGQGRC-NH_2) as a fluffy, yellow solid. Cysteine (605.8 mg, 5 mmol, 20x) was codissolved with intermediate peptide in a dH_2O/DMSO (90:10) solution (50 mL) and agitated for 24 h. Product was vacuum filtered and washed with dH_2O. The filtrate was frozen, lyophilized, and purified by RP-HPLC using a 42-min linear gradient (20–100% of acetonitrile and 0.1% trifluoroacetic acid) and lyophilized to give the intermediate (FAM-GRGPQGIWGQGR<u>C(C)</u>-NH_2 linked *via* a cysteine-cysteine <u>disulfide bridge</u>) as a fluffy, yellow solid. N_3-OSu (13.6 mg, 0.06 mmol, 2x) was reacted overnight with the peptide in minimal DMF containing DIEA (15.5 mg, 0.12 mmol, 4x). The peptide was purified by RP-HPLC using a 42-min linear gradient (20–100% of acetonitrile and 0.1% trifluoroacetic acid) and lyophilized to give the product (FAM-GRGPQGIWGQGR<u>C(C-N_3)</u>-NH_2 linked *via* a cysteine-cysteine <u>disulfide bridge</u>, denoted FAM-EvR) as a fluffy, yellow solid (21.7 mg, 11.1 µmol) with an overall yield of 4.4%. Peptide purity was confirmed with analytical RP-HPLC and matrix-assisted laser desorption-ionization time-of-flight mass spectrometry using α-cyano-4-hydroxycinnamic acid/2,5-dihydroxybenzoic acid (2:1) matrix: MALDI-TOF: calculated for $C_{85}H_{111}N_{27}O_{24}S_2^+$ $[M + {}^1H]^+$, 1959.1; found 1959.5.

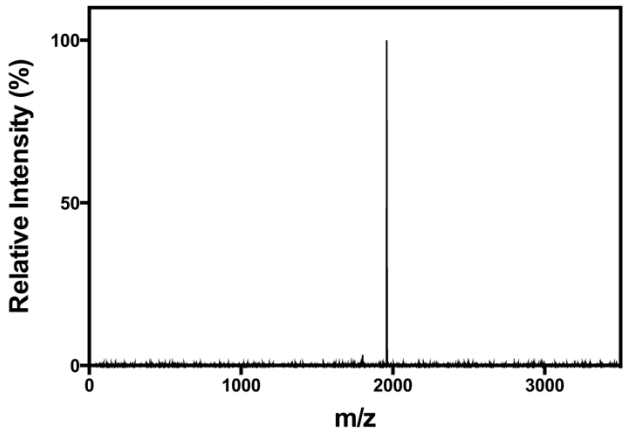

Method S6: Synthesis of FAM-EvRvP

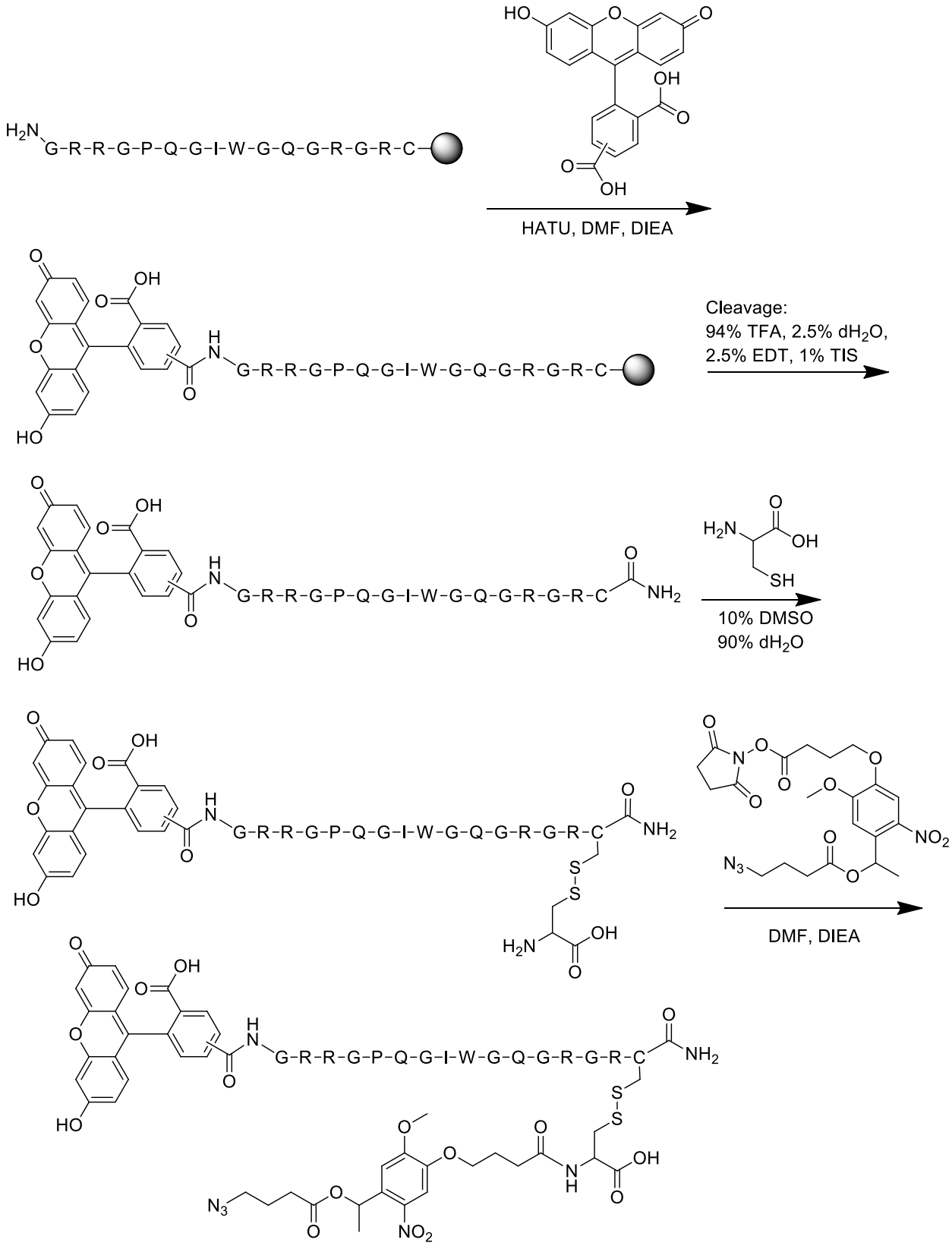

The base peptide H-GRRGPQGIWGQGRGRC-NH_2 was synthesized (0.25 mmol scale) on rink amide resin (ChemPep, loading capacity = 0.8 mmol/g) *via* standard microwave-assisted Fmoc solid-phase methodologies with HBTU activation. Microwave-assisted coupling of 5,6-Carboxyfluorescein (4x, 376 mg, Fisher) was conducted at 60 °C and 25W for 30 min on resin with HATU (3.9x, 370 mg) dissolved in minimal DMF containing DIEA (8x, 258 mg). Resin was treated with trifluoroacetic acid/1,2-ethanedithiol/water/triisopropylsilane (94:2.5:2.5:1) for 2 h, and the crude peptide was precipitated in and washed (2x) with ice-cold diethyl ether. The crude peptide was purified by RP-HPLC using a 55-min linear gradient (5–100% of acetonitrile and 0.1% trifluoroacetic acid) and lyophilized to give the intermediate (FAM-GRRGPQGIWGQGRGRC-NH_2) as a fluffy, yellow solid. Cysteine (606 mg, 5 mmol, 20x) was codissolved with the intermediate peptide in a dH_2O/DMSO (90:10) solution (50 mL) and agitated for 24 h. Product was vacuum filtered and washed with dH_2O. The filtrate was frozen, lyophilized, and purified by RP-HPLC using a 42-min linear gradient (20–100% of acetonitrile and 0.1% trifluoroacetic acid) and lyophilized to give the intermediate (FAM-GRRGPQGIWGQGRGRC(C)-NH_2 linked *via* a cysteine-cysteine disulfide bridge) as a fluffy, yellow solid. N_3-*o*NB-OSu (28.4 mg, 0.056 mmol, 1.3x) was dissolved in minimal DMF containing DIEA (22.2 mg, 0.172 mmol, 4x) and added to peptide to react overnight. The peptide was purified by RP-HPLC using a 42-min linear gradient (20–100% of acetonitrile and 0.1% trifluoroacetic acid) and lyophilized to give the product (FAM-GRRGPQGIWGQGRGRC(C-*o*NB-N_3)-NH_2 linked *via* a cysteine-cysteine disulfide bridge, denoted FAM-EVRVP) as a fluffy, yellow solid (60.0 mg, 23 μmol) with an overall yield of 9.2%. Peptide purity was confirmed with analytical RP-HPLC and matrix-assisted laser desorption-ionization time-of-flight mass spectrometry using α-cyano-4-hydroxycinnamic acid/2,5-dihydroxybenzoic acid (2:1) matrix: MALDI-TOF: calculated for $C_{112}H_{153}N_{37}O_{33}S_2^+$ $[M + {}^1H]^+$, 2609.8; found 2609.9.

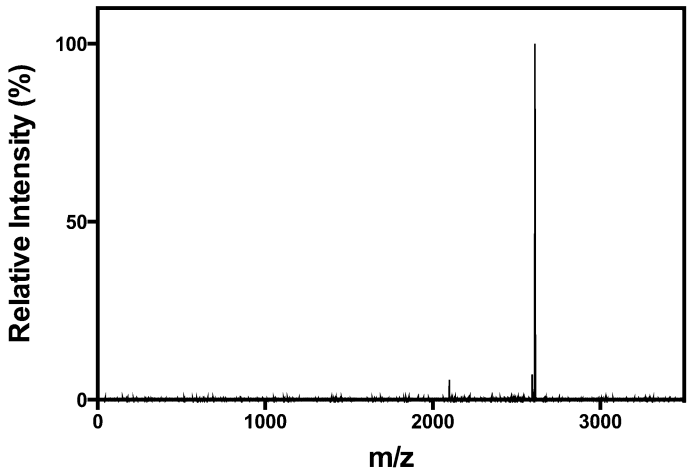

Method S7: Synthesis of FAM-EΛR

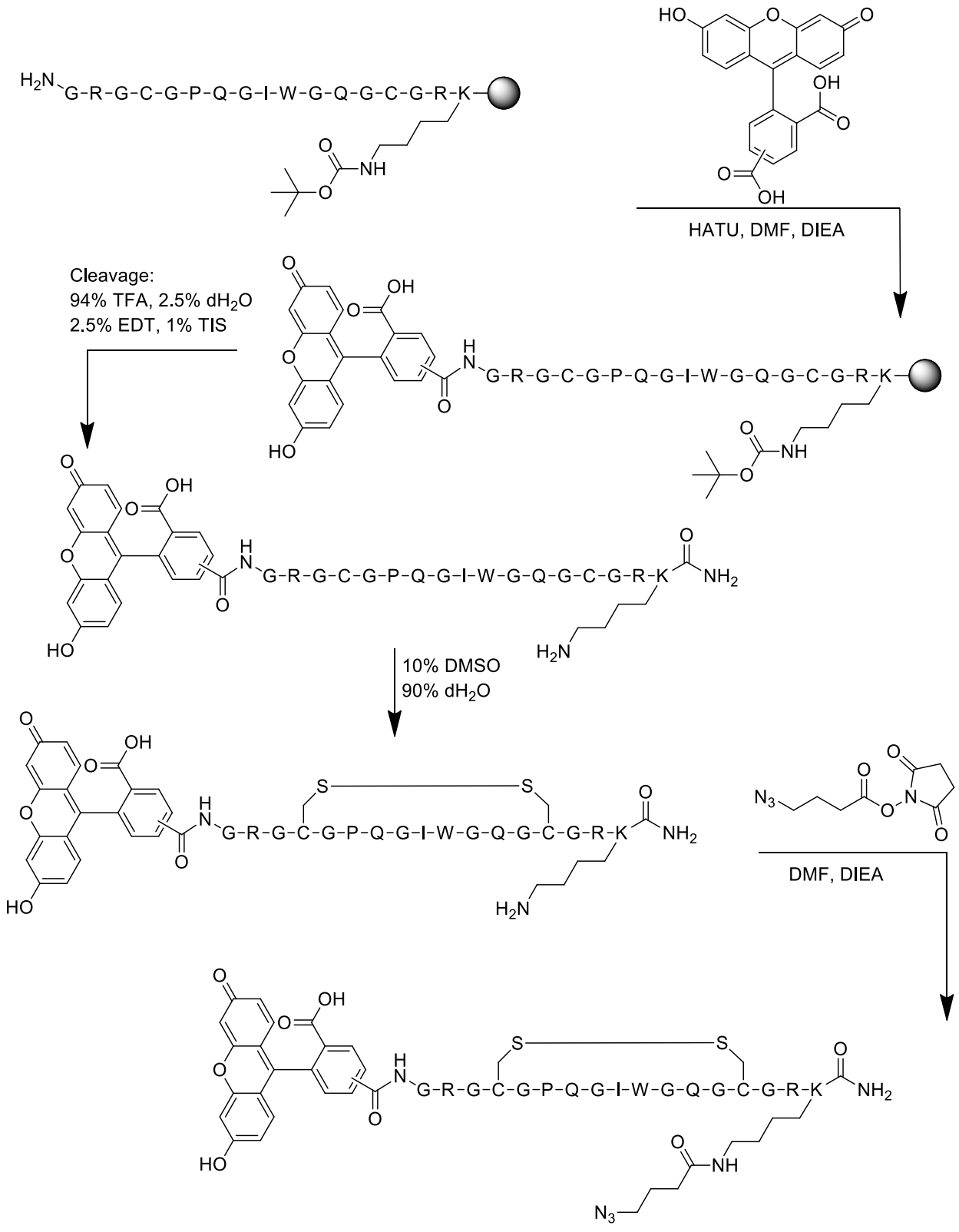

The base peptide H-GRGCGPQGIWGQGCGRK-NH_2 was synthesized (0.25 mmol scale) on rink amide resin (ChemPep, loading capacity = 0.8 mmol/g) *via* standard microwave-assisted Fmoc solid-phase methodologies with HBTU activation. Microwave-assisted coupling of 5,6-Carboxyfluorescein (282.2 mg, 0.75 mmol, 4x Fisher) was conducted at 60 °C and 25W for 30 min on resin with HATU (280.9 mg, 0.73 mmol, 2.95x) dissolved in minimal DMF containing DIEA (193.9 mg, 1.5 mmol, 6x). Resin was treated with trifluoroacetic acid/1,2-ethanedithiol/water/triisopropylsilane (94:2.5:2.5:1) for 2 h, and the crude peptide was precipitated in and washed (2x) with ice-cold diethyl ether. The crude peptide was purified by RP-HPLC using a 55-min linear gradient (5–100% of acetonitrile and 0.1% trifluoroacetic acid) and lyophilized to give the intermediate (FAM-GRGCGPQGIWGQGCGRK-NH_2) as a fluffy, yellow solid. The purified peptide (<0.5 mM) was dissolved in a dH_2O/DMSO (90:10) solution (50 mL) and agitated for 24 h. Product was concentrated, lyophilized, and subsequently purified by RP-HPLC using a 55-min linear gradient (5–100% of acetonitrile and 0.1% trifluoroacetic acid). Lyophilization afforded the purified intermediate (FAM-GRGCGPQGIWGQGCGRK-NH_2 cyclized *via* cysteine-cysteine disulfide bridge) as a fluffy, yellow solid. N_3-OSu (2.65 mg, 0.012 mmol, 1.2x) was coupled overnight with the peptide in minimal DMF containing DIEA (4.65 mg, 0.04 mmol, 4x). The peptide was purified by RP-HPLC using a 55-min linear gradient (5–100% of acetonitrile and 0.1% trifluoroacetic acid) and lyophilized to give the product (FAM-GRGCGPQGIWGQGCGRK(N_3)-NH_2 cyclized *via* cysteine-cysteine disulfide bridge, denoted FAM-E∧R) as a fluffy, yellow solid (5.7 mg, 2.6 µmol) with an overall yield of 1.1%. Peptide purity was confirmed with analytical RP-HPLC and matrix-assisted laser desorption-ionization time-of-flight mass spectrometry using α-cyano-4-hydroxycinnamic acid matrix: MALDI-TOF: calculated for $C_{95}H_{127}N_{31}O_{33}S_2^+$ $[M + {}^1H]^+$, 2183.3; found 2183.2.

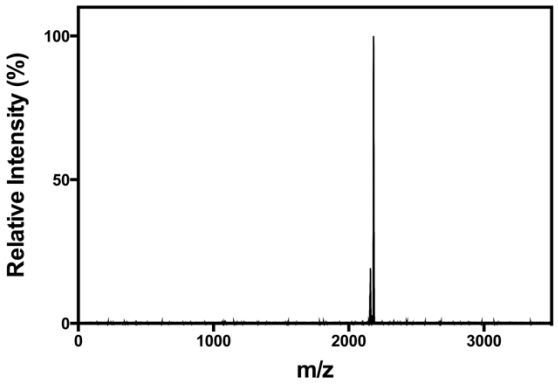

Method S8: Synthesis of FAM-PΛR

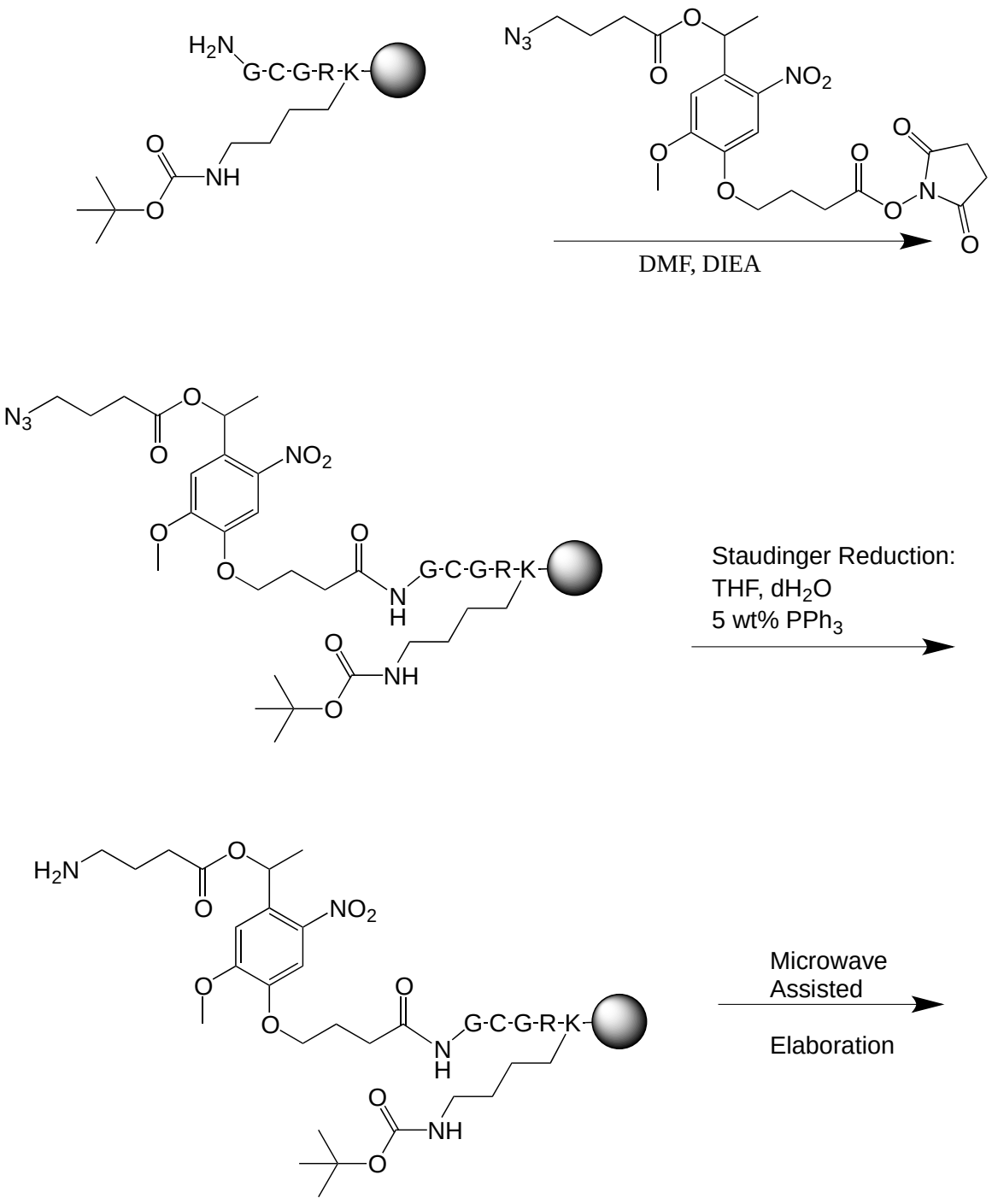

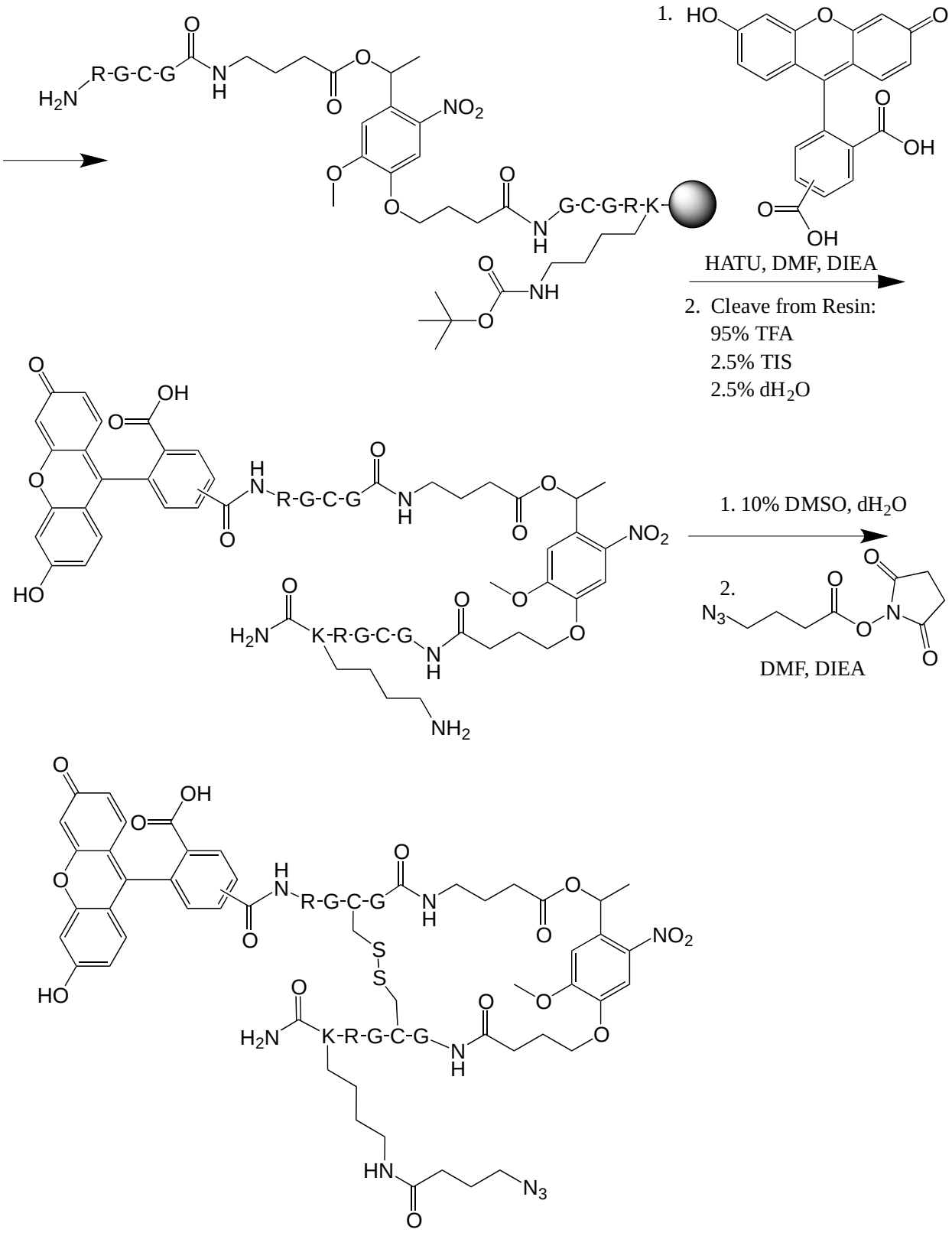

The base peptide H-GCGRK-NH_2 was synthesized (0.25 mmol scale) on rink amide resin (ChemPep, loading capacity = 0.8 mmol/g) *via* standard microwave-assisted Fmoc solid-phase

methodologies with HBTU activation. N_3-*o*NB-OSu (329.55 mg, 0.325 mmol, 1.3x) was dissolved in minimal DMF containing DIEA (129.2 mg, 1.0 mmol, 4x) and added to peptide on resin to react overnight at room temperature. The peptide's N-terminal azide was reduced by Staudinger reduction[13]: the resin was first rinsed with a solution of tetrahydrafuran/dH_2O (90:10, 3 x 20 mL), followed by overnight reaction in a solution of triphenylphospine (5 wt%, 1.5 g, Sigma) in tetrahydrafuran/dH_2O (90:10, 30 mL). Peptide was rinsed with DMF (3 x 10 mL) and DCM (3 x 10 mL), and standard microwave-assisted Fmoc solid-phase methodologies with HBTU activation was used to elaborate the peptide to form the peptide H-RGCG-*o*NB-GCGRK-NH_2. 5,6-Carboxyfluorescein (377 mg, 1.0 mmol, 4x Fisher) was coupled at room temperature overnight on resin with HATU (371 mg, 0.98 mmol, 3.9x) dissolved in minimal DMF containing DIEA (8x, 258.3 mg). Resin was treated with trifluoroacetic acid/water/triisopropylsilane (95:2.5:2.5) for 2 h, and the crude peptide was precipitated in and washed (2x) with ice-cold diethyl ether. The crude peptide was purified by RP-HPLC using a 42-min linear gradient (20–100% of acetonitrile and 0.1% trifluoroacetic acid) and lyophilized to give the intermediate (FAM-RGCG-*o*NB-GCGRK-NH_2) as a fluffy, yellow solid. The purified peptide (<0.5 mM) was dissolved in a dH_2O/DMSO (90:10) solution (35 mL) and agitated for 24 h, then frozen and lyophilized. Intermediate product was purified by RP-HPLC using a 42-min linear gradient (20–100% of acetonitrile and 0.1% trifluoroacetic acid) and lyophilized to give the intermediate (FAM-RGCG-*o*NB-GCGRK-NH_2 cyclized *via* cysteine-cysteine disulfide bridge) as a fluffy, yellow solid. N_3-OSu (6.2 mg, 0.0274 mmol, 1.2x) was coupled overnight with the peptide in minimal DMF containing DIEA (10.9 mg, 14 µL, 0.084 mmol, 4x). The peptide was purified by RP-HPLC using a 42-min linear gradient (20–100% of acetonitrile and 0.1% trifluoroacetic acid) and lyophilized to give the product (FAM-RGCG-*o*NB-GCGRK(N_3)-NH_2 cyclized *via* cysteine-cysteine disulfide bridge, denoted FAM-PΛR) as a fluffy, yellow solid (1.33 mg, 0.77 µmol) with an overall yield of 0.15%. Peptide purity was confirmed with analytical RP-HPLC and matrix-assisted laser desorption-ionization time-of-flight mass spectrometry using α-cyano-4-hydroxycinnamic acid matrix: MALDI-TOF: calculated for $C_{74}H_{96}N_{22}O_{23}S_2^+$ $[M + {}^1H]^+$, 1725.8; found 1726.0.

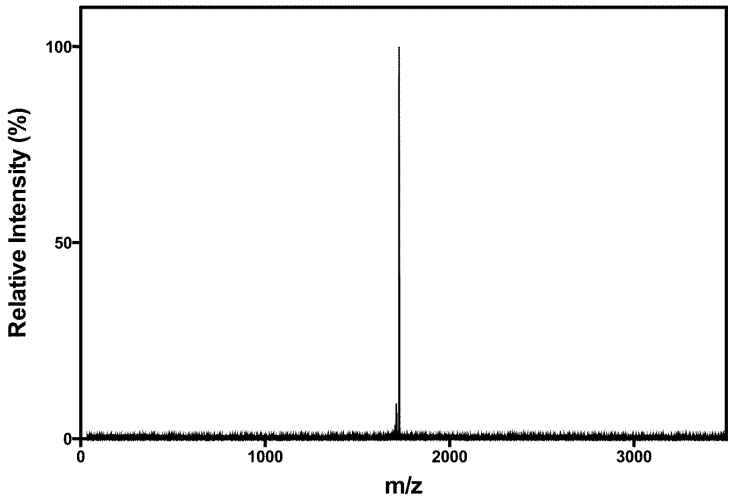

Method S9: Synthesis of FAM-RVP

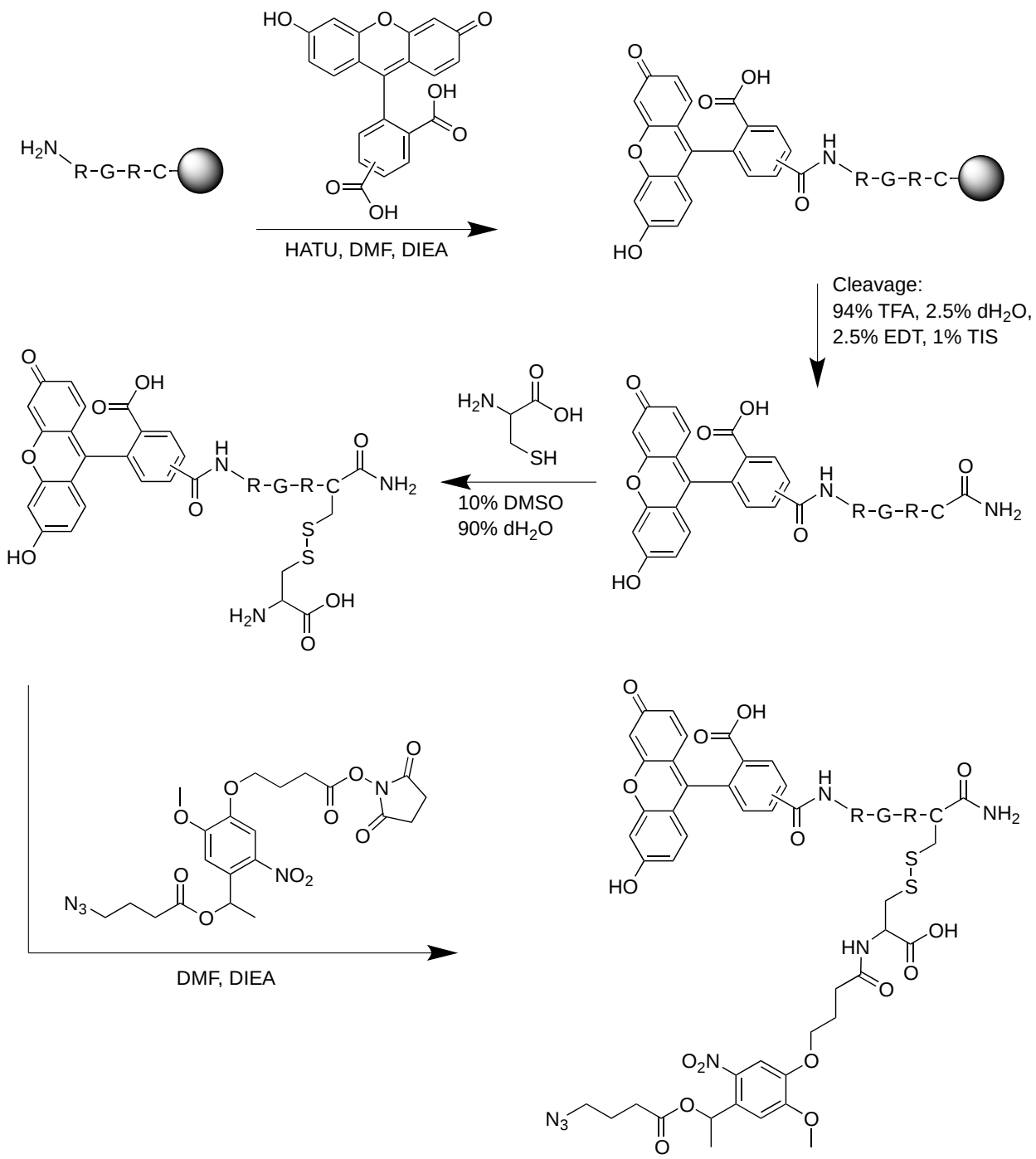

The base peptide H-RGRC-NH_2 was synthesized (0.25 mmol scale) on rink amide resin (ChemPep, loading capacity = 0.8 mmol/g) *via* standard microwave-assisted Fmoc solid-phase methodologies with HBTU activation. Microwave-assisted coupling of 5,6-Carboxyfluorescein (4x, 377 mg, Fisher) was conducted at 60 °C and 25W for 30 min on resin with HATU (3.9x, 371 mg) dissolved in minimal DMF containing DIEA (8x, 258.3 mg). Resin was treated with trifluoroacetic acid/1,2-ethanedithiol/water/triisopropylsilane (94:2.5:2.5:1) for 2 h, and the crude

peptide was precipitated in and washed (2x) with ice-cold diethyl ether. The crude peptide was purified by RP-HPLC using a 42-min linear gradient (20–100% of acetonitrile and 0.1% trifluoroacetic acid) and lyophilized to give the intermediate (FAM-RGRC-NH_2) as a fluffy, yellow solid. Cysteine (606 mg, 5 mmol, 20x) was codissolved with intermediate peptide in a dH_2O/DMSO (90:10) solution (50 mL) and agitated for 24 h. Additional cysteine (606 mg, 5 mmol, 20x) was added to solution and reacted for 24 h while agitating at room temperature. Product was vacuum filtered and washed with dH_2O. The filtrate was frozen, lyophilized, and purified by RP-HPLC using a 42-min linear gradient (20–100% of acetonitrile and 0.1% trifluoroacetic acid); lyophilization afforded the purified intermediate (FAM-RGRC(C)-NH_2 linked *via* a cysteine-cysteine disulfide bridge) as a fluffy, yellow solid (105 mg, 0.108 mmol). N_3-*o*NB-OSu (68 mg, 0.13 mmol, 1.2x) was coupled overnight with the peptide in minimal DMF containing DIEA (55.8 mg, 0.43 mmol, 4x). The crude peptide was purified by RP-HPLC using a 42-min linear gradient (20–100% of acetonitrile and 0.1% trifluoroacetic acid) and lyophilized to give the product (FAM-RGRC(C-*o*NB-N_3)-NH_2 linked *via* a cysteine-cysteine disulfide bridge, denoted FAM-RvP) as a fluffy, yellow solid (86.7 mg, 0.064 mmol) with a good overall yield (25.4%). Peptide purity was confirmed with analytical RP-HPLC and matrix-assisted laser desorption-ionization time-of-flight mass spectrometry using α-cyano-4-hydroxycinnamic acid matrix: MALDI-TOF: calculated for $C_{58}H_{71}N_{16}O_{19}S_2^+$ $[M + {}^1H]^+$, 1360.4; found 1359.5.

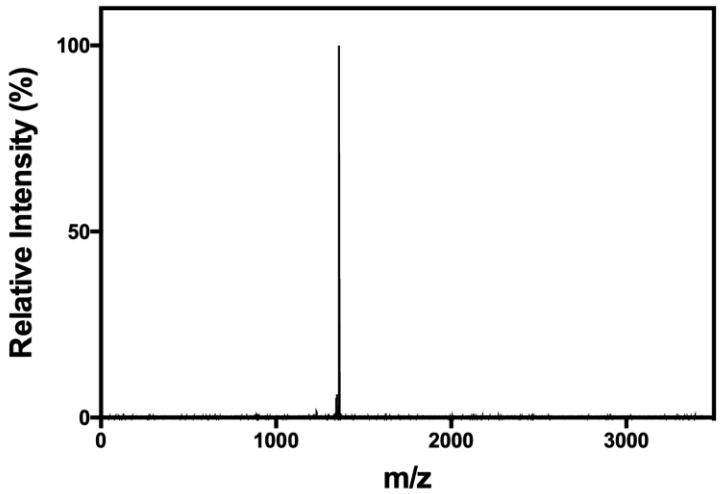

Figure S1: Small Molecule Release from Gels Containing FAM-P∧R Pendant

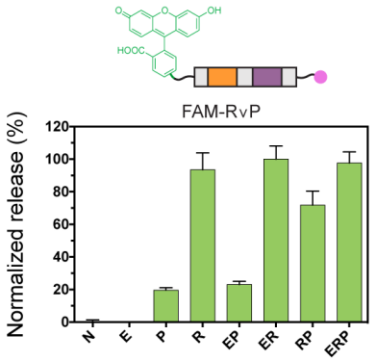

FAM is selectively released from gels for conditions involving either light OR reductant. X-axis labels indicate material treatment conditions (N indicates no treatment, E is MMP enzyme, R is a chemical reductant, P is UV light). The extent of release was normalized between 0% (corresponding to N) and 100% (in treatment with highest release) for each pendant. Green bars signify conditions expected to result in release; red bars indicate conditions expected not to yield release. Error bars correspond to ±1 standard deviation about the mean with propagated uncertainties for n = 3 experimental replicates.

References

1. DeForest, C. A. & Anseth, K. S. Cytocompatible click-based hydrogels with dynamically tunable properties through orthogonal photoconjugation and photocleavage reactions. *Nat. Chem.* **3,** (2011).
2. DeForest, C. A. & Tirrell, D. A. A photoreversible protein-patterning approach for guiding stem cell fate in three-dimensional gels. *Nat. Mater.* **14,** 523–531 (2015).
3. Badeau, B. A., Comerford, M. P., Arakawa, C. K., Shadish, J. A. & DeForest, C. A. Engineered modular biomaterial logic gates for environmentally triggered therapeutic delivery. *Nat. Chem.* **10,** 251–258 (2018).

VITA

EDUCATION

2014-2020 Ph.D. in Chemical Engineering (March 2020)
M.S. in Chemical Engineering
University of Washington, *Seattle, WA*
Cumulative GPA: 3.45/4.00

2010-2014 B.S. in Chemical Engineering
Minor in Mathematics
University of Nevada, Reno, *Reno, NV*
Cumulative GPA: 3.82/4.00, *Cum Laude*

PROFESSIONAL EXPERIENCE

Graduate Research Assistant – University of Washington, Seattle WA
Jan. 2015 – Mar. 2020 · *Dept of Chemical Engineering · PI: Dr. Cole DeForest*

- Applied genetic code expansion to install a single photocaged amino acid (in-house synthesized) into proteins for spatial and temporal control over their bioactivity within hydrogel biomaterials and mammalian cells
- Engineered fusion proteins and cloned DNA plasmids for protein expression in *E. coli* and mammalian cells
- Established in-house protocols to perform label-based proteome-wide investigations including sample preparation, LC-MS/MS operation, and large data-set processing
- Synthesized, modified, and engineered biomaterials to innovate 4D-tunable cell culture platforms

Undergraduate Research Assistant – University of Nevada, Reno, NV
Aug. 2013 – June 2014 · *Dept of Civil & Environmental Engineering · PI: Dr. Edward Kolodziej*

- Optimized extraction and GC/MS-based analysis of steroid metabolites in bovine tissue samples
- Measured photo- & anaerobic-degradation of environmentally persistent synthetic testosterone and estrogen metabolites

Nov. 2010 – Jan. 2013 · *Dept of Civil & Environmental Engineering · PI: Dr. Amy Childress*

- Constructed a benchtop osmotic membrane bioreactor coupled with forward/reverse osmosis units for wastewater processing
- Conducted reverse osmosis experiments monitoring flux of high salt concentration feed streams

PUBLICATIONS

1. **Ruskowitz ER**, Kurniawan S, Shadish JA, DeForest CA. Fully genetically encoded, spatiotemporally controlled protein tethering and release from protein hydrogel networks. *In preparation.*
2. **Ruskowitz ER**, Kurniawan S, DeForest CA. A genetically encoded protein-protein photoligation through light-activated SpyCatcher. *In preparation.*
3. **Ruskowitz ER** & DeForest CA. Proteome-wide analysis of cellular response to ultraviolet light for biomaterial synthesis and modification. *ACS Biomater Sci & Eng.* **5** (5), 2111-2116 (2019).
4. **Ruskowitz ER***, Comerford MP*, Badeau BA, DeForest CA. Logical stimuli-triggered delivery of small molecules from hydrogel biomaterials. *Biomater Sci.* **7** (2), 542-546 (2019). **These authors contributed equally to this work*
5. Adelmund SM, **Ruskowitz ER**, Farahani PE, Wolfe JV, DeForest CA. Light-activated proteomic labeling *via* photocaged bioorthogonal non-canonical amino acids. *ACS Chem Bio*. **13** (3) 573-577 (2018).
6. **Ruskowitz ER** & DeForest CA. Photoresponsive biomaterials for targeted drug delivery and 4D cell culture. *Nat Rev Mat.* **3** (2), 17087 (2018). Cover article.

PRESENTATIONS

1. **Ruskowitz ER**. A genetically encoded photoligation strategy for 4D protein patterning in biomaterials. UW ChemE Awards Day – Seattle WA, December 2019. *Invited Oral Presentation*
2. **Ruskowitz ER**. Photoactivatable proteins for instantaneous 4D control over microenvironmental cell signaling. ACES Graduate Student Symposium – Seattle WA, September 2019. *Oral Presentation*
3. **Ruskowitz ER**. Photoactivatable proteins for instantaneous 4D control over microenvironmental cell signaling. Gordon Research Seminar – Tissue Engineering and Biomaterials – Casteldefels, Spain, July 2019. *Invited Oral Presentation*
4. **Ruskowitz ER** & DeForest CA. Photoactivatable proteins for instantaneous 4D control over microenvironmental cell signaling. Gordon Research Conference – Tissue Engineering and Biomaterials – Casteldefels, Spain, July 2019. *Poster Presentation*
5. **Ruskowitz ER**. Proteome-wide analysis of cellular response to ultraviolet light for biomaterial synthesis and modification. Society for Biomaterials Conference – Seattle WA, April 2019. *Oral Presentation*
6. **Ruskowitz ER** & DeForest CA. A proteome-wide analysis of cells after exposure to UV light using pSILAC. ACES Graduate Student Symposium – Seattle WA, September 2018. *Poster Presentation*

LEADERSHIP & OUTREACH

Lab Manager, UW ChemE Cell Culture Laboratory, 2015 – 2020
Set up and maintained a shared departmental lab space with 36 users to-date; trained 12 users on sterile culture practices

Director, UW Distinguished Young Scholars Seminar, 2018

Led a team of 3 graduate assistants, organizing a summer-long seminar series featuring speakers from across the nation

Demo Organizer, Expanding Your Horizons, 2016 – 2018
Led a team of 4 graduate students in an all-day event featuring hands-on science activities for >60 7^{th}-12^{th} graders

Panel Leader, Women in Chemical Engineering Industry Panel, 2016
Facilitated a panel discussion on "The Role of ChemE's in Biotech"

Elected Organizer & Panel Leader, UW ChemE Graduate Student Symposium, 2016
Organized a 6-hr. symposium for ~100 attendees featuring an inaugural industry panel – fundraised $2100

Co-Founder & Vice President, Women in Chemical Engineering (WChE) UW, 2016-2017
Founding member of the nation's first student organization seeking to educate, empower, and advocate for women in chemical engineering through professional development, community networking and outreach

- *Implemented mental health and professional development workshops and multiple fundraising events*
- *Instituted annual department-wide donation drive for a local women's homeless shelter*
- *Established the first WChE-Invited Speaker Seminar featuring 4-star General Dr. Ellen Pawlikowski*

Volunteer, UW Engineering Day, 2016 – 2019
Volunteer, MLK Day of Service, 2015

MENTORSHIP & TEACHING

Research Mentor
Sept. 2018 to present · *Department of Chemical Engineering · University of Washington*

- Trained & mentored 3 UG students, 1 MS & 1 PhD on genetic cloning, protein expression & biomaterial modification

June 2016 · *WiSE UP*

- Introduced an incoming female engineering UG student to research over 1 week resulting in a research poster

June – Aug. 2013 · *GATE Internship Program · University of Nevada, Reno*

- Mentored a high school student and taught basic laboratory skills

Teaching Assistant – University of Washington, Seattle WA
Thermodynamics II (Winter 2018), Thermodynamics I – *"flipped" classroom requiring 1-on-1 teaching each class* (Fall 2017), Polymer Chemistry Laboratory – *assisted in course experiment design and implementation* (Spring 2016 & 2017), Senior Design (Spring 2015)

AWARDS

Faculty Lecture Award, *UW Chemical Engineering*, 2019
Krieger-Brocker Travel Award, *UW Chemical Engineering*, 2019
Travel Award, *UW Graduate School*, 2019
Invited Oral Presenter, *Gordon Research Seminar – Tissue Engineering & Biomaterials*, 2019
Outstanding Female Award, *SWE Evening with Industry*, 2016-2017
Presidential Scholar, *University of Nevada, Reno*, 2010-2014
Governor Guinn Millennium Scholar, *University of Nevada, Reno*, 2010-2014